

A SPECTROSCOPIC STUDY OF A LARGE SAMPLE OF WOLF-RAYET GALAXIES

Natalia G. Guseva, Yuri I. Izotov¹

Main Astronomical Observatory, Ukrainian National Academy of Sciences, Goloseevo, Kiev 03680, Ukraine

Electronic mail: guseva@mao.kiev.ua, izotov@mao.kiev.ua

and

Trinh X. Thuan¹

Astronomy Department, University of Virginia, Charlottesville, VA 22903

Electronic mail: txt@virginia.edu

ABSTRACT

We analyze long-slit spectral observations of 39 Wolf-Rayet (WR) galaxies with heavy element mass fraction ranging over 2 orders of magnitude, from $Z_{\odot}/50$ to $2Z_{\odot}$. Nearly all galaxies in our sample show broad WR emission in the blue region of the spectrum (the blue bump) consisting of an unresolved blend of N III $\lambda 4640$, C III $\lambda 4650$, C IV $\lambda 4658$ and He II $\lambda 4686$ emission lines. Broad C IV $\lambda 5808$ emission (the red bump) is detected in 30 galaxies. Additionally, weaker WR emission lines are identified, most often the N III $\lambda 4512$ and Si III $\lambda 4565$ lines, which have very rarely or never been seen and discussed before in WR galaxies. These emission features are characteristic of WN7 – WN8 and WN9 – WN11 stars respectively.

We derive the numbers of early WC (WCE) and late WN (WNL) stars from the luminosities of the red and blue bumps, and the number of O stars from the luminosity of the $H\beta$ emission line. Additionally, we propose a new technique for deriving the numbers of WNL stars from the N III $\lambda 4512$ and Si III $\lambda 4565$ emission lines. This technique is potentially more precise than the blue bump method because it does not suffer from contamination of WCE and early WN (WNE) stars and nebular gaseous emission.

It is found that the relative number of WR stars $N(\text{WR})/N(\text{O} + \text{WR})$ decreases with decreasing metallicity, in agreement with predictions of evolutionary synthesis models. The relative number ratios $N(\text{WC})/N(\text{WN})$ and the equivalent widths of the blue bump $EW(\lambda 4650)$ and of the red bump $EW(\lambda 5808)$ derived from observations are also in satisfactory agreement with theoretical predictions, except for the most metal-deficient WR galaxies. A possible source of disagreement is too low a line emission luminosity adopted for a single WCE star in low-metallicity models.

¹Visiting astronomer, Kitt Peak National Observatory, National Optical Astronomical Observatories, operated by the Association of Universities for Research in Astronomy, Inc., under contract with the National Science Foundation.

We assemble a sample of 30 H II regions with detected He II $\lambda 4686$ nebular emission to analyze the possible connection of this emission with the hard UV radiation of the WR stars. The theoretical predictions satisfactorily reproduce the observed intensities and equivalent widths of the He II $\lambda 4686$ nebular emission line. However, galaxies with nebular He II $\lambda 4686$ emission do not always show WR emission. Therefore, in addition to the ionization of He⁺ in the H II region by WR stars, other mechanisms for the origin of He II $\lambda 4686$ such as radiative shocks probably need to be invoked.

Subject headings: galaxies: abundances — galaxies: starburst — galaxies: stellar content — H II regions — stars: Wolf-Rayet

1. INTRODUCTION

Galaxies with Wolf-Rayet (WR) star features in their spectra have long been known, beginning with the discovery of such features in the spectrum of the blue compact galaxy He 2-10 by Allen, Wright & Goss (1976). Osterbrock & Cohen (1982) and Conti (1991) introduced the concept of WR galaxies, defining them to be those galaxies which show broad stellar emission lines in their spectra. These WR galaxies are thought to be undergoing present or very recent star formation which produces massive stars evolving to the WR stage. WR galaxies are therefore ideal objects for studying the early phases of starbursts, determining burst properties and constraining parameters of the high mass end of the initial mass function.

More than 130 WR galaxies are now known (Conti 1999; Schaerer, Contini & Pindao 1999b). Morphologically, they constitute a very inhomogeneous class, including such diverse objects as galaxies with active galactic nuclei (AGN), ultraluminous far-infrared galaxies, spiral galaxies, starbursts and blue compact dwarf (BCD) galaxies. Individual WR stars cannot be usually observed as single stars in distant galaxies. They have been observed only in our Galaxy (Massey & Conti 1980; Torres & Conti 1984; Hamman, Koesterke & Wessolowski 1995; Koesterke & Hamann 1995; Esteban & Peimbert 1995; Crowther, Smith & Hillier 1995b; Crowther et al. 1995c; Crowther, Smith & Willis 1995d; Crowther & Bohannan 1997), in the Magellanic Clouds (Moffat et al. 1987; Conti & Massey 1989; Bohannan & Walborn 1989; Smith, Shara & Moffat 1990a; Russell & Dopita 1990; Crowther, Hillier & Smith 1995a; Crowther & Smith 1997; Crowther & Dessart 1998) and in some members of the Local Group: M31 and M33 (Conti & Massey 1981; D’Odorico & Rosa 1981; Massey & Conti 1983; Massey, Conti & Armandroff 1987; Schild, Smith & Willis 1990; Willis, Schild & Smith 1992; Smith, Crowther & Willis 1995; Crowther et al. 1997; Massey & Johnson 1998), IC 10 (Massey, Armandroff & Conti 1992), NGC 6822, IC 1613, NGC 300, and NGC 55 (Massey & Johnson 1998).

Much effort has been expended recently to construct a reliable quantitative scheme for classifying WR stars, based on observations of these stars in our Galaxy and in the nearest galaxies, mainly the LMC. As a result, a quantitative classification of WN, WC and WO stars has been elaborated (Smith, Shara & Moffat 1990ab, 1996; Smith & Maeder 1991; Kings-

burgh, Barlow & Storey 1995; Crowther, De Marco & Barlow 1998). Additionally, evolutionary synthesis models for young starbursts have been developed with the use of the latest stellar evolution models, theoretical stellar spectra and compilation of observed emission line strengths from WR stars (Krüger et al. 1992; Cerviño & Mas-Hesse 1994; Meynet 1995; Schaerer & Vacca 1998, hereafter SV98).

WR stars in more distant objects are detected indirectly by observing integrated galaxy spectra. Strong star formation activity in a galaxy results in a large number of massive stars, the most massive of which will evolve through the WR phase. Thus, at a definite stage of the starburst evolution, many WR stars make their appearance during a short time interval. Despite their small number relative to that of massive stars, especially in low-metallicity galaxies, WR stars are numerous enough for their integrated emission to be detected. In this paper, we shall follow Osterbrock & Cohen (1982) and Conti (1991) in defining a WR galaxy as one whose integrated spectrum of the whole or a part shows detectable WR broad features emitted by unresolved star clusters. While this definition is dependent on the quality of the spectrum and the location and size of the aperture, it has the advantage of distinguishing a distant WR galaxy from nearby galaxies, where WR stars can be studied individually.

The ratio of the number of WR stars to that of all massive stars is a very strong function of metallicity. Theoretical evolutionary models (Mas-Hesse & Kunth 1991; Maeder 1991; Krüger et al. 1992; Cerviño & Mas-Hesse 1994; Maeder & Meynet 1994; Meynet 1995; SV98) predict that for a fixed metallicity, this ratio varies strongly with time elapsed since the beginning of the starburst. Its maximum value decreases from 1 to 0.02 when the heavy element mass fraction Z decreases from Z_{\odot} to $Z_{\odot}/50$. The duration of the WR stage in the starburst also decreases with decreasing metallicity. Hence the number of galaxies with extremely low metallicities containing a WR stellar population is expected to be very small.

A systematic search for WR features in emission-line galaxies was first carried out by Kunth & Joubert (1985). They examined 45 extragalactic H II regions and found 17 WR galaxies, based on the detection in their spectra of a broad emission excess in the $\lambda 4600$ – 4700 wavelength region. Conti (1991) compiled from the literature a first catalog containing 37 WR galaxies. Vacca & Conti (1992) performed a search for WR stars in a sample of 14 emission-line galaxies and

developed a quantitative scheme for estimating WR populations. All these searches resulted in the detection of WR features in the blue region of the spectrum at $\lambda 4650$ (hereafter called the “blue bump”). It is interesting to note that, in the first WR galaxy observed, He 2-10, Allen et al. (1976) detected not only the blue bump, but also a broad N III feature at $\lambda 4511$ – 4535 . In subsequent studies of WR galaxies this feature was not generally seen or discussed. An exception is the most metal-deficient WR galaxy known, I Zw 18, where Izotov et al. (1997) also identified the N III $\lambda 4511$ – 4535 feature.

Evolutionary synthesis models predict a significant number of WC4 stars which radiate strong broad C III/C IV $\lambda 4650$ and C IV $\lambda 5808$ features (Schaerer & Vacca 1996; Schaerer et al. 1997). The observed ratio $N(\text{WC})/N(\text{WN})$ is ~ 1 in the solar neighborhood (Conti & Vacca 1990), and ~ 0.1 – 0.2 within a $10''$ radius of the 30 Doradus nebula (Moffat et al. 1987). In starbursting galaxies with $1/5 \leq Z/Z_{\odot} \leq 1$ $\sim 30\%$ of WR stars are of WC subtype (Schaerer & Vacca 1996; Schaerer et al. 1997). The first detections of the C IV $\lambda 5808$ emission line (hereafter called the “red bump”) in integrated galaxy spectra were reported by Kunth & Schild (1986) and Dinerstein & Shields (1986). However, the red bump was not seen in other early observations (Gonzalez-Riestra, Rego & Zamorano 1987; Vacca & Conti 1992). Later higher signal-to-noise ratio observations allowed to detect the red WC bump (CIV $\lambda 5808$) in an increasing number of galaxies (Izotov, Thuan & Lipovetsky 1994, 1997, hereafter ITL94 and ITL97; Izotov et al. 1996; Thuan, Izotov & Lipovetsky 1996; Izotov & Thuan 1998b, hereafter IT98; Schaerer et al. 1997; Schaerer et al. 1999a; Huang et al. 1999). WR stars of both WN and WC subtypes have even been detected in I Zw 18 with $Z \sim Z_{\odot}/50$ (Izotov et al. 1997; Legrand et al. 1997; De Mello et al. 1998). Hence, we have now at our disposal WR galaxies with metallicities ranging over two orders of magnitude, from $Z_{\odot}/50$ to $\sim 2Z_{\odot}$. This allows us to study the properties of massive stellar populations in metal-poor environments which are not available in the Local Group.

In 1993, a program was begun to obtain high signal-to-noise spectra for a large sample of a low-metallicity blue compact dwarf galaxies in order to measure the primordial helium abundance (ITL94, ITL97, IT98, Thuan, Izotov & Lipovetsky 1995). A large fraction of these spectra ($\sim 50\%$) showed broad emission characteristic of WN and WC stars.

While some of these objects are known to contain WR stars from previous studies, the majority are newly discovered WR galaxies. We have assembled here, from our large data base, a sample of 39 WR galaxies with the aim of studying their spectroscopic properties. In particular, we wish to determine the $N(\text{WR})/N(\text{O+WR})$ and $N(\text{WC})/N(\text{WN})$ ratios for all these galaxies, and use the data to constrain models of massive star evolution. Section 2 describes the observations and data reduction. In section 3 we discuss heavy element abundances for a subsample of WR galaxies, with previously unpublished observations. In Section 4 we describe the WR features detected in our spectra, some of which have not been discussed before in the literature. In section 5 we present a new method for deriving the numbers of WR and O stars. In section 6 we compare our results with other observational data as well as with theoretical models, and discuss the effects of metallicity and starburst age on the WR stellar population. In section 7 we discuss the origin of the nebular He II $\lambda 4686$ line emission. Section 8 contains a summary of our main results and conclusions.

2. OBSERVATIONS AND DATA REDUCTION

Spectrophotometric observations of 38 galaxies with detected or suspected broad WR emission features were obtained with the Ritchey-Chrétien spectrograph at the Kitt Peak National Observatory (KPNO) 4m telescope, and with the GoldCam spectrograph at the 2.1m KPNO telescope. The 4m observations were carried out during the period 1993–1994 while the 2.1m observations were obtained in 1996. The majority of the galaxies in our sample were selected from the First Byurakan Survey (Markarian et al. 1989), and from a complete sample of ~ 250 BCDs (Izotov et al. 1993) discovered in the Second Byurakan Objective Prism Survey (SBS, Markarian, Lipovetsky & Stepanian 1983). Four low-metallicity galaxies are from the Michigan Survey (Salzer, MacAlpine & Boroson 1989). We have also included the BCD II Zw 40, known to possess WR features (Conti 1991). In addition to these 38 galaxies observed at KPNO, we have included the BCD I Zw 18 because of its extremely low metallicity. The spectrum of I Zw 18 was obtained in 1997 with the Multiple Mirror Telescope (Izotov et al. 1997). Hence the total sample contains 39 galaxies. Because of the high signal-to-noise ratio required to determine an accurate helium abundance,

our spectra allow to detect WR features not only in the blue region, but also in the rarely observed C IV $\lambda 5808$ region. Several other lower intensity WR emission lines are also seen.

Table 1 lists the studied galaxies with their IAU names, coordinates α , δ at the 1950.0 epoch, apparent magnitudes m_{pg} from Markarian et al. (1989) and Zwicky et al. (1961–1968), absolute magnitudes M_{pg} (a Hubble constant $H_0 = 75 \text{ km s}^{-1} \text{ Mpc}^{-1}$ is adopted), observed redshifts z , oxygen abundances $12 + \log(\text{O}/\text{H})$ and other designations.

The journal of observations is given in Table 2. All observations were performed in the same way. The slit was centered on the brightest part of each galaxy. Total exposure times varied between 10 and 180 minutes. Each exposure was broken up into 2 – 6 subexposures to allow for more effective cosmic ray removal, except for SBS 0948+532 for which only one exposure was obtained. For the majority of galaxies, a $2''$ wide slit was used set at the position angle given in Table 2. The exception is I Zw 18 which was observed with a $1''.5$ wide slit. The spectral resolution was 6–7 Å in all cases. Except for three objects observed at airmass ~ 1.6 and position angle 90 degrees, the vast majority of galaxies were observed at small airmasses, so that no correction for atmospheric dispersion was performed. Several spectrophotometric standard stars were observed each night for flux calibration. Spectra of He-Ne-Ar comparison lamps were obtained before and after observation of each galaxy to provide wavelength calibration. Data reduction was performed with the IRAF² software package and included bias subtraction, cosmic ray removal, flat-field correction, flux and wavelength calibrations, correction for atmospheric extinction and subtraction of the night sky background. The residuals of the night sky lines after subtraction are $\leq 1\%$.

3. HEAVY ELEMENT ABUNDANCES

Line intensities and heavy element abundances for the majority of the WR galaxies have been given previously in a series of papers on the primordial helium abundance (ITL94, ITL97, IT98) and on heavy element abundances (Thuan et al. 1995, Izotov & Thuan

1999). To derive heavy element abundances for the twelve remaining galaxies we follow the procedure described in ITL94 and ITL97.

The extracted one-dimensional spectra of the brightest regions in these twelve galaxies are shown in Figure 1. All emission line fluxes were corrected for interstellar extinction with the use of the extinction coefficient $C(\text{H}\beta)$ derived from the Balmer decrement. For this purpose we adopted the extinction curve of Whitford (1958) as fitted by ITL94. The theoretical ratios of hydrogen Balmer emission lines are taken from Brocklehurst (1971) at the electron temperature derived from the observed ratio $[\text{O III}](\lambda 4959 + \lambda 5007) / \lambda 4363$ when the auroral emission line $\lambda 4363$ is detected. This is the case for 30 out of the 39 WR galaxies in our sample. The electron temperature for the nine galaxies with non-detected $[\text{O III}]\lambda 4363$ was derived from the empirical calibration of total oxygen emission line flux $[\text{O II}]\lambda 3727 + [\text{O III}](\lambda 4959 + \lambda 5007)$ vs. electron temperature (Pagel et al. 1979). The observed $F(\lambda)$ and corrected $I(\lambda)$ emission line fluxes relative to the $\text{H}\beta$ emission line fluxes for the 12 galaxies listed in Table 2 are shown in Table 3. Also given in Table 3 are the extinction coefficient $C(\text{H}\beta)$, the observed absolute flux of the $\text{H}\beta$ emission line and its equivalent width $EW(\text{H}\beta)$ and the equivalent width of the hydrogen absorption lines $EW(\text{abs})$. The latter is set to be the same for all hydrogen lines. We note that the intensity of the He I $\lambda 5876$ emission line in II Zw 40 is reduced, because of absorption by Galactic neutral sodium, just as in the case of I Zw 18 (Izotov & Thuan 1998a). The He I $\lambda 5876$ emission line in Mrk 178 is contaminated by the strong nearby WR C IV $\lambda 5808$ emission line (Figure 1), while this line in the spectrum of Mrk 1329 is on a bad CCD column, making its intensity unreliable.

The ionic and total heavy element abundances of the four galaxies in Table 2 with detected $[\text{O III}]\lambda 4363$ emission line are shown in Table 4. The oxygen abundance $12 + \log(\text{O}/\text{H})$ derived in these galaxies ranges from 7.82 to 8.23 and is in fair agreement with previous determinations. For Mrk 178, Gonzalez-Riestra et al. (1987) derived oxygen $12 + \log(\text{O}/\text{H}) = 7.72$ as compared to our value of 7.82. For II Zw 40, Walsh & Roy (1993), Masegosa, Moles & Campos-Aguilar (1994) and Martin (1997) derived respectively an oxygen abundance of 8.25, 8.18 and 8.12 compared to our value of 8.09. As for Mrk 1236, Vacca & Conti (1992) derived $12 + \log(\text{O}/\text{H}) = 8.09$ as compared to our value of 8.07. The element abundance ratios

²IRAF: the Image Reduction and Analysis Facility is distributed by the National Optical Astronomy Observatories, which is operated by the Association of Universities for Research in Astronomy, Inc. (AURA) under cooperative agreement with the National Science Foundation (NSF).

in these four galaxies (Table 4) are in good agreement with typical ratios in low-metallicity blue compact dwarf galaxies (Izotov & Thuan 1999).

We adopt the calibration between oxygen abundance and $[\text{N II}](\lambda 6548 + \lambda 6584)$ to $\text{H}\alpha$ $\lambda 6563$ flux ratio from van Zee et al. (1998) to derive oxygen abundance in the nine galaxies with nondetected $[\text{O III}] \lambda 4363$

$$12 + \log(\text{O}/\text{H}) = 1.02 \log([\text{NII}]/\text{H}\alpha) + 9.36. \quad (1)$$

This calibration is insensitive to uncertainties in interstellar extinction and agrees with that of Edmunds & Pagel (1984), to within 0.1 dex in the derived oxygen abundance. The oxygen abundances for the galaxies with nondetected $[\text{O III}] \lambda 4363$ are shown in Table 1. It can be seen that they are considerably larger than those of galaxies with detected $[\text{O III}] \lambda 4363$, exceeding in some cases the solar oxygen abundance. The oxygen abundance of 9.03 derived us for Mrk 710 is in good agreement with the values of 9.09 obtained by Vacca & Conti (1992) and that of 9.00 obtained by Schaerer et al. (1999a).

Examination of Table 1 shows that the WR galaxies in our sample span an oxygen abundance range extending over two orders of magnitude ($Z_{\odot}/50$ to $2Z_{\odot}$). This unique sample allows us to study the properties of WR stellar populations in a wide range of heavy element abundances.

4. WR EMISSION FEATURES

We now discuss the properties of WR galaxy spectra. In low-resolution spectra of WR galaxies the blue bump at $\lambda 4650$ is most often seen. This unresolved bump is a blend of the $\text{N V } \lambda 4605, 4620$, $\text{N III } \lambda 4634, 4640$, $\text{C III/C IV } \lambda 4650, 4658$ and $\text{He II } \lambda 4686$ broad WR lines. These are emitted mainly by late WN (WNL) and early WC (WCE) stars, although some contribution of early WN (WNE) stars might be present (SV98). Superposed on the blue bump are much narrower $[\text{Fe III}] \lambda 4658$, $\text{He II } \lambda 4686$, $\text{He I} + [\text{Ar IV}] \lambda 4711$ and $[\text{Ar IV}] \lambda 4740$ nebular emission lines. The detectability of the weaker red bump, emitted mainly by WCE stars, is lower. Hence, the observed characteristics of WR galaxies are restricted to a narrow range of WR star subtypes, most often WNL and WCE stars.

Can other WR subtypes be seen in integrated spectra of WR galaxies? Each WR star, depending on the metallicity and mass of the progenitor, may evolve

through different WR subtypes from WNL to WCE. WNE stars emit $\text{N V } \lambda 4605, 4620$, $\text{C IV } \lambda 4658$, $\text{He II } \lambda 4686$ and $\text{C IV } \lambda 5808$ (e.g. Smith et al. 1996) and hence cannot be distinguished from other WR stars in low-resolution spectra. Additionally, WNE stars are not as luminous as WNL stars in the optical range. The WR star lifetime in the WNE stage is short compared to that in the WNL stage for nearly all metallicities and progenitor star masses (Maeder & Meynet 1994). Therefore, in the majority of cases the contribution of WNE stars to the blue bump is expected to be small. However, evolution models of Maeder & Meynet (1994) predict that at high metallicities and low WR progenitor star masses, the WNE lifetime is greater than the WNL one. Hence, at late stages of instantaneous bursts in metal-rich WR galaxies the contribution of WNE stars can be significant.

The $\text{C III } \lambda 4650, \lambda 5696$ emission lines are seen mainly in late-type WC stars (WC7 – WC9). No normal WC star of type later than WC9 has been detected. However, some central stars of planetary nebulae have characteristics of WR stars and are classified as $[\text{WC10}] - [\text{WC12}]$ (e.g. Leuenhagen & Hamann 1994, 1998; Leuenhagen, Hamann & Jeffery 1996). In the spectra of these stars, $\text{C II } \lambda 4267$ emission and some other C II lines are observed. It is thought that late WC stars are to be seen only in regions with metallicity greater than solar (Smith 1991; Smith & Maeder 1991; Phillips & Conti 1992). Since the majority of starburst WR galaxies have lower metallicities than solar, they are not expected to contain WCL stars.

As for the late WN (WN9 – WN11) stars, they produce N II , N III and Si III lines (e.g. Smith et al. 1995; Crowther et al. 1997; Crowther & Smith 1997) and are bright, therefore they should be detected in the spectra of WR galaxies. However, high signal-to-noise ratio spectra are required because these WNL features are weak. Probably, the first detection of very late WN and WC stars was done by Kunth & Schild (1986) in the galaxy Tol 9. They saw $\text{N II } \lambda 5679, \lambda 5747-67$ and $\text{C III } \lambda 5696$ and attributed those lines to WN10 and WC7 stars respectively. The presence of WC7 stars in Tol 9 is surprising because its metallicity was lower than solar ($Z_{\odot}/15$). Later, Phillips & Conti (1992) and Schaerer et al. (1999a) detected the $\text{C III } \lambda 5696$ emission line in the high-metallicity galaxies NGC 1365 ($\sim 3Z_{\odot}$) and Mrk 710 ($1.2Z_{\odot}$) respectively.

In Figure 2 we show spectra of our sample of 39

WR galaxies. All spectra have been corrected to rest wavelengths and are restricted to the wavelength range $\lambda\lambda 4150 - 6100\text{\AA}$ which contains the WR features of interest. The spectra are of varying quality depending on the brightness of the galaxy, exposure time and the size of the telescope used (2.1, 4m or MMT). Identifications for certain or suspected WR emission lines are given for each spectrum. Many of the emission lines represent blends of several lines. For simplicity, we mark the most often detected N III $\lambda 4511-4534$ blend as N III $\lambda 4512$, the Si III $\lambda 4552-4576$ blend as Si III $\lambda 4565$, N V $\lambda 4605, 4620$ as N V $\lambda 4619$ and N III $\lambda 4634, 4640$ as N III $\lambda 4640$. From those identifications, it is clear that several new lines have been detected in the spectra of some of our WR galaxies which have rarely or never been seen before in the spectra of WR galaxies. Those new line identifications constitute one of the most important results of our work. We discuss in more detail the emission WR features observed in each galaxy in the following.

0112-011 \equiv *UM 311*. — Masegosa, Moles & del Olmo (1991) first noticed the presence of a WR population in this galaxy. IT98 detected both blue and red bumps. The unresolved blue bump is particularly strong in this galaxy. Additionally, N III $\lambda 4512$, Si III $\lambda 4565$ and He I/N II $\lambda 5047$ are present, which are characteristic of WN7 – WN8 and WN9 – WN10 stars respectively (e.g. Massey & Conti 1980, 1983; Crowther & Smith 1997). In the red part of the spectrum, the C IV $\lambda 5808$ emission line is clearly detected which indicates the presence of WCE stars.

0207-105 \equiv *Mrk 1026*. — Only two possible WR features N II $\lambda 4620, \lambda 5720-40$ and one certain C IV $\lambda 5808$ line are detected in this galaxy. Most likely, these features are due to WNL and WCE stars. However, the spectrum is too noisy to allow definite conclusions.

0211+038 \equiv *Mrk 589*. — In the blue region, several features are present which we identify as N III $\lambda 4512$, Si III $\lambda 4565$, N V $\lambda 4619$, N III $\lambda 4640$, He II $\lambda 4686$ and Si II $\lambda 5056$ emission lines. The C IV $\lambda 5808$ line is present in the red part of spectrum. These lines suggest the presence of WCE, WNE and WNL stars.

0218+003 \equiv *UM 420*. — Noisy spectrum. However, broad C IV $\lambda 4658$, He II $\lambda 4686$ and C IV $\lambda 5808$ indicate the possible presence of WCE stars.

0252-102 \equiv *Mrk 1063*. — Broad bump consisting of N V $\lambda 4619$, N III $\lambda 4640$, He II $\lambda 4686$. Additionally, N III $\lambda 4512$, Si III $\lambda 4565$ and Si II $\lambda 5046$ are observed

in the blue region. The C IV $\lambda 5808$ line is observed in the red region.

0459-043 \equiv *NGC 1741* \equiv *Mrk 1089*. — Kunth & Schild (1986) detected N III $\lambda 4640$ and He II $\lambda 4686$ lines. These features are also present in our spectrum. Additionally, we note the presence of N III $\lambda 4512$ and Si III $\lambda 4565$ emission lines. In the red part of the spectrum N II $\lambda 5720-40$ emission is detected. The WR population is dominated by WNL stars.

0553+033 \equiv *II Zw 40*. — Kunth & Sargent (1981) detected a broadened He II $\lambda 4686$ emission line. No broad WR emission was seen by Walsh & Roy (1993). Our observations reveal the presence of Si III $\lambda 4565$, N III $\lambda 4640$ /C IV $\lambda 4658$, He I/N II $\lambda 5047$, N II $\lambda 5720-40$ and C IV $\lambda 5808$ emission lines. The WR lines in the blue bump are contaminated by the strong nebular lines [Fe III] $\lambda 4658$, He II $\lambda 4686$, He I + [Ar IV] $\lambda 4711$ and [Ar IV] $\lambda 4740$.

0635+756 \equiv *Mrk 5*. — Noisy spectrum. The N III $\lambda 4640$ and He II $\lambda 4686$ emission lines are detected, implying the presence of WNL stars.

0720+335 \equiv *Mrk 1199*. — The N III $\lambda 4512$, Si III $\lambda 4565$, N V $\lambda 4619$, C IV $\lambda 4658$, He II $\lambda 4686$, Si II $\lambda 5056$, N II $\lambda 5720-40$ and C IV $\lambda 5808$ emission lines are detected. This implies that WNL, WNE and WCE populations are present.

0723+692 \equiv *NGC 2363* \equiv *Mrk 71*. — Roy et al. (1992) have discussed the origin of the broad emission in nebular lines. The broad blue bump was present in their spectrum but not noticed. Gonzalez-Delgado et al. (1994) have detected both blue and red bumps. ITL97 confirmed the finding by Gonzalez-Delgado et al. (1994). The Si III $\lambda 4565$, N III $\lambda 4640$, C IV $\lambda 4658$, He II $\lambda 4686$, He I/N II $\lambda 5047$ and C IV $\lambda 5808$ emission lines are present in our high signal-to-noise ratio spectrum, indicating the presence of WNL and WCE stars. The blue bump is strongly contaminated by nebular emission.

0842+162 \equiv *Mrk 702*. — Broad WR bumps are detected in the blue and red regions. The N III $\lambda 4512$, Si III $\lambda 4565$, N V $\lambda 4619$, N III $\lambda 4640$, He II $\lambda 4686$ and C IV $\lambda 5808$ emission lines are seen. The WNL and WNE stars dominate in this galaxy.

0926+606 \equiv *SBS 0926+606*. — ITL97 first noticed the presence of WR stars in this galaxy. Reasonably strong Si III $\lambda 4565$ and He I/N II $\lambda 5047$ emission lines are detected indicating the presence of WN9 – WN10 stars. There is possibly a N II $\lambda 5720-40$ emission feature. The N III $\lambda 4640$ emission line is relatively

weak, while the N III $\lambda 4512$ line is not seen. The blue bump is strongly contaminated by nebular emission.

0930+554 \equiv *I Zw 18* \equiv *Mrk 116*. — Izotov et al. (1997) and Legrand et al. (1997) detected both the blue and red bumps in this BCD, the most metal-deficient WR galaxy known. Izotov et al. (1997) also saw N III $\lambda 4512$ and Si III $\lambda 4565$ emission lines. However, they misidentified the latter line as Mg I $\lambda 4571$. Possibly, N II $\lambda 5720$ –40 and $\lambda 5928$ –52 lines are detected, indicating the presence of WNL stars. In contrast, Legrand et al. (1997) who observed with a different position angle of the slit found evidence only for WCE stars.

0946+558 \equiv *Mrk 22*. — The WR stellar population in this galaxy was detected by ITL94. The main features are N III $\lambda 4512$, N III $\lambda 4640$, broadened He II $\lambda 4686$ and C IV $\lambda 5808$. The WR population is dominated by WNL and WCE stars.

0947+008 \equiv *Mrk 1236*. — A broad He II $\lambda 4686$ emission line in this galaxy was seen by Kunth & Schild (1986) and confirmed by Vacca & Conti (1992). However, those authors did not show the spectrum of the galaxy. The most striking features in our spectrum are the C II $\lambda 4267$ and C III $\lambda 5696$ emission lines which we attribute to late WC stars. We also identify the feature seen at 4620\AA as a possible C II $\lambda 4620$ emission line. The presence of these features in a low-metallicity BCD such as Mrk 1236 (its oxygen abundance is $12 + \log(\text{O}/\text{H}) = 8.06$ or $\sim Z_{\odot}/7$) is unexpected. New observations are required to confirm our finding. Other lines are the C IV $\lambda 4658$ / He II $\lambda 4686$ blend and the C IV $\lambda 5808$ emission line, indicating the presence of WCE stars. No strong nitrogen lines are present, although the spectrum is noisy.

0948+532 \equiv *SBS 0948+532*. — Broad WR emission was detected by ITL94. The Si III $\lambda 4565$, N III $\lambda 4640$ and He II $\lambda 4686$ lines are seen, indicating the presence of WNL stars. Probably, N II $\lambda 5720$ –40 and C IV $\lambda 5808$ are also present, however the spectrum is noisy. The blue bump is strongly contaminated by nebular emission.

0952+095 \equiv *NGC 3049* \equiv *Mrk 710*. — Kunth & Schild (1986) detected broad N III $\lambda 4640$, He II $\lambda 4686$ and C IV $\lambda 5808$ emission lines. A broad WR bump in the blue region was also seen by Vacca & Conti (1992). Schaerer et al. (1999a) discussed the presence of N III $\lambda 4640$, He II $\lambda 4686$, C III $\lambda 5696$ and C IV $\lambda 5808$ broad features indicating the presence of early and late WC and late WN stars. We confirm their

findings. Additionally, we find N III $\lambda 4512$, Si III $\lambda 4565$ and N V $\lambda 4619$ features implying the presence of WNE and WNL stars.

1030+583 \equiv *Mrk 1434*. — A broad He II $\lambda 4686$ emission line was detected by ITL97. The Si III $\lambda 4565$ and C IV $\lambda 5808$ emission lines are seen in this low-metallicity galaxy ($12 + \log(\text{O}/\text{H}) = 7.79$ or $Z \sim Z_{\odot}/14$).

1036-069 \equiv *Mrk 1259*. — Ohya, Taniguchi & Terlevich (1997) identified broad N V $\lambda 4619$, N III $\lambda 4640$ and He II $\lambda 4686$ emission lines. We confirm the presence of these lines in our higher signal-to-noise ratio spectrum. Additionally, we identify N III $\lambda 4512$, N III $\lambda 4905$ and Si II $\lambda 5056$ features. We find also the C IV $\lambda 5808$ emission line in the red part of the spectrum.

1053+064 \equiv *Mrk 1271*. — IT98 detected a broad blue bump. Here we identify the N III $\lambda 4512$, Si III $\lambda 4565$, N II $\lambda 4620$ and He II $\lambda 4686$ emission lines. Possibly, C IV $\lambda 5808$ is also present, although higher signal-to-noise ratio observations are required to be certain. The blue bump is strongly contaminated by nebular emission.

1054+365 \equiv *CG 798*. — ITL97 noticed a broad He II $\lambda 4686$ emission line. Here we identify additionally Si III $\lambda 4565$ and possibly C III $\lambda 5696$ emission lines.

1130+495 \equiv *Mrk 178*. — Gonzalez-Riestra, Rego & Zamorano (1988) detected a broad He II $\lambda 4686$ emission line. In our high signal-to-noise ratio spectrum the WR features are very pronounced. We identify them with the N III $\lambda 4640$, C IV $\lambda 4658$ and He II $\lambda 4686$ lines in the blue region, and with the C IV $\lambda 5808$ emission line in the red region.

1134+202 \equiv *Mrk 182*. — Noisy spectrum. However, a broad WR emission is present in the blue part of the spectrum.

1135+581 \equiv *Mrk 1450*. — ITL94 noted broad WR features in the blue and red regions. We identify the N III $\lambda 4512$, Si III $\lambda 4565$, N III $\lambda 4640$, He II $\lambda 4686$, N III $\lambda 4905$, He I/N II $\lambda 5047$ and C IV $\lambda 5808$ lines. The blue bump is strongly contaminated by nebular emission.

1139+006 \equiv *Mrk 1304* \equiv *UM 448*. — Broad He II $\lambda 4686$ was detected by Masegosa et al. (1991). Our observations show that the intensities of WR features are atypical. Although broadened, the He II $\lambda 4686$ line is weak, while the N III $\lambda 4512$, Si III $\lambda 4565$, N II $\lambda 4620$, He I/N II $\lambda 5047$, N II $\lambda 5720$ –40, C IV $\lambda 5808$ lines are strong.

1140–080 \equiv *Mrk 1305*. — Noisy spectrum. N V $\lambda 4619$, C IV $\lambda 4658$, He II $\lambda 4686$ and C IV $\lambda 5808$ features are present. Higher signal-to-noise ratio observations are necessary to confirm the detection of the WR features.

1147+153 \equiv *Mrk 750*. — Kunth & Joubert (1985) found broad He II $\lambda 4686$ while Conti (1991) noted the existence of N III $\lambda 4640$. IT98 confirmed the presence of WR features. The signal-to-noise ratio of the spectrum is relatively low. C II $\lambda 4267$, Si III $\lambda 4565$, C II $\lambda 4620$ are possibly present. The C IV $\lambda 4658$ emission line is blended with the He II $\lambda 4686$ line. Additionally, the C IV $\lambda 5808$ line is detected.

1150–021 \equiv *Mrk 1307* \equiv *UM 462*. — The presence of WR stars in this galaxy is suspected. The He II $\lambda 4686$ emission line is broadened. The Si III $\lambda 4565$ and He I/N II $\lambda 5047$ lines are detected.

1152+579 \equiv *Mrk 193*. — Only Si III $\lambda 4565$ and N II $\lambda 5720–40$ are fairly well detected. The presence of the N II $\lambda 4620$, N III $\lambda 4640$ and He I/N II $\lambda 5047$ lines is suspected. The blue bump is strongly contaminated by nebular emission.

1211+540 \equiv *SBS 1211+540*. — Only the broadened He II $\lambda 4686$ line is detected fairly well. The signal-to-noise ratio of the spectrum is too low to definitely detect other WR features in this very low-metallicity galaxy ($12 + \log(O/H) = 7.64$ or $Z \sim Z_{\odot}/19$).

1222+614 \equiv *SBS 1222+614*. — ITL97 noted the presence of both blue and red bumps. We identify N III $\lambda 4512$, Si III $\lambda 4565$, He II $\lambda 4686$, N II $\lambda 5720–40$, C IV $\lambda 5808$ emission lines. The N III $\lambda 4640$ and C IV $\lambda 4658$ lines are blended.

1223+487 \equiv *Mrk 209*. — ITL97 noted the presence of a blue bump in this galaxy. We identify a broadened He II $\lambda 4686$ emission line, and weak N III $\lambda 4512$, He I/N II $\lambda 5047$ and C IV $\lambda 5808$ emission lines. The Si III $\lambda 4565$ line is strong and the N II $\lambda 5720–40$ emission line is suspected. The blue bump is strongly contaminated by nebular emission.

1234+072 \equiv *Mrk 1329*. — Noisy spectrum. Strong broad He II $\lambda 4686$ is present. We also identify N III $\lambda 4512$, He II $\lambda 4541$, Si III $\lambda 4565$, N III $\lambda 4640$, He I/N II $\lambda 5047$, He II $\lambda 5411$ and weak C IV $\lambda 5808$ emission lines.

1249+493 \equiv *SBS 1249+493*. — Noisy spectrum. Two broad features (C IV $\lambda 4658$ and He II $\lambda 4686$) are probably present in this low-metallicity galaxy ($12 + \log(O/H) = 7.72$ or $Z \sim Z_{\odot}/15$). Further

observations are required to confirm the presence of WR stars.

1256+351 \equiv *NGC 4861* \equiv *Mrk 59*. — Both blue and red bumps have been detected by Dinerstein & Shields (1986) and ITL97. We identify in our high quality spectrum N III $\lambda 4512$, Si III $\lambda 4565$, N V $\lambda 4619$, He II $\lambda 4686$, He I/N II $\lambda 5047$ and C IV $\lambda 5808$ broad emission lines. The N III $\lambda 4640$ and C IV $\lambda 4658$ lines are blended. The blue bump is strongly contaminated by nebular emission.

1319+579A \equiv *SBS 1319+579A*. — Noisy spectrum. WR features were noted by ITL97. We detect the Si III $\lambda 4565$, C IV $\lambda 4658$, He II $\lambda 4686$, He I/N II $\lambda 5047$, N II $\lambda 5720–40$ and C IV $\lambda 5808$ emission lines which suggest the presence of WNL and WCE stars. The blue bump is strongly contaminated by nebular emission.

1437+370 \equiv *Mrk 475*. — Conti (1991) noted the presence of a broad He II $\lambda 4686$ emission line and possibly of the N III $\lambda 4640$ emission line. ITL94 detected strong blue and red bumps. We identify Si III $\lambda 4565$, He II $\lambda 4686$, He I/N II $\lambda 5047$ and C IV $\lambda 5808$ emission-line features. Possibly, the N III $\lambda 4640$ line is present as well. The blue bump is strongly contaminated by nebular emission.

1533+574B \equiv *SBS 1533+574B*. — Noisy spectrum. We detect the Si III $\lambda 4565$, N III $\lambda 4640$, He II $\lambda 4686$, He I/N II $\lambda 5047$, N II $\lambda 5720–40$ and C IV $\lambda 5808$ emission lines. The blue bump is strongly contaminated by nebular emission.

2329+286 \equiv *Mrk 930*. — Noisy spectrum. We identify the N III $\lambda 4512$, Si III $\lambda 4565$, He II $\lambda 4686$, He I/N II $\lambda 5047$, N II $\lambda 5720–40$ and C IV $\lambda 5808$ emission lines.

5. DERIVATION OF THE NUMBER OF WR AND O STARS

The following quantitative analysis of massive stellar populations in WR galaxies is based on only 33 objects. We have excluded from the original sample of 39 WR galaxies (Table 1) the 6 galaxies 0207–105, 1134+202, 1140–080, 1152+579, 1249+493, 1533+574B because their spectra were noisy and their WR features were either weak or uncertain.

5.1. Flux measurements of H β and WR emission lines

In this section we describe our procedure for determining the number of O and WR stars from the spectroscopic data. In general, the number of WR stars is derived from the luminosity of a WR line, while the number of O stars is deduced from the H β luminosity after subtracting the contribution of WR stars from it. Because the H β emission is extended and the slit usually does not cover the whole region of ionized gas emission, care should be exercised to correct for lost light. Therefore, one-dimensional spectra with one pixel step along the spatial axis of the slit have been extracted from the two-dimensional spectrum. The H β fluxes were then measured for each one-dimensional spectrum where this line was detected. As for the equivalent width of H β , it was measured in the one-dimensional spectrum extracted in the largest possible aperture with diameter equal to the whole spatial extent of the slit. The WR fluxes are derived from one-dimensional spectra with aperture covering the regions where WR emission is present. The measured H β flux cannot be used directly for the determination of the number of ionizing O stars because of the aperture effect discussed by Conti (1991) and Vacca & Conti (1992): while the region with the brightest H β emission where the stellar cluster is located is usually covered by the slit, a significant fraction of the H β emission from the extended H II region may be outside of it. H β emission can spread far away from the center of the O and WR star cluster.

To take into account this effect the following procedure has been adopted. We assume that the brightness distribution of each object has a circular symmetry, with the center of the cell with the maximum H β flux (all H β fluxes are extinction-corrected) chosen to be the center of symmetry. However, if the flux in adjacent cells exceeds 0.7 the flux in the brightest cell, the center was shifted by half a cell in the direction of that cell. Since the distribution of fluxes on opposite sides from the center would generally not be equal, we consider each object as a set of homogeneous half-rings. This yields a correction factor C_{cor}^i for each cell i along the slit of the form:

$$C_{cor}^i = \begin{cases} \frac{\pi(r_{max}^2 - r_{min}^2)}{2ab}, & \text{if } \frac{r_{min} + r_{max}}{2} \geq \frac{b}{2}, \\ 1, & \text{otherwise.} \end{cases} \quad (2)$$

Here a and b are the cell sizes along and across the slit expressed in arcsec, r_{max} and r_{min} are the dis-

tances from the center of symmetry to the near and far edges of the cell. C_{cor}^i is thus just the ratio of the area of a half-ring to that of a cell. This procedure is used for all cells along the slit. The H β fluxes in each half-ring are then summed together to give the extinction and aperture-corrected H β flux and the mean correction factor C_{cor} is derived as the ratio of the extinction and aperture-corrected H β flux to the H β flux corrected only for extinction. The corrected H β fluxes are shown in Table 5 together with the correction factors C_{cor} . Here $F_{cor}(H\beta)$, is the absolute flux, corrected for interstellar extinction and aperture, while $F(H\beta)$ is the absolute flux measured along the slit and corrected only for interstellar extinction. We also show in Table 5 other relevant parameters for the H II regions: the coefficient for interstellar extinction $C(H\beta)$ derived from the observed Balmer decrement in the spectrum of the brightest region, the equivalent width of the H β emission line, the age of the star formation burst derived from $EW(H\beta)$ and the parameter η_0 to be discussed below. $EW(H\beta)$ is also subject to aperture effects and its aperture correction factor may be as large as C_{cor} for the H β flux. Therefore, H β equivalent widths of star-forming regions not corrected for aperture effects are lower limits and ages of star formation bursts derived from noncorrected $EW(H\beta)$ should be considered as an upper limits. We cannot however derive correction factors for $EW(H\beta)$ from the spectra alone, as the underlying galaxy can also contribute to the continuum and decrease $EW(H\beta)$ as compared to the case where the continuum is produced by the star-forming region only.

The above aperture correction procedure has not been applied to the WN and WC bump fluxes because that emission comes from very compact regions with angular sizes usually not greater than the slitwidth. Those fluxes have been measured instead in the integrated spectrum obtained by summing in the spatial direction all one-pixel-sized one-dimensional spectra where WR emission features are detected. In only five galaxies 0635+756, 0952+095, 1030+583, 1053+064 and 1211+540, is the angular size of WR regions along the slit slightly larger than the slit width. For those galaxies, the measured fluxes of WR features should be considered as lower limits. The correction factors are however very close to unity.

A careful subtraction of the continuum is essential for deriving accurate WR bump fluxes and hence numbers of WR stars. To define the continuum, we

carefully select several points in spectral regions free of nebular and stellar lines. The continuum is then fitted by cubic splines. The quality of the continuum fit is visually checked and if deemed satisfactory is subtracted from the spectrum.

On top of the blue bump are superposed [Fe III] $\lambda 4658$, He II $\lambda 4686$, [Ar IV] + He I $\lambda 4712$ and [Ar IV] $\lambda 4740$ narrow nebular emission lines. These nebular lines have been subtracted from the bump using the IRAF SPLOT software package. We then measure the fluxes of the broad components within a specified wavelength range which is varying because of the changing appearance of broad components in galaxies with different burst ages. Similar measurements have been done for other weaker WR lines. The results of the measurements are shown in Table 6. Here $F(\lambda)$ and $EW(\lambda)$ are the total fluxes corrected for interstellar extinction and equivalent widths of different WR lines.

5.2. The number of WR stars

We estimate the number of WR stars from the luminosity of the blue ($\lambda 4650$) and red ($\lambda 5808$) bumps. In principle, if the luminosity of one WR star in a specific broad line or in the whole bump is known, we can derive the number of WR stars:

$$N_{\text{WR}} = \frac{L_{\text{WR}}}{L_{\text{WR}}^0} \quad (3)$$

where L_{WR} is the absolute luminosity of the WR bump (or of one WR line) corrected for interstellar extinction, and L_{WR}^0 is the luminosity of the WR bump (or of one WR line) of a single WR star. Usually, WC4 stars are considered as representatives of WCE stars, while WN7 stars are considered as representatives of WNL stars. In the following, to derive the numbers of WR stars we shall use parameters relevant to WC4 and WN7 stars. However, one should keep in mind that WNE stars can contribute to the blue bump at late WR stages in high-metallicity galaxies.

The luminosity of the red bump includes only the C IV $\lambda 5808$ line and gives directly the number of WCE stars. The situation with the blue bump is more complicated. To determine the number of WNL stars, the contribution of WCE stars to the blue bump should be removed. To do this we use the luminosity of the red bump and introduce the coefficient

$$k = \frac{L_{\text{WC4}}(\lambda 4658)}{L_{\text{WC4}}(\lambda 5808)}. \quad (4)$$

Then the luminosity of WC4 stars which should be subtracted from the total luminosity of the blue bump is equal to $kL_{\text{WC4}}(\lambda 5808)$. The value of the coefficient k not well known. Smith (1991) gives $k = 1.52$, while SV98 obtain $k = 1.71 \pm 0.53$, consistent with the Smith value within the errors. The value of k is uncertain because the relative fluxes of individual lines vary strongly even within the same WR subtype (see Tables 1 and 2 in SV98).

Luminosities of single WR stars are also known poorly. Smith (1991) adopts a luminosity of 3.2×10^{36} ergs s^{-1} for a single WNL star in the blue bump and for a single WC4 star in the red bump from observations of WR stars in the Large Magellanic Cloud, while Vacca & Conti (1992) favor a luminosity of 2.5×10^{36} ergs s^{-1} for a single WC4 star in the red bump. SV98 have compiled the luminosities of WR stars in different emission lines. They find the luminosities of single WNL and WC4 stars in the red bump to be 9.9×10^{34} and 3.0×10^{36} ergs s^{-1} respectively. Furthermore, the luminosity of a single WNL star in the blue bump is metallicity-dependent because of the varying contribution of the N III $\lambda 4640$ emission line, which is smaller at lower metallicity. The luminosity of a single WNL star in the blue bump is equal to $(2.0 - 2.6) \times 10^{36}$ ergs s^{-1} in the range of heavy element mass fraction from $Z = 0.007$ (LMC) to $Z = 0.02$ (Milky Way), while the contribution of a single WC4 star to the blue bump is 5.1×10^{36} ergs s^{-1} .

To derive the number of WCE and WNL stars we have adopted the calibration by SV98. For this purpose, only a few lines are needed. We use the flux of the C IV $\lambda 5808$ line to derive the number of WCE stars. In the blue region, to derive the number of WNL stars we measure the flux of the whole bump including the unresolved N III $\lambda 4640$, C III / C IV $\lambda 4650 / \lambda 4658$ and He II $\lambda 4686$ emission lines, and subtract from it the flux contributed by WCE stars. We adopt the luminosity of a single WNL star in the blue bump to be 2.0×10^{36} ergs s^{-1} for $Z < Z_{\odot}$ and 2.6×10^{36} ergs s^{-1} for $Z \geq Z_{\odot}$ (SV98). For a single WCE star, a luminosity $L(\text{C IV } \lambda 5808)$ of 3.0×10^{36} ergs s^{-1} and a coefficient $k = 1.71$ are adopted. The numbers of WNL and WCE stars so derived are given in Table 7.

This technique does not always give reasonable results because of observational uncertainties and uncertainties in the adopted values of k and the luminosities of single WR stars. The number of WCE

stars in the two galaxies 1211+540 and 1223+487 is less than unity. The spectra of the galaxies 0218+003 and 2329+286 are noisy. This leads to too low or even negative numbers of WNL stars. In those cases, another technique to be discussed in the following is used.

5.3. The number of WNL and WCL stars from the weak WR lines

The detection of many weak features in the spectra of our galaxies allows us to derive the number of WR stars by another independent method and even to study the distribution of stars with different subtypes. Our spectra show mainly features of WNL stars, most often N III $\lambda 4512$ which is characteristic of WN7 – WN8 stars. The Si III $\lambda 4565$ line present in WN9 – WN11 stars is also often seen. Alternatively, this line and some other permitted lines such as N II $\lambda 4620$, Si II $\lambda 5056$ could be nebular in origin and excited by absorption of UV starlight or strong UV He I line emission (e.g., Grandi 1976). However in our objects, the intensities of these lines relative to $H\beta$ (Tables 5 – 6) are in general several times larger than those predicted by Grandi. Thus, despite a possible contribution of nebular emission, the Si III $\lambda 4565$ line is most likely related to WR stars. This line and the N III $\lambda 4512$ line are not contaminated by the emission of other WR subtypes and can in principle yield quite reliable determinations of the numbers of WN stars. In contrast, the determination of the number of the WNL stars from the blue bump at $\lambda 4650$ is subject to more uncertainties caused by the contamination from WCE and WNE stars, strong nebular lines and uncertainties in the poorly known intensity ratio C IV $\lambda 4658/\lambda 5808$ (SV98).

However, the intensities of weak N III $\lambda 4512$ and Si III $\lambda 4565$ in single stars are not well known. We estimate from the spectrum of a WN8 star by Massey & Conti (1980) that the strength of N III $\lambda 4512$ is ~ 3 times weaker than the strength of N III $\lambda 4640$ + He II $\lambda 4686$ lines. Similar values are obtained by Crowther et al. (1995a) from the spectra of WN9 stars for both the N III $\lambda 4512$ and Si III $\lambda 4565$ lines. Therefore, we adopt for the luminosity of WNL stars in these lines the value of 6.6×10^{35} ergs s^{-1} , which is 1/3 that for the N III $\lambda 4640$ + He II $\lambda 4686$ lines derived by SV98.

The results are shown in Table 7. The numbers of WNL stars derived from different lines are in fair agreement (they are generally within a factor of 2) when uncertainties in input data are taken into ac-

count. In particular, for the BCD I Zw 18 the numbers of WNL stars derived from the blue bump, and from the N III $\lambda 4512$ and Si III $\lambda 4565$ lines agree well. Further observations with higher signal-to-noise ratio and better calibration of the N III $\lambda 4512$ and Si III $\lambda 4565$ line luminosities are desirable to test this method which promises to yield more reliable determinations of the number of WNL stars.

The emission line C III $\lambda 5696$ which is characteristic of WCL stars is detected in three galaxies. We estimate the number of WCL stars adopting the luminosity of a single WC7 star in the C III $\lambda 5696$ emission line to be $L_{WC7}^0 = 8.1 \times 10^{35}$ ergs s^{-1} (SV98). Then, for the C III $\lambda 5696$ extinction-corrected fluxes of 1.91×10^{-15} , 4.39×10^{-15} and 0.50×10^{-15} ergs $s^{-1} \text{ cm}^{-2}$ in the galaxies 0947+008 (Mrk 1236), 0952+095 (Mrk 710) and 1054+365 (CG 798) respectively, the derived numbers of WCL stars are 178, 254 and 5. These values are comparable to the numbers of WCE and WNL stars. Although Schaerer et al. (1999a) have not derived the number of WCL stars in Mrk 710 from their data, their measured flux of C III $\lambda 5696$ (relative to $H\beta$) is in satisfactory agreement with ours. While the presence of WCL stars in this high-metallicity galaxy ($Z \sim 1.3 Z_{\odot}$) is expected (Smith & Maeder 1991), the presence of late WC stars in the lower metallicity galaxies Mrk 1236 and CG 798 (both with $Z \sim Z_{\odot}/8$) is more surprising. New observations are required to confirm the presence of WCL stars in these galaxies.

5.4. The number of O stars

The number of O stars can be derived from the number of ionizing photons Q_0^{cor} which is related to the total luminosity of the $H\beta$ emission line $L_{cor}(H\beta)$ by

$$L_{cor}(H\beta) = 4.76 \times 10^{-13} Q_0^{cor}. \quad (5)$$

We take as representative an O7V star and set the number of Lyman continuum photons emitted by such a star to be $Q_0^{O7V} = 1 \times 10^{49} \text{ s}^{-1}$ (Leitherer 1990). The total number of O stars is then derived from the number of O7V stars by correcting for other O stars subtypes. In order to estimate the number of OV stars in WR galaxies, Vacca & Conti (1992) and Vacca (1994) have considered the parameter η_0 , defined to be the ratio of the number of O7V stars to the number of all OV stars. The quantity η_0 depends on the parameters of the initial mass function for massive stars and is, in general, a function of time because of massive

star evolution (Schaerer 1996). SV98 have calculated η_0 as a function of time elapsed from the beginning of an instantaneous burst, and we use their calculations to derive $\eta_0(t)$ for each of our galaxies at age t as determined from the equivalent width $EW(H\beta)$ (SV98). We adopt an IMF with a Salpeter slope $\alpha = 2.35$ and low and upper mass limits of $0.8 M_\odot$ and $120 M_\odot$. Derived ages and $\eta_0(t)$ are shown in Table 5.

It is also necessary to subtract the contribution of WR stars to the total number of ionizing photons. Following Schaerer et al. (1999a) who assumed that the average Lyman continuum flux per WR star is comparable to Q_0^{O7V} , we adopt the average Lyman continuum photon flux per WR star to be $Q_0^{WR} = Q_0^{O7V} = 1.0 \times 10^{49} \text{ s}^{-1}$. Then the number of O stars $N(O)$ is given by:

$$N(O) = \frac{Q_0^{cor} - N_{WR} Q_0^{WR}}{\eta_0(t) Q_0^{O7V}}. \quad (6)$$

The number of O stars derived from Eq. (6) is given in Table 7 together with the relative numbers of massive stars $N(WR)/N(O+WR)$ and $N(WC)/N(WN)$, where $N(WR) = N(WN) + N(WC)$ and assuming $N(WC) = N(WCE)$ and $N(WN) = N(WNL)$. The number of WNL stars is derived from the $\lambda 4650$ bump except for two galaxies, 0218+003 and 2329+286. The blue bump gives a too small $N(WNL)$ in the case of 0218+003, and a negative $N(WNL)$ in the case of 2329+286. We use instead the flux of the Si III $\lambda 4565$ emission line to derive $N(WNL)$ in both cases.

6. COMPARISON WITH EVOLUTIONARY SYNTHESIS MODELS

Figure 3 shows the luminosity of the blue bump at $\lambda 4650$ in our sample galaxies vs. metallicity (as denoted by $12 + \log(O/H)$). It is seen that there is a general trend for the luminosity of the blue bump to decrease with decreasing metallicity. However there is a very large spread of points at a fixed metallicity. At $12 + \log(O/H) \sim 7.9$, the spread spans some three orders of magnitude. This large spread is thought to reflect different stages during the burst of star formation. To check for possible selection effects, we have plotted in different symbols the bright ($M_B < -18$) non-dwarf and dwarf ($M_B \geq -18$) galaxies. It is seen that all galaxies with large $L(\lambda 4650)$ ($> 10^{39} \text{ ergs s}^{-1}$) are bright. Can the lack of galaxies with faint $L(\lambda 4650)$ in the $8.2 \leq 12 + \log(O/H) \leq 9.1$

abundance range simply be due to the selection effect that, in bright galaxies, WR bumps with small $L(\lambda 4650)$ (those with $< 10^{39} \text{ ergs s}^{-1}$) cannot be detected? We cannot completely exclude this possibility as we observed only nuclear starbursts in the bright highest-metallicity galaxies. There exists the possibility that WR stars can be found with high S/N observations in faint non-nuclear metal-rich H II regions. However, we believe that the most likely reason for the non-detection of galaxies with faint $L(\lambda 4650)$ in the $8.2 \leq 12 + \log(O/H) \leq 9.1$ abundance range, is not because their WR bumps cannot be detected, but simply because there are no dwarf galaxies in this high metallicity range.

Thus we believe the general decrease of $L(\lambda 4650)$ with O/H to be real. This decrease is expected from massive stellar evolution models (Maeder 1991; Maeder & Meynet 1994; Meynet 1995; SV98) and it is consistent with earlier observations of WR galaxies (Vacca & Conti 1992; Masegosa et al. 1991; Kunth & Schild 1986; Kunth & Joubert 1985) where no galaxy with oxygen abundance $12 + \log(O/H) \leq 7.9$ was ever seen to contain WR stars. A possible exception was the galaxy Zw 0855+06, although there was some controversy about its oxygen abundance: Vacca & Conti (1992) derived $12 + \log(O/H) = 7.72$ while Kunth & Joubert (1985) obtained a value of 8.40. However, the increase in detector sensitivity and the use of large telescopes for the detection of weak low-contrast WR features in galaxies have changed the situation. The discovery of WR stars in I Zw 18 ($Z_\odot/50$, Izotov et al. 1997; Legrand et al. 1997) and SBS 0335-052 ($Z_\odot/40$, Izotov et al. 1999a) implies that the luminosity of the WR bump cannot keep on decreasing with decreasing metallicity. Instead, the data in Fig. 3 for those galaxies suggest that the luminosity of the blue bump appears to become roughly constant for $12 + \log(O/H) \leq 7.9$, although this conclusion is based only on a few data points. The data on WR populations in low-metallicity galaxies is very scarce for two reasons. First, such low-metallicity objects are extremely rare and second, the time spent by massive stars in the WR stage is very short at low metallicities, which make them hard to detect.

The discovery of WR stellar populations in the two most metal-deficient galaxies known has increased substantially the metallicity range for WR galaxies. Our WR galaxy sample spans two orders of magnitude in metallicity, from $Z_\odot/50$ (I Zw 18) to $\sim 2Z_\odot$ (0720+335 \equiv Mrk 1199), allowing to compare ob-

served and predicted relative numbers of WR stars and check the validity of theoretical models in a wide range of metal abundances. In the following we compare the properties of the observed WR population in our galaxies with predictions of evolutionary synthesis models by SV98 for the range of heavy element mass fraction $Z = 0.001 - 0.02$ and by Schaerer (1998, private communication) for $Z = 0.0004$.

6.1. Metallicity effects on the relative numbers of WR stars

Figure 4 shows the number ratio $N(\text{WR}) / N(\text{O} + \text{WR})$ for our sample galaxies (filled circles) vs. metallicity. For comparison we also show the data from Schaerer et al. (1999a) (open circles), Kunth & Joubert (1985) (asterisks) and Vacca & Conti (1992) (diamonds). While the relative numbers of WR stars are derived by Schaerer et al. (1999a) in the same way as ours, they are derived differently by Kunth & Joubert (1985) and Vacca & Conti (1992) and cannot be compared directly with our data. Therefore, we have recalculated the relative numbers of WR stars by the same method, using the fluxes and equivalent widths of nebular and WR emission lines published by those authors. However, the red bumps were not detected in their observations and therefore we have no information about the relative contribution of WCE stars to the blue bump. Furthermore, for other authors' data, we cannot correct the flux in the $\text{H}\beta$ emission line for aperture effects for lack of information. Inspection of Table 5 shows that the mean correction factor for aperture effects is $\sim 2 - 3$. Therefore, $\text{H}\beta$ fluxes are underestimated and the relative numbers of WR to $(\text{O} + \text{WR})$ stars derived from the data by Kunth & Joubert (1985), Vacca & Conti (1992) and Schaerer et al. (1999a) are slightly overestimated as is evidenced by a small upward shift of their data compared to ours. Note that the detectability limit of WR populations in our galaxies is better compared to other observations because of the generally higher signal-to-noise ratio of our spectra.

For each of the four galaxies in our sample with metallicity greater than solar (0211+038, 0720+335, 0952+095, 1036-069) we show two values of $N(\text{WR}) / N(\text{O} + \text{WR})$ connected by dashed lines. Lower limits are calculated assuming the correction factor η_0 to be 1. However, the equivalent widths of the $\text{H}\beta$ emission line in these galaxies are $\leq 30\text{\AA}$ and hence the ages of the star bursts are ≥ 5.3 Myr (Table 5). For these ages, high-metallicity O stars are not ex-

pected, the definition of η_0 becomes meaningless and the ionizing flux is provided by stars of type B or later and WR stars (SV98). Therefore, upper limits are set to $N(\text{WR})/N(\text{O}+\text{WR}) = 1$ for the four metal-rich galaxies. At the low-metallicity end, the $N(\text{WR})/N(\text{O}+\text{WR})$ ratio for I Zw 18 (filled circle) is probably underestimated by a factor of ~ 2 because the equivalent width of the $\text{H}\beta$ emission line in the BCD's NW component, equal to 67\AA , and the parameter $\eta_0 = 0.2$ give a relatively large age of 5.9 Myr. A burst age of 4–5 Myr, seems more reasonable as it is only slightly larger than the age estimated from the $\text{H}\beta$ equivalent width of the SE component of I Zw 18 (128\AA) where WR stars are not seen. To illustrate how $N(\text{WR})/N(\text{O} + \text{WR})$ changes as a function of adopted age, we show respectively by an open rectangle and an open triangle the $N(\text{WR})/N(\text{O}+\text{WR})$ ratios expected in I Zw 18 for instantaneous burst ages of 4 Myr ($EW(\text{H}\beta) \sim 100\text{\AA}$) and 3 Myr ($EW(\text{H}\beta) \sim 200\text{\AA}$), in addition to the ratio for a burst age of 5.9 Myr (filled circle). For the other galaxies, the $N(\text{WR})/N(\text{O}+\text{WR})$ ratio may increase slightly when their $\text{H}\beta$ equivalent width is corrected for aperture effects. This is because a correction would increase $EW(\text{H}\beta)$, which would increase η_0 and decrease the number of O stars.

Despite these uncertainties, it is clear from Fig. 4 that the fraction of WR stars relative to other massive stars increases with increasing metallicity, as first noted by Kunth & Schild (1986). This increase is in agreement with predictions of evolutionary synthesis models (Mas-Hesse & Kunth 1991; Krüger et al. 1992; Cerviño & Mas-Hesse 1994; Meynet 1995; SV98).

The solid line in Fig. 4 shows the maximum theoretical values of $N(\text{WR})/N(\text{O}+\text{WR})$ ratios as a function of metallicity as predicted by SV98 and Schaerer (1998, private communication). We have used the instantaneous burst models with a Salpeter IMF slope $\alpha=2.35$ and $M_{up}=120M_{\odot}$, except for the metallicity $Z = Z_{\odot}/50$ for which $M_{up} = 150 M_{\odot}$ is adopted. Nearly all our galaxies lie below the solid line, in agreement with the theoretical predictions. The spread of points can be understood as caused by the strong dependence on time of the WR star relative numbers during the short WR stage of the starburst. Evolutionary synthesis models predict that the number of WR stars rises to a maximum value and then falls down to zero on the short time scale of 1 Myr for $Z = Z_{\odot}/50$ and of 5 Myr for $Z = Z_{\odot}$. The maximum value depends on the IMF and the heavy ele-

ment mass fraction Z , since at a higher metallicity the minimum mass limit for a star which undergoes the WR phase is lower. In Fig. 4 the evolutionary track of a galaxy undergoing a star formation burst would describe a loop. An object rushes up and reaches the maximum $N(\text{WR})/N(\text{O}+\text{WR})$ value (solid line), and after that drops down, drifting slightly to higher Z , because massive stars would enrich the surrounding environment with heavy elements via stellar winds and supernova explosions (Maeder & Meynet 1994; Esteban & Peimbert 1995; Pilyugin 1994). In this scenario we would expect different objects at different stages of WR evolution to scatter in the region under the solid line, as is observed. The lack of galaxies with high Z and small relative number of WR stars can be understood as a selection effect. We have observed only nuclear starbursts in highest-metallicity galaxies as nuclear regions constitute an especially favorable environment for the formation of numerous massive stars. It is likely that this region will be filled in when higher signal-to-noise ratio observations of non-nuclear metal-rich H II regions are carried out. Another factor which may account for the observed spread of points is the finite duration of the starburst. The assumption of an instantaneous burst where all stars are formed at the same time, represents a limiting case. High spatial resolution studies of blue compact dwarf galaxies (e.g. Thuan, Izotov & Lipovetsky 1997; Papaderos et al. 1998) show that star forming regions consist of several clusters with an age spread of several Myr. Thus real star formation should be intermediate between the instantaneous burst and continuous star formation cases. The dot-dashed line in Fig. 4 shows the theoretical prediction for the other limiting case, a continuous star formation model. The data scatters nicely between the two limiting cases, implying that the models are basically correct.

6.2. The $N(\text{WC})/N(\text{WN})$ ratio

Figure 5 shows the dependence of the WC-to-WN star number ratio on metallicity. It is seen that galaxies with relatively large numbers of WC stars (the so-called WC galaxies) possess a very narrow range of metallicities, with $12 + \log(\text{O}/\text{H})$ going only from 7.8 to 8.2. These large $N(\text{WC})/N(\text{WN})$ ratios can be explained in terms of the bursting nature of the star formation. The thick solid line in Figure 5 shows the maximum values of $N(\text{WC})/N(\text{WN})$ as a function of oxygen abundance as predicted by theoretical models (SV98; Schaerer 1998, private communi-

cation). These instantaneous burst models use stellar evolution models with enhanced mass-loss (Maeder & Meynet 1994), and are characterized by the same parameters as described before. The theoretical curve delineates quite well the left boundary of the region where the data points in the range of oxygen abundance $12 + \log(\text{O}/\text{H}) = 7.6 - 8.3$ scatter.

However, the agreement for the extremely metal-deficient galaxy I Zw 18 is not so good. The observed $N(\text{WC})/N(\text{WN})$ in this galaxy is ~ 0.28 while models predict $N(\text{WC})/N(\text{WN}) \approx 0.09$. This discrepancy cannot be due to our adopted values of line luminosities of single WR stars since we use the same values as SV98. In contrast to the relative number of WR stars, the $N(\text{WC})/N(\text{WN})$ ratio does not suffer from aperture effects. The numbers of WNL stars in I Zw 18 of 45 and 36 derived from the weaker lines N III $\lambda 4512$ and Si III $\lambda 4565$ respectively (Table 7) are very close to the value of 44 derived from the blue bump. These values are derived with a distance of 20 Mpc to I Zw 18 (Izotov et al. 1999b). On the other hand, if the same distance is adopted, Legrand et al. (1997) detect only 3 – 6 WCE stars and no WN star, so that their $N(\text{WC})/N(\text{WN})$ ratio is uncertain. De Mello et al. (1998) obtain $N(\text{WN}) \sim 30$ from analysis of *Hubble Space Telescope* images, which results in an even larger $N(\text{WC})/N(\text{WN})$ ratio for I Zw 18. Hence, we conclude that models fail to predict the correct $N(\text{WC})/N(\text{WN})$ ratio at very low metallicity. However, because of the small numbers of WR stars in I Zw 18 (~ 45 WNL and ~ 12 WCE stars) and the small slit width of $1''.5$ used in the spectroscopic observations, we cannot exclude the possibility that we are observing in I Zw 18 a region with a locally enhanced number of WCE stars. Therefore, high signal-to-noise ratio (SNR) two-dimensional spectroscopic mapping is necessary to check this possibility. The existing two-dimensional spectroscopic data on I Zw 18 by Vílchez & Iglesias-Páramo (1998) have too low a SNR for WR features to be seen.

The $N(\text{WC})/N(\text{WN})$ ratio derived for the galaxies in our sample is very different from that expected in the case of continuous star formation as derived empirically by observations of Local Group galaxies. We show by diamonds in Fig. 5 the $N(\text{WC})/N(\text{WN})$ ratios in the Local Group galaxies M33, M31, NGC 6822, SMC, LMC, IC 10 and the Milky Way based on observations of individual WR stars (Massey & Johnson 1998). The linear fit to these data excluding the 2 deviant points of IC 10 and the Milky Way given

by Massey & Johnson (1998) is shown by the dashed line. This fit can be considered as an empirical determination of the dependence of the $N(\text{WC})/N(\text{WN})$ ratio on metallicity in the case of continuous star formation. It predicts $N(\text{WC})/N(\text{WN})$ to approach 0 for galaxies with oxygen abundance $12 + \log(\text{O}/\text{H}) \leq 8.1$ and agrees well with the predictions of massive stellar evolution models with enhanced mass-loss for continuous star formation with a constant rate.

The galaxy IC 10 was excluded by Massey & Johnson (1998) from the determination of the correlation because of its very large $N(\text{WC})/N(\text{WN})$ ratio of ~ 2 (although that ratio may be as small as 1.4 if uncertainties are taken into account). Those authors suggest that such a high value is caused by the bursting nature of star formation in IC 10. Indeed, this galaxy, together with our galaxies with oxygen abundances in the range from 7.8 to 8.2, can be understood in terms of models with an instantaneous starburst as shown by the solid line in Fig. 5.

The five galaxies in our sample at the high end of oxygen abundance $12 + \log(\text{O}/\text{H}) \geq 8.6$ lie systematically below the fit of Massey & Johnson (1998) while no galaxy with high metallicity is found above it. The same result has been obtained by Schaerer et al. (1999a) for two metal-rich galaxies He 2-10 ($Z \sim Z_{\odot}/2$) and Mrk 710 ($Z \sim Z_{\odot}$). These low values may be partly due to the assumption that WCE stars dominate among WC stars. If we assume instead that WC7 stars are the main contributors to the C IV $\lambda 5808$ emission line in high-metallicity galaxies then the relative number of WC-to-WN stars is increased by a factor of ~ 4 because of the lower luminosity of WC7 stars, just accounting for the discrepancy between the values given by the fit for continuous star formation (dashed line) and the observed values. However, in this case an appreciable C III $\lambda 5696$ emission line is expected in the spectra of high-metallicity galaxies because the luminosity ratio $L(\text{C III } \lambda 5696)/L(\text{C IV } \lambda 5808)$ for a single WC7 star is ~ 0.5 (SV98). Thus far, the C III $\lambda 5696$ line has been seen only in Mrk 710 (Schaerer et al. 1999a; this paper). Additionally, WNE stars can significantly contribute to the luminosity of blue bump in these galaxies, decreasing even more the $N(\text{WC})/N(\text{WN})$ ratio because the luminosity of a single WNE star in this bump is ~ 3 times lower than that of a WNL star (SV98).

But, probably, the main reason for the low $N(\text{WC})/N(\text{WN})$ ratios in high-metallicity galaxies is the

bursting nature of star formation in these galaxies, with different durations of the successive WNL, WNE and WCE stages. All five galaxies have low equivalent widths of $\text{H}\beta$ (Table 5) and hence they are in the late stage of the WR episode with starburst ages ≥ 5.3 Myr, when mainly WN stars are present while the number of WC stars drops to 0 (SV98).

In summary, analysis of the $N(\text{WC})/N(\text{WN})$ ratio shows good general agreement between the observational data and the model predictions, except in the case of the very low metallicity galaxy I Zw 18. The detection of WR stars in other extremely metal-deficient galaxies is necessary to clarify the situation at the low-metallicity end.

6.3. Age dependence

Due to the bursting nature of star formation in WR galaxies, the relative number of WR stars is a sensitive function of time elapsed since the beginning of the star formation episode. The equivalent width of the $\text{H}\beta$ emission line $EW(\text{H}\beta)$ can be used with a certain degree of confidence as an indicator of the age of star formation region. The hydrogen ionizing flux of a star cluster gradually decreases as the most massive stars disappear. As a result the equivalent width of $\text{H}\beta$ decreases with time. The theoretical behavior of $EW(\text{H}\beta)$ with time for an instantaneous burst is given by SV98 for a set of metallicities ranging from $Z_{\odot}/20$ to $2Z_{\odot}$.

Figure 6 shows the dependence of the $N(\text{WR})/N(\text{O}+\text{WR})$ ratio as a function of the age of an instantaneous burst occurring at time $t = 0$. Because this ratio is a strong function of the heavy element mass fraction Z , we divided objects from our sample (filled circles) and from Kunth & Joubert (1985) (asterisks), Vacca & Conti (1992) (diamonds) and Schaerer et al. (1999a) (open circles) into four groups: the highest-metallicity objects with $12 + \log(\text{O}/\text{H}) > 8.63$ are shown in Figure 6a, those with $8.43 < 12 + \log(\text{O}/\text{H}) \leq 8.63$ are shown in Figure 6b, those with $7.93 < 12 + \log(\text{O}/\text{H}) \leq 8.43$ are shown in Figure 6c and the lowest-metallicity objects with $12 + \log(\text{O}/\text{H}) \leq 7.93$ are shown in Figure 6d. We compare the observed distributions with predictions of evolutionary synthesis models by SV98 shown by solid lines and labeled by their heavy element mass fraction. For metal-rich galaxies we again show two values of $N(\text{WR})/N(\text{O}+\text{WR})$: 1 and the ratio expected for the parameter $\eta_0 = 1$. They are connected by dashed lines in Figure 6a. At the low-metallicity end

(Fig. 6d), three values of $N(\text{WR})/N(\text{O}+\text{WR})$ are shown for I Zw 18 corresponding as before to three choices of starburst age: 3, 4 and 5.9 Myr. They are connected by a dashed line. Taking into account the uncertainties in deriving the $N(\text{WR})/N(\text{O}+\text{WR})$ ratio (observational errors, uncertainties in the age of starburst, breakdown of the instantaneous burst approximation and other model assumptions), we find a good general agreement between the relative numbers of WR stars predicted by the theoretical models and those inferred from observations, especially for objects in the range of heavy element mass fraction $Z = 0.002 - 0.010$ (Figures 6b, 6c). The agreement is not so good for the most metal-deficient galaxies (Figure 6d), including I Zw 18. For the latter, we expect that part of the disagreement may come from uncertainties in the age determination with the use of the $\text{H}\beta$ equivalent width. It is known that the ionized gas distribution in the NW component of I Zw 18 is very complex with WR stars located in a hole with very low $EW(\text{H}\beta)$ (Izotov et al. 1997). The presence of a large $\text{H}\alpha$ halo in I Zw 18 suggests that some of the H II regions in it are density-bounded (Dufour & Hester 1990; Martin 1996). In this case part of the ionizing photons will escape the H II region, resulting in a lower equivalent width of the $\text{H}\beta$ emission line. The most deviant point in Figure 6d belongs to the galaxy Mrk 178. This discrepancy may be caused by small statistics in the number of WR stars which are only a few ($\sim 2 - 3$) in this galaxy, and by uncertainties in the burst age determination.

The equivalent widths of the blue and red bumps as a function of $\text{H}\beta$ equivalent width are shown respectively in Figures 7 and 8. We again divide our galaxy sample into 4 subsamples according to heavy element mass fraction, in the same manner as in Figure 6. Solid lines show the theoretical predictions by SV98 for stellar populations with IMF slope $\alpha = 2.35$, while dashed lines in Fig. 7d and 8d are those with IMF slope $\alpha = 1.0$. We expect the main contribution to the red bump equivalent width to come from the C IV $\lambda 5808$ line. However, because of the low resolution and large width of this line, some contribution of N II $\lambda 5720-40$, although small, might be present. By contrast, different subtypes of WR stars contribute to the blue bump. Therefore, while the theoretical curves in Figure 8 represent only $EW(\lambda 5808)$, for the blue bump the theoretical curves shown in Figure 7 are the sum of the N III $\lambda 4640$, C III/C IV $\lambda 4658$ and He II $\lambda 4686$ WR emission line equivalent widths.

Note that the points with high values ($EW(\lambda 4650) > 5\text{\AA}$ and $EW(\lambda 5808) > 3\text{\AA}$) in Figures 7d and 8d are highly uncertain, because they belong to galaxies with very few ($\leq 1 - 3$) WR stars (1130+495, 1223+487, 1437+370 in Tables 6 and 7), or galaxies with noisy spectra (0218+003). We do not consider these galaxies in our analysis. Again, we find general good agreement between observations and theory for $EW(\lambda 4650)$ and $EW(\lambda 5808)$ of objects with heavy element fraction $Z > 0.002$ (Fig. 7a–7c and 8a–8c). The relatively low values of the observed $EW(\lambda 5808)$ in Fig. 8a and 8b can be understood in the following manner. High-metallicity objects in our sample are likely to be in a late WR stage and hence they are observed after the WC bump equivalent width reaches its maximum value. This supports our previous conclusion in section 6.2 that the low $N(\text{WC})/N(\text{WN})$ ratios in high-metallicity galaxies are lower than those predicted by the continuous star formation empirical relationship (Fig. 5) because of the bursting nature of star formation in these galaxies. In both Figures 7 and 8, there appears to be a slight systematic shift of the data points to the left of the theoretical curves by $\log EW(\text{H}\beta) \sim 0.4$. This implies that the models predict systematically larger $EW(\text{H}\beta)$ by a factor of ~ 2.5 , i.e. smaller burst ages as compared to those implied by the observations. However, we expect that correction for aperture effects will increase $EW(\text{H}\beta)$ making the agreement better.

Agreement is not so good however for the galaxies with lowest metallicities. Theoretical predictions with the Salpeter IMF slope $\alpha = 2.35$ are below our observed data points for both $EW(\lambda 4650)$ and $EW(\lambda 5808)$. Models with a very shallow IMF slope $\alpha = 1.0$ also fail to explain the observed points. We note that, in contrast, de Mello et al. (1998) found satisfactory agreement between the predicted $EW(\lambda 4650)$ and $EW(\lambda 5808)$ and the values observed by Legrand et al. (1997). However, those authors' observations did not include the region of maximum WR emission. This region was found by Izotov et al. (1997) to have several times larger $EW(\lambda 4650)$ and $EW(\lambda 5808)$, leading to the discrepancy between models and observations discussed here. It is likely, that the disagreement comes from the different properties of WCE stars at low metallicities as compared to those in the Galaxy and Local Group galaxies. We suspect that single low-metallicity WCE star luminosities in the C IV $\lambda 4658$ and C IV $\lambda 5808$ lines are $\sim 2 - 4$ times larger than those adopted by SV98.

The use of Smith’s (1991) WR star emission line luminosities would increase $EW(\lambda 4650)$ and $EW(\lambda 5808)$ (SV98, de Mello et al. 1998), but by an amount not large enough to account for the observed values in I Zw 18. Observational data for single WR stars are not available at such low metallicities. However, some arguments in favor of a larger WCE star line luminosity at low metallicity come from the calculations of Maeder & Meynet (1994). They have shown that, for a given fixed mass of the progenitor star, both the total luminosity of a WCE star and its surface C/He abundance ratio are larger at very low metallicities. The luminosity of a WNL star also increases with decreasing metallicity, but by not such a large amount. Hence, we expect that the net effect might be an increase of both the blue and red bump model equivalent widths, in better agreement with observations. A higher line luminosity of low-metallicity WCE stars would also result in a better agreement between the observed and predicted $N(\text{WC})/N(\text{WN})$ ratio for I Zw 18 (Fig. 5), since the observed value would be reduced.

There is another factor which may increase the equivalent widths of the blue and red bumps. Theory predicts that WR stars in massive close binary systems in the late ($\gtrsim 5$ Myr) phases of an instantaneous burst of star formation may have larger equivalent widths (SV98). However the properties of WR stars in binaries are still poorly known.

7. THE ORIGIN OF THE NEBULAR HE II $\lambda 4686$ EMISSION

The strong nebular He II $\lambda 4686$ emission line has been detected in many low-metallicity blue compact galaxies (in $\sim 50\%$ of the sample) observed by ITL94, ITL97, Thuan et al. (1995), IT98, Izotov et al. (1996, 1997). Its intensity, exceeding $\sim 3\%$ that of $\text{H}\beta$ in some objects, is several orders of magnitude larger than theoretical values predicted by models of photoionized H II regions (e.g. Stasińska 1990). It was suggested by Bergeron (1977), that the He II emission in dwarf emission-line galaxies could arise in the atmospheres of Of stars. Garnett et al. (1991) obtained observations of nebulae in nearby dwarf galaxies with strong narrow He II $\lambda 4686$ emission lines and examined several possible excitation mechanisms, concluding that the radiation field associated with star-forming regions can be harder than previously suspected. More recently Schaerer & de Koter (1997) cal-

culated non-LTE atmosphere models taking into account line blanketing and stellar winds and found that the flux in the He II continuum is increased by 2 to 3 orders of magnitudes compared to predictions from plane-parallel non-LTE model atmospheres and by 3 to 6 orders of magnitudes compared to predictions from plane parallel LTE model atmospheres. However, for young starbursts dominated by O stars ($t \leq 3$ Myr), typical values of $I(\text{He II})/I(\text{H}\beta)$ are between 5×10^{-4} and 2×10^{-3} , still far below the observed intensities. Schaerer (1996) synthesized the nebular and Wolf-Rayet He II $\lambda 4686$ emission in young starbursts. For heavy element mass fractions $Z_{\odot}/5 \leq Z \leq Z_{\odot}$, he predicted a strong nebular He II emission due to a significant fraction of WC stars in the early WR phases of the burst, and concluded that the predictions (typically $I(\text{He II})/I(\text{H}\beta) \sim 0.01 - 0.025$) agree well with the observations. SV98 proposed that hot WN stars may also play a role. Another mechanism, suggested by Garnett et al. (1991), is that radiative shocks in giant H II regions can produce relatively strong He II emission under certain conditions. The strength of the He II emission is sensitive mostly to the velocity of the shock, reaching a maximum for $V_{\text{shock}} \sim 120 \text{ km s}^{-1}$, and dropping rapidly at higher velocities.

To study the possible mechanisms responsible for the emission of the nebular He II $\lambda 4686$ line, we gathered a sample of galaxies from the present study and previous papers (ITL94, ITL97, IT98, Thuan et al. 1995) showing nebular He II $\lambda 4686$. The galaxies are listed in Table 8. No nebular He II $\lambda 4686$ emission was detected in galaxies with $12 + \log(\text{O}/\text{H}) > 8.13$. Also shown are the intensities and equivalent widths of the nebular He II $\lambda 4686$ line together with the equivalent width of the $\text{H}\beta$ emission line and the oxygen abundance. WR stellar emission was detected only in 18 out of the 30 H II regions in Table 8, a 60% detection rate. A non-detection of WR features means that a galaxy contains no or too few WR stars (several to a few tens depending on the distance of the galaxy) to produce detectable WR emission. The number of WR stars responsible for a broad feature with peak intensity comparable to the continuum rms is approximately given by $d^2/(S/N)$, where d is the distance to the galaxy in Mpc. Typically, our spectra with no WR lines detected have $S/N \sim 30$. Then, at a distance of ~ 10 Mpc, a broad blue bump produced by $\gtrsim 3$ WR stars can be detected. We believe that the non-detection of WR emission in some galaxies is not the result of a selection effect as the spectra of all galaxies

possess approximately the same signal-to-noise ratio: it has to be large enough so we could measure accurately the intensities of the weak He I lines necessary for the primordial helium problem. Moreover, they have approximately the same relative intensity and equivalent width of the nebular He II $\lambda 4686$ emission line. Because the nebular He II emission region is generally smaller than the $H\beta$ emission region, we have not corrected the He II $\lambda 4686$ line intensity for aperture effect. We present in Table 8 He II $\lambda 4686$ line intensities relative $H\beta$ for two cases: in column 4, $H\beta$ is corrected only for extinction, while in column 5 $H\beta$ is corrected for both extinction and aperture effect. The aperture correction factors for $H\beta$ in the WR galaxies are given in Table 5. For the remaining objects we assume the correction factor to be 2.5, a typical value for the objects in Table 5.

Figure 9 displays the dependence of the equivalent width and intensity of the nebular He II $\lambda 4686$ line as a function of the $H\beta$ equivalent width. Theoretical predictions are also shown for stellar populations with $Z = 0.0004, 0.001, 0.004$ by dashed, solid and dotted lines, respectively (SV98, Schaerer 1998, private communication). The observed equivalent widths of the nebular He II $\lambda 4686$ emission line in WR galaxies (filled circles) and in the galaxies with nondetected WR features (open circles) are in good agreement with values predicted by models with $Z = 0.0004$ and 0.001 (Figure 9b). As before, the observed values of $EW(H\beta)$ are systematically shifted to the left of the theoretical curves by $\log EW(H\beta) \sim 0.4$, implying that predicted burst ages are systematically younger as compared to observations. However, as previously, correction for aperture effect would increase $EW(H\beta)$ and result in better agreement. The agreement with data is not so good however for the model with $Z = 0.004$ which predicts $EW(\text{He II } \lambda 4686)$ that are systematically higher (Figure 9a).

Figure 9b shows that the intensities of He II $\lambda 4686$ relative to $H\beta$, the latter being corrected only for interstellar extinction, are systematically larger than predicted values. Correction of $H\beta$ for aperture effect does result in a better agreement (Figure 9c). Again we see a systematic shift of the data points to the left of the evolutionary synthesis models which may be due in part to the fact that the $H\beta$ equivalent width has not been corrected for aperture effect. Overall, we find a satisfactory general agreement between models and observations, implying that the hard radiation of WR stars can account for many properties of the He

II $\lambda 4686$ nebular emission in WR galaxies.

However, the galaxies with lowest metallicities tend to have slightly larger nebular He II $\lambda 4686$ line intensities compared to those with higher metallicities (Table 8). No nebular He II $\lambda 4686$ emission has been observed in galaxies with $Z > 0.004$. This trend is just the opposite of what is expected from the evolutionary synthesis models by SV98 which predict nebular $I(\text{He II } \lambda 4686)/I(H\beta)$ as high as $0.05 - 0.10$ at solar and higher metallicities. We conclude that high-metallicity stellar models overpredict the number of photons with $\lambda < 228 \text{ \AA}$ responsible for the ionization of He^+ .

Additionally, the points representing galaxies with detected and nondetected WR features mingle indistinctly in Figure 9. This implies that, despite the good agreement between the observed and predicted characteristics of the nebular He II $\lambda 4686$ emission line, WR stars are probably not the sole origin of He II $\lambda 4686$ emission in star-forming regions. Other mechanisms such as for example radiative shocks, are probably also at work. These mechanisms may play an important role in the late stages of star formation bursts (indicated by a lower equivalent width of the $H\beta$ emission line) when the supernova activity increases.

8. SUMMARY AND CONCLUSIONS

We present here the results of a spectroscopic study of a sample of 39 WR galaxies spanning two orders of magnitude in heavy element abundances, from $Z_{\odot}/50$ to $2Z_{\odot}$. Our main goal is to search for WN and WC stars in these galaxies, compare their numbers with predictions from evolutionary synthesis models and test massive stellar evolution models in a wide range of metallicities.

Our principal results are the following:

1. The broad WR emission in the blue region of the spectrum at $\lambda 4650$ (the blue bump), an unresolved blend of N V $\lambda 4605, 4620$, N III $\lambda 4634, 4640$, C III $\lambda 4650$, C IV $\lambda 4658$ and He II $\lambda 4686$ emission lines, is present in 37 galaxies and suspected in 2 more. The red bump mainly produced by the emission of broad C IV $\lambda 5808$ is detected in 30 galaxies. The WR population in the majority of our galaxies is dominated by late WN and early WC stars. However, a nonnegligible population of early WN stars can be present in the highest-metallicity galaxies in our sample.

2. Weak WR emission lines are present in the spec-

tra of many of our galaxies which are very rarely or never seen before. The N III $\lambda 4512$ and Si III $\lambda 4565$ lines are most often present and they are tracers of WN7–WN8 and WN9–WN11 stars respectively. These features have been detected in particular in the most metal-deficient blue compact galaxy known, I Zw 18 (Izotov et al. 1997). The C III $\lambda 5696$ emission line is detected in three galaxies suggesting the presence of late WC stars. We confirm the detection of C III $\lambda 5696$ by Schaerer et al. (1999a) in the spectrum of the high-metallicity galaxy Mrk 710. This line is expected in high-metallicity environments. However, its presence in the spectra of Mrk 1236 and CG 798 with $\sim Z_{\odot}/8$ is more surprising and needs confirmation by higher signal-to-noise ratio spectral observations.

3. A new technique is proposed for the determination of the WNL star numbers from the fluxes of the N III $\lambda 4512$ and Si III $\lambda 4565$ emission lines. The advantage of this technique is that these lines are only seen in WNL stars, while the blue bump, usually used to derive their number, is a mixture of WNE, WNL and WCE stellar emission contaminated by nebular gaseous emission. The numbers of WNL stars derived from the N III $\lambda 4512$ and Si III $\lambda 4565$ emission lines are in satisfactory agreement with values derived from the blue bump. This new technique allows potentially to study the distribution of WNL stars within narrow subtypes. However, a more precise calibration of the N III $\lambda 4512$ and Si III $\lambda 4565$ emission lines in WR stars is necessary.

4. Good general agreement is found between the relative numbers of WR stars $N(\text{WR})/N(\text{O}+\text{WR})$ inferred from observations and those predicted by evolutionary synthesis models. The relative numbers of WR stars decrease with decreasing metallicity in the whole metallicity range discussed in this paper ($Z_{\odot}/50 - 2Z_{\odot}$), in agreement with predictions by massive stellar evolution models with enhanced stellar wind (Maeder & Meynet 1994).

5. The relative numbers $N(\text{WC}) / N(\text{WN})$ of WR stars of different subtypes in the galaxies of our sample can be explained by the bursting nature of star formation, and are in general good agreement with predictions of evolutionary synthesis models by SV98. The relative numbers $N(\text{WR}) / N(\text{O}+\text{WR})$ and observed equivalent widths of the blue and red bumps also compare favorably with predictions of evolutionary synthesis models by the same authors for metallicities larger than $\sim 1/10$ solar. However, the agreement is not so good for galaxies at

the low-metallicity end, where $N(\text{WC}) / N(\text{WN})$, $EW(\lambda 4650)$ and $EW(\lambda 5808)$ derived from observations are several times larger compared to model predictions. Part of the disagreement may come from the poor statistics of WR stars in these low-metallicity WR galaxies. In the case of I Zw 18 ($Z_{\odot}/50$) however, the difference between observations and models may be explained by too low single WCE star line luminosities adopted in the SV98 models, or by an additional contribution by WR stars in binaries.

6. The nebular He II $\lambda 4686$ emission is analyzed in 30 H II regions to study its origin, whether it can be due to the ionization of He⁺ by the hard UV radiation of WR stars. A WR population is detected in only 18 of these H II regions. No H II region with detected nebular He II $\lambda 4686$ emission has oxygen abundance $12 + \log(\text{O}/\text{H}) > 8.13$. Models by SV98 reproduce satisfactorily the observed intensities and equivalent widths of the nebular He II $\lambda 4686$ emission line. Hence, in WR galaxies, He II $\lambda 4686$ emission can in general be accounted for by the hard UV radiation of WR stars. However, their models predict the existence of nebular He II $\lambda 4686$ emission at the early stages of a burst of star formation with $EW(\text{H}\beta) = 200 - 300\text{\AA}$ while the data are systematically shifted to lower $EW(\text{H}\beta) \leq 100\text{\AA}$ implying larger ages. For I Zw 18 in particular, models predict the existence of nebular He II $\lambda 4686$ emission with $EW(\text{H}\beta) > 300\text{\AA}$, while the observed $EW(\text{H}\beta)$ is only 67\AA . While this disagreement can be explained in part by aperture effects in the $EW(\text{H}\beta)$ measurements, WR stars cannot be the sole cause of He II $\lambda 4686$ emission. The properties of this emission are similar whether galaxies contain WR stars or not (Fig. 9). Hence, to addition to WR star ionization other mechanisms (e.g. radiative shocks) need to be invoked to account for He II $\lambda 4686$ nebular emission, especially at the late stages of the star formation burst.

It is a pleasure to thank Daniel Schaerer for the use of his evolutionary synthesis models and useful comments. Phil Massey and the referee Crystal Martin also contributed helpful comments. This international collaboration was possible thanks to the partial financial support of INTAS grant No. 97-0033 for which N.G.G. and Y.I.I. are grateful. T.X.T. and Y.I.I. acknowledge the partial financial support of NSF grant AST-9616863. Y.I.I. thanks the staff of the University of Virginia for their kind hospitality.

REFERENCES

- Allen, D. A., Wright, A. E., & Goss W. M. 1976, MNRAS, 177, 91
- Bergeron, J., 1977, ApJ, 211, 62
- Bohannon, B., & Walborn, N. R. 1989, PASP, 101, 520
- Brocklehurst, M. 1971, MNRAS, 153, 471
- Cerviño, M., & Mas-Hesse, J. M. 1994, A&A, 284, 749
- Conti, P. S. 1991, ApJ, 377, 115
- . 1999, PASP, 111, 251
- Conti, P. S., & Massey, P. 1981, ApJ, 249, 471
- . 1989, ApJ, 337, 251
- Conti, P. S., & Vacca, W. D. 1990, AJ, 100, 431
- Crowther, P. A., & Bohannon, B. 1997, A&A, 317, 532
- Crowther, P. A., De Marco, O., & Barlow, M. J. 1998, MNRAS, 296, 367
- Crowther, P. A., & Dessart, L. 1998, MNRAS, 296, 622
- Crowther, P. A., Hillier, D. J., & Smith, L. J. 1995a, A&A, 293, 172
- Crowther, P. A., & Smith, L. J. 1997, A&A, 320, 500
- Crowther, P. A., Smith, L. J., & Hillier, D. J. 1995b, A&A, 302, 457
- Crowther, P. A., Smith, L. J., Hillier, D. J., & Schmutz, W. 1995c, A&A, 293, 427
- Crowther, P. A., Smith, L. J., & Willis, A. J. 1995d, A&A, 304, 269
- Crowther, P. A., Szeifert, T., Stahl, O., & Zickgraf, F.-J. 1997, A&A, 318, 543
- de Mello, D. F., Schaerer, D., Heldmann, J., & Leitherer, C. 1998, ApJ, 507, 199
- Dinerstein, H. L., & Shields, G. A. 1986, ApJ, 311, 45
- D’Odorico, S., & Rosa, M. 1981, ApJ, 248, 1015
- Dufour, R. J., & Hester, J. J. 1990, ApJ, 350, 149
- Edmunds, M. G., & Pagel, B. E. J. 1984, MNRAS, 211, 507
- Esteban, D. & Peimbert, M. 1995, Rev. Mexicana Astron. Asrtrofis., Ser. Conf., 3, 133
- Garnett, D. R., Kennicutt, R. C., Chu, Y.-H., & Skillman, E. D. 1991, ApJ, 373, 458
- Gonzalez-Delgado, R. M., Perez, E., Tenorio-Tagle, G., Vilchez, J. M., Terlevich, E., Terlevich, R., Telles, E., Rodriguez-Espinosa, J. M., Mas-Hesse, M., Garcia-Vargas, M. L., Diaz, A. I., Cera, J., & Castañeda, H. 1994, ApJ, 437, 239
- Gonzales-Riestra, R., Rego, M., & Zamorano, J. 1987, A&A, 186, 64
- . 1988, A&A, 202, 27
- Grandi, S. A. 1976, ApJ, 206, 658
- Hamman, W.-R., Koesterke, L., & Wessolowski, U. 1995, A&AS, 113, 459
- Huang, J. H., Gu, Q. S., Ji, L., Li, W. D., Wei, J. Y., & Zheng, W. 1999, ApJ, 513, 215
- Izotov, Y. I., Chaffee, F. H., Foltz, C. B., Green, R. F., Guseva, N. G., & Thuan, T. X. 1999a, ApJ, December 20
- Izotov, Y. I., Dyak, A. B., Chaffee, F. H., Foltz, C. B., Kniazev, A. Y., & Lipovetsky, V. A. 1996, ApJ, 458, 524
- Izotov, Y. I., Foltz, C. B., Green, R. F., Guseva, N. G., & Thuan, T. X. 1997, ApJ, 487, L37
- Izotov, Y. I., Lipovetsky, V.A., Guseva, N.G., Kniazev, A. Y., Neizvestny, S. I., & Stepanian, J. A. 1993, Astron. Astrophys. Trans., 3, 193
- Izotov, Y. I., Papaderos, P., Thuan, T. X., Foltz, C. B., Fricke, K. J., & Guseva, N. G. 1999b, A&A, in press
- Izotov, Y. I., & Thuan, T. X. 1998a, ApJ, 497, 227
- . 1998b, ApJ, 500, 188 (IT98)
- . 1999, ApJ, 511, 639
- Izotov, Y. I., Thuan, T. X., & Lipovetsky, V. A. 1994, ApJ, 435, 647 (ITL94)
- . 1997, ApJS, 108, 1 (ITL97)
- Kingsburgh, R. L., Barlow, M. J., & Storey, P. J. 1995, A&A, 295, 75
- Koesterke, L., & Hamann, W.-R. 1995, A&A, 299, 503
- Krüger, H., Fritze-von Alvensleben, U., Fricke, K. J., & Loose, H.-H. 1992, A&A, 259, L73
- Kunth, D., & Joubert, M. 1985, A&A, 142, 411
- Kunth, D., & Sargent, W. L. W. 1981, A&A, 101, L5

- Kunth, D., & Schild, H. 1986, *A&A*, 169, 71
- Legrand, F., Kunth, D., Roy, J.-R., Mas-Hesse, J. M., & Walsh, J. R. 1997, *A&A*, 326, L17
- Leitherer, C. 1990, *ApJS*, 73, 1
- Leuenhagen, U., & Hamann, W.-R. 1994, *A&A*, 283, 567
- . 1998, *A&A*, 330, 265
- Leuenhagen, U., Hamann, W.-R., & Jeffery, C. S. 1996, *A&A*, 312, 167
- Maeder, A. 1991, *A&A*, 242, 93
- Maeder, A., & Meynet, G. 1994, *A&A*, 287, 803
- Markarian, B. E., Lipovetsky, V. A., & Stepanian, J. A. 1983, *Astrophysics*, 19, 14
- Markarian, B. E., Lipovetsky, V. A., Stepanian, J. A., Erastova, L. K., & Shapovalova, A. I. 1989, *Commun. Special Astrophys. Obs. USSR*, 62, 5
- Martin, C. L. 1996, *ApJ*, 465, 680
- . 1997, *ApJ*, 491, 561
- Masegosa, J., Moles, M., & Campos-Aguilar, A. 1994, *ApJ*, 420, 576
- Masegosa, J., Moles, M., & del Olmo, A. 1991, *A&A*, 244, 273
- Mas-Hesse, J. M., & Kunth, D. 1991, *A&AS*, 88, 399
- Massey, P., Armandroff, T. E., & Conti, P. S. 1992, *AJ*, 103, 1159
- Massey, P., & Conti, P. 1980, *ApJ*, 242, 638
- . 1983, *PASP*, 95, 440
- Massey, P., Conti, P. S., & Armandroff, T. E. 1987, *AJ*, 94, 1538
- Massey, P., & Johnson, O. 1998, *ApJ*, 505, 793
- Meynet, G. 1995, *A&A*, 298, 767
- Moffat, A. F. J., Niemela, V. S., Phillips, M. M., Chu, Y.-H., & Seggewiss, W. 1987, *ApJ*, 312, 612
- Ohyama, Y., Taniguchi, Y., & Terlevich, R. 1997, *ApJ*, 480, L9
- Osterbrock, D. E., & Cohen, R. D. 1982, *ApJ*, 261, 64
- Pagel, B. E. J., Edmunds, M. G., Blackwell, D. E., Chun, M. S., & Smith, G. 1979, *MNRAS*, 179, 95
- Papaderos, P., Izotov, Y. I., Fricke, K. J., Thuan, T. X., & Guseva, N. G. 1998, *A&A*, 338, 43
- Phillips, A. C., & Conti, P. S. 1992, *ApJ*, 395, L91
- Pilyugin, L. S. 1994, *A&A*, 287, 387
- Roy, J.-R., Aube, M., McCall, M. L., & Dufour, R. J. 1992, *ApJ*, 386, 498
- Russell, S. C. & Dopita, M. A. 1990, *ApJS*, 74, 93
- Salzer, J. J., MacAlpine, G. M., & Boroson, T. A. 1989, *AJ*, 70, 477
- Schaerer, D. 1996, *ApJ*, 467, L17
- Schaerer, D., Contini, T., Kunth, D., & Meynet, G. 1997, *ApJ*, 481, L75
- Schaerer, D., Contini, T., & Kunth, D. 1999a, *A&A*, 341, 399
- Schaerer, D., Contini, T., & Pindao, M. 1999b, *A&AS*, 136, 35
- Schaerer, D., & de Koter, A. 1997, *A&A*, 322, 598
- Schaerer, D., & Vacca, W. D. W. 1996, in: *WR stars in the Framework of Stellar evolution*, 33rd Liege Int. Astroph. Coll., Eds. Vreux et al., p. 641
- . 1998, *ApJ*, 497, 618 (SV98)
- Schild, H., Smith, L. J., & Willis, A. J. 1990, *A&A*, 237, 169
- Smith, L. F. 1991, in *IAU Symp. 143, Wolf-Rayet Stars and Interrelations with Other Stars in Galaxies*, ed. K.A. van der Hucht & B. Hidayat (Dordrecht: Kluwer), 601
- Smith, L. F., & Maeder, A. 1991, *A&A*, 241, 77
- Smith, L. F., Shara, M. M., & Moffat, A. F. G. 1990a, *ApJ*, 348, 471
- . 1990b, *ApJ*, 358, 229
- . 1996, *MNRAS*, 281, 163
- Smith, L. J., Crowther, P. A., & Willis, A. J. 1995, *ApJ*, 302, 830
- Stasińska, G. 1990, *A&AS*, 83, 501
- Thuan, T. X., Izotov, Y. I., & Lipovetsky, V. A. 1995, *ApJ*, 445, 108
- . 1996, *ApJ*, 463, 120
- . 1997, *ApJ*, 477, 661
- Torres, A. V., & Conti, P. S. 1984, *ApJ*, 280, 181
- Vacca, W. D. 1994, *ApJ*, 421, 140
- Vacca, W. D., & Conti, P. S. 1992, *ApJ*, 401, 543
- van Zee, L., Salzer, J. J., Haynes, M. P., O'Donoghue, A. A., & Balonek, T. J. 1998, *AJ*, 116, 2805

- Vílchez, J. M., & Iglesias-Páramo, J. 1998, ApJ, 508, 248
- Walsh, J. R., & Roy, J.-R. 1993, MNRAS, 262, 27
- Whitford, A. E. 1958, AJ, 63, 201
- Willis, A. J., Schild, H., & Smith, L. J. 1992, A&A, 261, 419
- Zwicky, F., Herzog, E., Wild, P., Karpovicz, M., & Kowal, C. T., 1961-1968, Catalogue of galaxies and cluster of galaxies, vv. 1-6. Calif. Inst. of Technology, Pasadena

TABLE 1
GENERAL PARAMETERS OF GALAXIES

Galaxy	$\alpha(1950.0)$	$\delta(1950.0)$	m_{pg}	M_{pg}	z	$12 + \log(O/H)$	Other name
0112-011	1 13 00.5	-01 07 22	17.0	-14.8	0.00570	8.31	UM 311
0207-105	2 07 50.2	-10 33 19	15.0	-18.6	0.01338	9.04 ^a	Mrk 1026, NGC 848
0211+038	2 11 08.7	+03 52 08	14.3	-19.0	0.01148	8.99 ^a	Mrk 589, UGC 1716
0218+003	2 18 20.4	+00 19 42	16.5	-20.3	0.05844	7.93	UM 420
0252-102	2 52 08.0	-10 13 46	13.0	-18.5	0.00501	8.46 ^a	Mrk 1063, NGC 1140
0459-043	4 59 09.4	-04 19 43	15.0	-18.7	0.01343	8.04	Mrk 1089, NGC 1741
0553+033	5 53 04.9	+03 23 07	15.5	-14.5	0.00249	8.09	II Zw 40, UGCA 116
0635+756	6 35 24.4	+75 40 14	17.0	-13.1	0.00264	8.04	Mrk 5, UGCA 130
0720+335	7 20 28.5	+33 32 24	13.7	-20.0	0.01353	9.13 ^a	Mrk 1199, UGC 3829
0723+692	7 23 23.7	+69 17 33	11.6	-16.1	0.00036	7.85	Mrk 71, NGC 2363
0842+162	8 42 45.3	+16 16 46	15.7	-20.9	0.05303	8.60 ^a	Mrk 702, PG 0842+162
0926+606	9 26 20.0	+60 40 02	17.5	-16.2	0.01371	7.91	
0930+554	9 30 30.3	+55 27 46	17.6	-13.9 ^b	0.00274	7.16	I Zw 18, Mrk 116, UGCA 166
0946+558	9 46 03.1	+55 48 46	15.6	-16.0	0.00525	8.00	Mrk 22, UGCA 184
0947+008	9 47 19.9	+00 51 00	13.5	-18.5	0.00626	8.07	Mrk 1236
0948+532	9 48 10.2	+53 13 41	18.0	-18.3	0.04629	8.00	
0952+095	9 52 10.2	+09 30 32	13.5	-18.0	0.00494	9.03 ^a	Mrk 710, NGC 3049, UGC 5325
1030+583	10 30 56.3	+58 19 20	16.5	-15.9	0.00757	7.79	Mrk 1434
1036-069	10 36 03.0	-06 54 37	13.5	-18.8	0.00718	8.95	Mrk 1259, IC 630
1053+064	10 53 33.3	+06 26 24	14.8	-15.9	0.00339	7.99	Mrk 1271
1054+365	10 54 59.8	+36 31 30	16.0	-13.5	0.00198	7.97	CG 798
1130+495	11 30 45.2	+49 30 43	13.9	-13.5	0.00074	7.82	Mrk 178, UGC 6541
1134+202	11 34 17.7	+20 12 14	17.0	-17.6	0.02083	8.74 ^a	Mrk 182
1135+581	11 35 51.3	+58 09 04	15.5	-15.2	0.00340	7.98	Mrk 1450, PG 1136+581
1139+006	11 39 38.5	+00 36 42	13.7	-20.6	0.01830	7.99	UM 448, Mrk 1304, UGC 6665
1140-080	11 40 24.6	-08 03 18	15.5	-17.6	0.01033	8.72 ^a	Mrk 1305, IC 723
1147+153	11 47 28.1	+15 18 05	15.4	-14.5	0.00243	8.11	Mrk 750
1150-021	11 50 03.8	-02 11 28	14.1	-16.6	0.00342	7.95	UM 462, Mrk 1307, UGC 6850
1152+579	11 52 51.9	+57 56 34	16.5	-17.9	0.01930	7.81	Mrk 193
1211+540	12 11 33.9	+54 01 58	17.8	-12.7	0.00308	7.64	
1222+614	12 22 44.5	+61 25 46	17.0	-12.9	0.00243	7.95	
1223+487	12 23 50.6	+48 46 07	15.3	-12.6	0.00096	7.77	Mrk 209, UGCA 281, I Zw 36
1234+072	12 34 29.9	+07 11 59	14.6	-17.0	0.00533	8.23	Mrk 1329, IC 3591, UGC 7790
1249+493	12 49 35.6	+49 19 43	18.8	-16.1	0.02430	7.72	
1256+351	12 56 38.2	+35 06 50	12.8	-17.4	0.00272	7.99	Mrk 59, NGC 4861, UGC 8098
1319+579A	13 19 25.2	+57 57 09	18.5	-13.6	0.00650	8.11	
1437+370	14 37 03.0	+37 01 07	17.0	-11.7	0.00137	7.93	Mrk 475, CG 493
1533+574B	15 33 03.3	+57 27 04	15.5	-17.8	0.01143	8.11	VII Zw 611
2329+286	23 29 29.5	+28 40 18	15.0	-19.3	0.01847	8.06	Mrk 930, PG 2329+286

^athe [O III] λ 4363 emission line is not detected. The oxygen abundance is derived using the calibration by van Zee et al. (1998) (see text).

^bthe distance of 20 Mpc is adopted (Izotov et al. 1999b).

TABLE 2
JOURNAL OF OBSERVATIONS

Galaxy	Telescope	Date	Number of Exposures	Exposure Time (minutes)	Airmass	P.A. (deg)
0112-011	2.1m	12/12/96	3	60	1.2	90
0207-105 ¹	2.1m	14/12/96	2	10	1.4	90
0211+038 ¹	2.1m	16/12/96	5	60	1.2	90
0218+038	2.1m	16/12/96	3	60	1.2	90
0252-102 ¹	2.1m	15/12/96	3	15	1.4	90
0459-043	2.1m	17/12/96	2	40	1.6	90
0553+033 ¹	2.1m	14,17/12/96	6	120	1.2	90
0635+756	2.1m	16/12/96	3	60	1.4	90
0720+335	2.1m	19/02/96	3	60	1.1	90
0723+692	4m	18/03/94	6	29	1.3	77
0842+162 ¹	2.1m	16/12/96	3	60	1.3	90
0926+606	4m	17/03/94	3	45	1.2	115
0930+554	MMT	29,30/04/97	6	180	1.2	139
0946+558	4m	23/03/93	2	30	1.2	90
0947+008 ¹	2.1m	19/12/96	2	40	1.2	90
0948+532	4m	24/03/93	1	15	1.2	90
0952+095 ¹	2.1m	14,16/12/96	4	60	1.4	90
1030+583	4m	16/03/94	2	30	1.1	92
1036-069 ¹	2.1m	19/02/96	4	20	1.4	91
1053+064	2.1m	15/12/96	3	60	1.6	90
1054+365	4m	18/03/94	3	45	1.0	97
1130+495 ¹	2.1m	17/12/96	3	55	1.1	133
1134+202 ¹	2.1m	18/02/96	2	10	1.0	91
1135+581	4m	24/03/93	3	30	1.2	90
1139+006	2.1m	16/12/96	2	40	1.6	90
1140-080 ¹	2.1m	17/02/96	2	10	1.3	35
1147+153	2.1m	17/12/96	2	30	1.1	90
1150-021	2.1m	16/12/96	3	60	1.3	62
1152+579	4m	24/03/93	3	45	1.1	90
1211+540	4m	23/03/93	3	60	1.1	90
1222+614	4m	16/03/94	3	45	1.2	90
1223+487	4m	17/03/94	4	55	1.1	145
1234+072 ¹	2.1m	18/02/96	2	30	1.4	91
1249+493	4m	23/03/93	3	55	1.1	90
1256+351	4m	17/03/94	8	70	1.0	59
1319+579A	4m	18/03/94	2	45	1.1	44
1437+370	4m	24/03/93	2	35	1.1	90
1533+574B	4m	16/03/94	3	45	1.1	112
2329+286	2.1m	16/12/96	3	60	1.0	90

¹Galaxies with not yet published data. The data for other galaxies are appeared in ITL94, ITL97, Izotov et al. 1997, IT98, Thuan et al. 1995.

TABLE 3
EMISSION LINE INTENSITIES

Ion	0207-105≡Mrk 1026		0211+038≡Mrk 589		0252-102≡Mrk 1063		0553+033≡II Zw 40	
	$F(\lambda)/F(H\beta)$	$I(\lambda)/I(H\beta)$	$F(\lambda)/F(H\beta)$	$I(\lambda)/I(H\beta)$	$F(\lambda)/F(H\beta)$	$I(\lambda)/I(H\beta)$	$F(\lambda)/F(H\beta)$	$I(\lambda)/I(H\beta)$
3727 [O II]	2.154±0.201	1.120±0.246	1.323±0.025	2.001±0.045	2.268±0.031	2.082±0.037	0.369±0.005	0.839±0.012
3750 H12	0.013±0.002	0.029±0.006
3770 H11	0.017±0.002	0.039±0.006
3798 H10	0.028±0.002	0.060±0.006
3835 H9	0.033±0.002	0.069±0.006
3868 [Ne III]	0.293±0.012	0.266±0.013	0.288±0.005	0.583±0.010
3889 He I + H8	0.092±0.003	0.184±0.007
3968 [Ne III] + H7	0.031±0.006	0.223±0.070	0.190±0.004	0.356±0.008
4026 He I	0.014±0.002	0.025±0.004
4101 H δ	0.086±0.010	0.242±0.038	0.076±0.009	0.279±0.051	0.152±0.004	0.258±0.007
4340 H γ	0.309±0.012	0.472±0.025	0.290±0.010	0.461±0.023	0.345±0.005	0.490±0.008
4363 [O III]	0.078±0.003	0.109±0.004
4471 He I	0.034±0.009	0.029±0.009	0.033±0.002	0.043±0.003
4658 [Fe III]	0.006±0.001	0.007±0.002
4686 He II	0.014±0.002	0.016±0.003
4713 [Ar IV] + He I	0.022±0.002	0.024±0.003
4740 [Ar IV]	0.014±0.002	0.015±0.002
4861 H β	1.000±0.120	1.000±0.294	1.000±0.021	1.000±0.025	1.000±0.017	1.000±0.022	1.000±0.010	1.000±0.010
4921 He I	0.010±0.002	0.010±0.002
4959 [O III]	0.525±0.103	0.237±0.102	0.267±0.014	0.232±0.013	1.039±0.017	0.851±0.017	2.618±0.021	2.462±0.021
5007 [O III]	0.944±0.120	0.424±0.119	0.672±0.017	0.574±0.017	3.072±0.036	2.507±0.036	8.113±0.060	7.409±0.056
5518 [Cl III]	0.007±0.001	0.004±0.001
5538 [Cl III]	0.004±0.001	0.002±0.001
5876 He I	0.118±0.079	0.049±0.072	0.152±0.011	0.096±0.008	0.150±0.009	0.115±0.008	0.151±0.003 ^a	0.086±0.002 ^a
6300 [O I]	0.081±0.012	0.045±0.007	0.047±0.008	0.035±0.007	0.034±0.003	0.016±0.001
6312 [S III]	0.034±0.002	0.016±0.001
6563 H α	6.124±0.533	2.882±0.604	5.476±0.085	2.892±0.055	3.771±0.048	2.882±0.049	6.975±0.052	2.872±0.024
6583 [N II]	2.696±0.249	1.065±0.234	1.887±0.033	0.975±0.021	0.385±0.010	0.283±0.009	0.155±0.004	0.063±0.002
6678 He I	0.054±0.012	0.027±0.007	0.048±0.008	0.035±0.007	0.081±0.003	0.032±0.001
6717 [S II]	1.304±0.148	0.511±0.135	0.583±0.017	0.291±0.010	0.396±0.011	0.289±0.010	0.173±0.004	0.067±0.002
6731 [S II]	1.118±0.142	0.437±0.128	0.562±0.017	0.280±0.010	0.295±0.010	0.215±0.009	0.140±0.004	0.054±0.001
7065 He I	0.019±0.008	0.009±0.004	0.028±0.007	0.020±0.006	0.126±0.003	0.042±0.001
7135 [Ar III]	0.111±0.011	0.050±0.006	0.087±0.007	0.062±0.006	0.235±0.004	0.077±0.001
$C(H\beta)$ dex	0.19±0.11		0.73±0.02		0.15±0.02		1.16±0.01	
$F(H\beta)$ ^b	0.8±0.1		1.2±0.1		6.7±0.1		9.1±0.1	
$EW(H\beta)$ Å	4.9±0.4		18.0±0.3		20.1±0.2		278±2	
$EW(abs)$ Å	5.8±0.4		1.9±0.2		4.3±0.2		0.1±0.4	

TABLE 3—Continued

Ion	0842+162≡Mrk 702		0947+008≡Mrk 1236		0952+095≡Mrk 710		1036-069≡Mrk 1259	
	$F(\lambda)/F(\text{H}\beta)$	$I(\lambda)/I(\text{H}\beta)$	$F(\lambda)/F(\text{H}\beta)$	$I(\lambda)/I(\text{H}\beta)$	$F(\lambda)/F(\text{H}\beta)$	$I(\lambda)/I(\text{H}\beta)$	$F(\lambda)/F(\text{H}\beta)$	$I(\lambda)/I(\text{H}\beta)$
3727 [O II]	2.104±0.051	2.221±0.062	1.539±0.018	1.513±0.019	0.979±0.019	1.261±0.027	1.463±0.010	2.103±0.016
3750 H12	0.019±0.004	0.088±0.020
3770 H11	0.027±0.004	0.103±0.017
3798 H10	0.032±0.005	0.110±0.020
3835 H9	0.035±0.004	0.109±0.014
3868 [Ne III]	0.219±0.017	0.226±0.019	0.302±0.007	0.296±0.007	0.021±0.009	0.026±0.012
3889 He I + H8	0.072±0.012	0.193±0.044	0.138±0.005	0.210±0.009	0.064±0.008	0.170±0.029
3968 [Ne III] + H7	0.090±0.013	0.207±0.040	0.208±0.006	0.279±0.009	0.049±0.008	0.149±0.034
4026 He I	0.016±0.007	0.019±0.009
4101 H δ	0.153±0.014	0.271±0.033	0.198±0.006	0.259±0.008	0.145±0.009	0.249±0.020	0.144±0.004	0.254±0.009
4340 H γ	0.365±0.017	0.460±0.028	0.401±0.007	0.447±0.009	0.365±0.011	0.470±0.018	0.355±0.005	0.467±0.008
4363 [O III]	0.045±0.004	0.043±0.004
4471 He I	0.041±0.014	0.039±0.015	0.028±0.004	0.027±0.004	0.021±0.007	0.022±0.008	0.033±0.004	0.036±0.004
4658 [Fe III]	0.012±0.008	0.012±0.008
4686 He II	0.012±0.005	0.011±0.005
4713 [Ar IV] + He I
4740 [Ar IV]
4861 H β	1.000±0.029	1.000±0.033	1.000±0.013	1.000±0.013	1.000±0.018	1.000±0.021	1.000±0.007	1.000±0.008
4921 He I
4959 [O III]	1.011±0.029	0.922±0.029	1.463±0.017	1.395±0.017	0.124±0.008	0.114±0.008	0.563±0.005	0.522±0.005
5007 [O III]	3.074±0.070	2.772±0.069	4.341±0.042	4.134±0.042	0.355±0.011	0.322±0.011	1.656±0.011	1.515±0.010
5518 [Cl III]
5538 [Cl III]
5876 He I	0.154±0.013	0.128±0.011	0.119±0.004	0.112±0.004	0.138±0.008	0.104±0.007	0.172±0.004	0.124±0.003
6300 [O I]	0.106±0.012	0.085±0.011	0.031±0.003	0.029±0.003	0.056±0.004	0.037±0.003
6312 [S III]	0.021±0.005	0.020±0.004	0.030±0.006	0.020±0.004
6563 H α	3.607±0.080	2.883±0.076	3.048±0.031	2.847±0.033	4.277±0.058	2.888±0.046	4.659±0.026	2.889±0.019
6583 [N II]	0.490±0.020	0.384±0.017	0.149±0.005	0.138±0.005	1.611±0.025	1.074±0.019	1.427±0.010	0.875±0.007
6678 He I	0.050±0.011	0.039±0.009	0.044±0.004	0.041±0.003	0.037±0.006	0.024±0.005	0.058±0.003	0.035±0.002
6717 [S II]	0.428±0.018	0.333±0.016	0.205±0.006	0.189±0.006	0.488±0.012	0.319±0.009	0.332±0.005	0.198±0.003
6731 [S II]	0.325±0.016	0.252±0.014	0.142±0.005	0.132±0.005	0.428±0.011	0.279±0.008	0.344±0.005	0.205±0.003
7065 He I	0.019±0.008	0.015±0.006	0.031±0.003	0.029±0.003	0.031±0.006	0.019±0.004	0.050±0.003	0.028±0.002
7135 [Ar III]	0.100±0.004	0.092±0.004	0.055±0.006	0.034±0.004	0.086±0.003	0.048±0.002
$C(\text{H}\beta)$ dex	0.20±0.03		0.04±0.01		0.45±0.02		0.58±0.01	
$F(\text{H}\beta)^b$	2.6±0.1		10.7±0.1		1.2±0.1		40.6±0.2	
$EW(\text{H}\beta)$ Å	36.6±0.7		118±1		35.9±0.5		36.3±0.2	
$EW(\text{abs})$ Å	3.4±0.4		5.5±0.2		2.3±0.3		1.7±0.1	

TABLE 3—Continued

Ion	1130+495≡Mrk 178		1134+202≡Mrk 182		1140-080≡Mrk 1305		1234+072≡Mrk 1329	
	$F(\lambda)/F(H\beta)$	$I(\lambda)/I(H\beta)$	$F(\lambda)/F(H\beta)$	$I(\lambda)/I(H\beta)$	$F(\lambda)/F(H\beta)$	$I(\lambda)/I(H\beta)$	$F(\lambda)/F(H\beta)$	$I(\lambda)/I(H\beta)$
3727 [O II]	1.167±0.029	1.264±0.035	2.168±0.059	2.659±0.078	4.198±0.134	4.022±0.170	1.116±0.008	1.152±0.008
3750 H12
3770 H11	0.041±0.002	0.048±0.003
3798 H10	0.048±0.002	0.056±0.003
3835 H9	0.061±0.002	0.070±0.003
3868 [Ne III]	0.427±0.019	0.454±0.022	0.181±0.030	0.170±0.035	0.376±0.004	0.386±0.004
3889 He I + H8	0.055±0.014	0.175±0.059	0.122±0.015	0.153±0.027	0.173±0.003	0.184±0.003
3968 [Ne III] + H7	0.166±0.016	0.214±0.022	0.077±0.014	0.097±0.025	0.268±0.003	0.281±0.004
4026 He I	0.013±0.002	0.014±0.002
4101 H δ	0.140±0.013	0.246±0.031	0.193±0.017	0.228±0.027	0.250±0.003	0.261±0.004
4340 H γ	0.393±0.017	0.481±0.026	0.439±0.021	0.483±0.028	0.293±0.028	0.463±0.067	0.475±0.004	0.485±0.005
4363 [O III]	0.119±0.015	0.119±0.016	0.046±0.002	0.046±0.002
4471 He I	0.043±0.002	0.044±0.002
4658 [Fe III]
4686 He II
4713 [Ar IV] + He I
4740 [Ar IV]
4861 H β	1.000±0.024	1.000±0.027	1.000±0.032	1.000±0.034	1.000±0.043	1.000±0.059	1.000±0.007	1.000±0.007
4921 He I	0.011±0.001	0.011±0.001
4959 [O III]	1.982±0.040	1.843±0.040	0.363±0.018	0.356±0.018	1.146±0.048	0.925±0.048	1.835±0.011	1.823±0.011
5007 [O III]	5.906±0.105	5.466±0.104	1.067±0.034	1.038±0.033	2.968±0.098	2.382±0.097	5.526±0.028	5.485±0.028
5518 [Cl III]
5538 [Cl III]
5876 He I	0.157±0.012 ^c	0.134±0.011 ^c	0.144±0.017	0.124±0.015	0.188±0.027	0.137±0.024	0.116±0.002 ^d	0.113±0.002 ^d
6300 [O I]	0.098±0.029	0.069±0.025	0.015±0.002	0.014±0.001
6312 [S III]	0.019±0.001	0.018±0.001
6563 H α	3.436±0.063	2.793±0.059	3.628±0.091	2.884±0.079	4.018±0.128	2.883±0.124	2.983±0.016	2.863±0.017
6583 [N II]	0.071±0.012	0.057±0.011	0.688±0.026	0.545±0.022	0.758±0.051	0.520±0.044	0.077±0.002	0.074±0.002
6678 He I	0.045±0.012	0.036±0.011	0.035±0.001	0.034±0.001
6717 [S II]	0.198±0.011	0.158±0.009	0.330±0.035	0.258±0.028	0.614±0.039	0.417±0.033	0.092±0.002	0.088±0.002
6731 [S II]	0.152±0.014	0.122±0.012	0.195±0.019	0.152±0.015	0.503±0.048	0.341±0.040	0.071±0.002	0.068±0.002
7065 He I	0.028±0.001	0.026±0.001
7135 [Ar III]	0.111±0.009	0.086±0.007	0.067±0.014	0.050±0.010	0.203±0.027	0.134±0.022	0.097±0.002	0.092±0.002
$C(H\beta)$ dex	0.20±0.02		0.30±0.03		0.23±0.04		0.05±0.01	
$F(H\beta)$ ^b	1.3±0.1		1.4±0.1		1.9±0.1		12.4±0.1	
$EW(H\beta)$ Å	24.3±0.4		54.2±1.2		8.5±0.3		276±1	
$EW(abs)$ Å	1.6±0.2		0.3±0.6		1.9±0.2		1.0±0.2	

^ais affected by Galactic neutral sodium absorption.^bin units of 10^{-14} ergs $s^{-1}cm^{-2}$.^cis affected by strong WR C IV $\lambda 5808$ emission.^dis affected by bad CCD column.

TABLE 4
HEAVY ELEMENT ABUNDANCES

Property	II Zw 40	Mrk 1236	Mrk 178	Mrk 1329
$T_e(\text{O III})(\text{K})$	13,400±190	11,700±390	15,800±1,000	10,900±150
$T_e(\text{O II})(\text{K})$	12,900±180	12,000±360	14,100± 860	11,500±140
$T_e(\text{S III})(\text{K})$	13,200±160	11,900±320	14,800± 840	11,200±130
$N_e(\text{S II})(\text{cm}^{-3})$	190±50	10±10	100±160	130±40
$\text{O}^+/\text{H}^+(\times 10^5)$	0.85±0.02	2.73±0.27	1.33±0.23	2.47±0.11
$\text{O}^{++}/\text{H}^+(\times 10^4)$	1.24±0.03	0.88±0.09	0.52±0.08	1.46±0.06
$\text{O}^{+++}/\text{H}^+(\times 10^5)$	0.19±0.03	0.10±0.04
$\text{O}/\text{H}(\times 10^4)$	1.22±0.04	1.16±0.09	0.66±0.09	1.71±0.06
$12 + \log(\text{O}/\text{H})$	8.09±0.02	8.07±0.03	7.82±0.06	8.23±0.02
$\text{N}^+/\text{H}^+(\times 10^6)$	0.63±0.03	1.62±0.16	0.48±0.08	0.96±0.04
ICF(N)	10.3	4.26	4.95	6.90
$\log(\text{N}/\text{O})$	-1.27±0.03	-1.23±0.08	-1.45±0.13	-1.41±0.04
$\text{Ne}^{++}/\text{H}^+(\times 10^5)$	2.01±0.09	1.58±0.17	0.95±0.16	2.70±0.13
ICF(Ne)	1.13	1.32	1.25	1.17
$\log(\text{Ne}/\text{O})$	-0.73±0.03	-0.75±0.07	-0.74±0.11	-0.73±0.03
$\text{S}^+/\text{H}^+(\times 10^6)$	0.16±0.01	0.48±0.03	0.31±0.03	0.26±0.01
$\text{S}^{++}/\text{H}^+(\times 10^6)$	1.21±0.10	2.20±0.54	...	2.51±0.21
ICF(S)	2.49	1.47	...	1.90
$\log(\text{S}/\text{O})$	-1.55±0.03	-1.47±0.08	...	-1.51±0.03
$\text{Ar}^{++}/\text{H}^+(\times 10^6)$	0.35±0.01	0.51±0.03	0.32±0.04	0.58±0.02
$\text{Ar}^{+3}/\text{H}^+(\times 10^6)$	0.29±0.04
ICF(Ar)	1.01	1.76	1.90	2.26
$\log(\text{Ar}/\text{O})$	-2.27±0.03	-2.11±0.04	-2.04±0.07	-2.12±0.02
$\text{Fe}^{++}/\text{H}^+(\times 10^6)$	0.19±0.05	0.41±0.30
ICF(Fe)	12.8	5.32
$\log(\text{Fe}/\text{O})$	-1.70±0.03	-1.72±0.14
[O/Fe]	0.28±0.03	0.30±0.14

TABLE 5
PARAMETERS OF H II REGIONS

Galaxy	$C(\text{H}\beta)$	$F(\text{H}\beta)^{\text{a,c}}$	C_{cor}	$F_{\text{cor}}(\text{H}\beta)^{\text{b,c}}$	$EW(\text{H}\beta)$	Age ^d	η_0
0112-011	0.15	15.8	2.06	32.6	252.2	4.2	0.40
0211+038	0.72	38.7	2.24	86.9	17.9	5.8	... ^e
0218+003	0.31	5.7	1.78	10.2	99.8	4.5	0.30
0252-102	0.16	16.7	3.11	52.0	21.8	6.0	0.30
0459-043	0.28	31.6	4.90	155.0	56.1	4.8	0.25
0553+033	1.20	238.0	2.86	680.0	272.2	4.0	0.50
0635+756	0.42	11.6	2.17	25.2	118.6	4.2	0.45
0720+335	0.55	44.5	2.06	91.7	20.3	5.5	... ^e
0723+692	0.12	114.0	5.05	576.0	264.4	3.6	0.85
0842+162	0.20	4.5	2.64	11.9	35.0	5.3	1.00
0926+606	0.18	6.5	3.60	23.4	108.6	4.4	0.35
0930+554	0.13	3.9	2.18	8.5	67.0	5.9	0.20
0946+558	0.18	6.3	2.24	14.1	99.5	4.5	0.40
0947+008	0.04	16.1	3.80	61.1	124.3	4.1	0.50
0948+532	0.04	4.1	2.00	8.1	169.8	3.9	0.65
0952+095	0.52	21.9	2.30	52.6	33.0	5.3	... ^e
1030+583	0.03	3.7	2.55	9.4	84.1	4.7	0.35
1036-069	0.60	210.0	2.13	448.0	32.1	5.3	... ^e
1053+064	0.16	13.6	2.62	35.7	78.0	4.7	0.30
1054+365	0.05	9.1	2.70	24.6	64.3	4.8	0.25
1130+495	0.21	4.0	5.02	19.9	20.1	8.0	0.10
1135+581	0.14	29.9	2.25	67.4	116.5	4.2	0.50
1139+006	0.34	56.5	4.05	229.0	48.9	5.3	0.20
1147+153	0.14	25.2	2.16	54.4	130.1	4.3	0.35
1150-021	0.29	37.7	6.02	227.0	87.8	4.6	0.30
1211+540	0.10	3.0	2.04	6.0	115.1	4.0	0.50
1222+614	0.00	9.3	3.37	31.2	85.2	4.6	0.30
1223+487	0.06	17.2	3.10	53.4	206.2	3.9	0.70
1234+072	0.05	17.2	2.00	34.4	166.5	4.2	0.45
1256+351	0.09	22.1	3.80	84.1	144.1	4.1	0.50
1319+579A	0.01	5.1	2.07	10.6	173.0	4.1	0.50
1437+370	0.14	8.4	3.17	26.6	127.4	4.1	0.50
2329+286	0.26	13.4	2.46	33.0	90.4	4.7	0.30

^aflux measured along the slit and corrected for extinction.

^btotal flux after correction for extinction and aperture: $F_{\text{cor}}(\text{H}\beta) = C_{\text{cor}}F(\text{H}\beta)$.

^cin units of 10^{-14} ergs $\text{cm}^{-2}\text{s}^{-1}$.

^din Myr.

^eparameter η_0 is undefined (see text).

TABLE 6
PARAMETERS OF WR EMISSION LINES

Galaxy	blue bump ($\lambda 4650$)		red bump ($\lambda 5808$)		N III $\lambda 4512$		Si III $\lambda 4565$	
	F^a	EW^b	F^a	EW^b	F^a	EW^b	F^a	EW^b
0112-011	1.04±0.02	17.58±0.31	0.22±0.01	6.28±0.43	0.03±0.01	0.39±0.15	0.16±0.01	2.49±0.24
0211+038	9.25±0.37	3.75±0.15	1.51±0.21	1.06±0.15	2.00±0.58	0.75±0.22	0.86±0.50	0.33±0.19
0218+003	0.38±0.03	9.25±0.76	0.22±0.03	8.17±1.20	0.10±0.03	2.31±0.68
0252-102	3.37±0.09	5.09±0.14	0.86±0.09	1.98±0.20	0.43±0.08	0.63±0.12
0459-043	1.50±0.05	7.81±0.26	0.21±0.05	1.27±0.27	0.57±0.09	1.75±0.26	0.29±0.11	0.92±0.34
0553+033	24.22±0.35	15.63±0.36	3.16±0.26	3.50±0.29	1.91±0.38	1.16±0.23
0635+756	1.39±0.05	14.06±0.47	0.20±0.04	3.08±0.60	0.09±0.04	0.90±0.42
0720+335	16.80±0.57	6.61±0.30	3.57±0.14	2.79±0.19	3.48±0.35	1.24±0.15	2.75±0.30	1.02±0.11
0723+692	1.66±0.02	5.58±0.07	0.52±0.02	3.15±0.15	0.10±0.01	0.29±0.05	0.29±0.02	0.94±0.06
0842+162	0.60±0.05	4.60±0.42	0.13±0.04	1.67±0.51	0.07±0.04	0.52±0.32
0926+606	0.27±0.01	4.84±0.18	0.04±0.01	1.26±0.23	0.04±0.02	0.63±0.17
0930+554	0.31±0.02	4.64±0.20	0.08±0.01	2.14±0.23	0.06±0.01	0.84±0.14	0.05±0.01	0.69±0.12
0946+558	0.35±0.02	5.52±0.30	0.05±0.01	1.06±0.25	0.07±0.03	0.97±0.22
0947+008	0.71±0.03	7.47±0.31	0.19±0.03	3.29±0.49	0.06±0.04	0.60±0.37	0.17±0.04	1.65±0.36
0948+532	0.22±0.01	9.04±0.50	0.05±0.01	3.36±0.60	0.03±0.01	1.02±0.27
0952+095	5.75±0.16	9.37±0.26	1.14±0.03	3.57±0.18	0.90±0.13	1.34±0.37	0.26±0.02	0.39±0.03
1030+583	0.24±0.01	5.04±0.14	0.04±0.01	1.69±0.22	0.03±0.01	0.64±0.21
1036-069	57.45±0.73	8.62±0.11	6.22±0.46	1.85±0.14	17.81±1.99	2.16±0.11	4.19±1.60	0.47±0.06
1053+064	1.29±0.03	7.44±0.16	0.06±0.02	0.48±0.16	0.18±0.05	0.94±0.14	0.20±0.06	0.94±0.14
1054+365	0.43±0.01	6.80±0.18	0.06±0.02	0.91±0.14
1130+495	1.54±0.02	15.92±0.50	0.57±0.02	10.51±0.84
1135+581	2.25±0.03	8.78±0.12	0.67±0.03	4.03±0.18	0.07±0.02	0.26±0.07	0.18±0.05	0.68±0.18
1139+006	4.56±0.16	5.75±0.20	1.88±0.17	2.51±0.23	0.97±0.26	0.82±0.21	1.08±0.33	0.91±0.28
1147+153	1.77±0.05	8.94±0.24	0.30±0.04	2.62±0.32	0.24±0.04	1.13±0.20
1150-021	1.50±0.04	3.74±0.14	0.07±0.02	0.32±0.11	0.23±0.09	0.45±0.11
1211+540	0.16±0.01	5.78±0.28	0.01±0.01	0.89±0.23	0.02±0.01	0.63±0.18
1222+614	0.63±0.01	6.18±0.10	0.23±0.01	3.60±0.17	0.02±0.01	0.22±0.11	0.05±0.01	0.50±0.12
1223+487	0.43±0.01	5.01±0.10	0.08±0.01	1.74±0.15	0.02±0.01	0.15±0.06	0.05±0.01	0.53±0.06
1234+072	0.69±0.03	10.00±0.42	0.06±0.02	1.42±0.45	0.07±0.05	0.96±0.32
1256+351	1.08±0.01	7.14±0.57	0.29±0.01	3.56±0.10	0.04±0.01	0.25±0.04	0.09±0.01	0.56±0.04
1319+579A	0.15±0.01	6.50±0.23	0.06±0.01	4.14±0.38	0.01±0.01	0.57±0.20	0.03±0.01	1.36±0.21
1437+370	0.56±0.01	12.83±0.38	0.25±0.02	6.08±0.40	0.04±0.01	0.97±0.31
2329+286	0.39±0.04	2.53±0.28	0.31±0.04	3.24±0.38	0.10±0.03	0.62±0.17	0.15±0.06	0.96±0.22

^aflux corrected for extinction in units of 10^{-14} erg s⁻¹ cm⁻².

^bin Å.

TABLE 7
NUMBERS OF MASSIVE STARS

Galaxy	$N(\text{O})$	$N(\text{WNL})$			$N(\text{WCE})$	$N(\text{WR})/N(\text{O}+\text{WR})^{\text{a}}$	$N(\text{WC})/N(\text{WN})^{\text{a}}$
		$\lambda 4650$	$\lambda 4512$	$\lambda 4565$			
0112–011	10038.6	209.6	25.7	147.4	45.6	0.025±0.001	0.218±0.018
0211+038	0.0 ^b	6508.1	7634.1	3281.0	1277.6	1.000 ^b	0.196±0.032
0218+003	419093.2	504.2	...	10026.1	4702.2	0.034±0.007	0.469±0.156
0252–102	15546.9	461.0	...	309.4	137.5	0.037±0.003	0.298±0.041
0459–043	441985.6	1977.9	2993.4	1516.2	246.5	0.005±0.001	0.125±0.028
0553+033	31497.3	1125.0	...	343.8	125.5	0.038±0.001	0.112±0.010
0635+756	1397.1	70.5	...	19.2	8.9	0.054±0.004	0.127±0.027
0720+335	0.0 ^b	14526.5	18452.0	14574.0	4179.1	1.000 ^b	0.288±0.020
0723+692	2082.2	5.7	2.1	6.5	2.6	0.004±0.001	0.453±0.034
0842+162	122502.4	10002.0	...	5691.0	2426.3	0.092±0.019	0.243±0.096
0926+606	49483.1	368.0	...	218.9	47.0	0.008±0.001	0.128±0.026
0930+554	3996.3 ^c	43.6 ^c	45.0 ^c	36.0 ^c	12.0 ^c	0.014±0.001	0.276±0.044
0946+558	3723.4	68.2	55.5	...	9.4	0.020±0.002	0.137±0.036
0947+008	18923.0	145.0	70.3	187.4	47.5	0.010±0.001	0.328±0.068
0948+532	102938.3	2707.7	...	1617.6	709.0	0.032±0.004	0.262±0.062
0952+095	0.0 ^b	687.7	633.7	180.2	178.0	1.000 ^b	0.259±0.013
1030+583	5890.1	89.5	...	53.5	16.3	0.018±0.001	0.182±0.027
1036–069	0.0 ^b	17891.3	26592.9	6255.6	2051.1	1.000 ^b	0.115±0.009
1053+064	5061.9	130.9	60.5	67.3	4.8	0.026±0.001	0.036±0.012
1054+365	1490.3	16.3	...	7.2	...	0.011±0.001	...
1130+495	389.4	3.0	2.0	0.013±0.001	0.668±0.049
1135+581	5938.1	122.7	24.1	60.3	49.8	0.028±0.001	0.406±0.028
1139+006	1504191.1	4350.3	9422.0	10497.9	4024.9	0.006±0.001	0.925±0.248
1147+153	3463.1	71.8	...	40.8	11.3	0.023±0.001	0.158±0.021
1150–021	35147.6	155.8	...	79.0	5.3	0.005±0.001	0.034±0.012
1211+540	435.6	12.3	...	5.3	0.9	0.029±0.002	0.071±0.020
1222+614	2402.3	13.5	4.0	9.1	8.6	0.009±0.001	0.638±0.065
1223+487	279.2	2.5	0.4	1.4	0.5	0.011±0.001	0.199±0.019
1234+072	8370.9	163.1	60.1	...	10.4	0.020±0.001	0.064±0.020
1256+351	4906.4	41.8	9.0	19.5	13.7	0.011±0.001	0.328±0.013
1319+579A	3540.7	19.7	16.9	39.4	15.7	0.010±0.001	0.798±0.182
1437+370	391.9	2.3	...	2.4	3.0	0.013±0.001	1.316±0.327
2329+286	143970.0	–445.9	1032.6	1531.2	668.6	0.015±0.004	0.437±0.164

^afor all galaxies, the ratio is derived from $N(\text{WNL})$ obtained with the blue bump $\lambda 4650$, except for 0218+003 and 2329+286 where $N(\text{WNL})$ obtained with Si III $\lambda 4565$ is used.

^bO stars are not expected (Schaerer & Vacca 1998) and the ratio $N(\text{WR})/N(\text{O}+\text{WR})$ is set to 1.

^cthe distance of 20 Mpc is adopted (Izotov et al. 1999b).

TABLE 8
PARAMETERS OF THE NEBULAR HE II $\lambda 4686$ EMISSION LINE

Galaxy	$EW(H\beta)^a$	$12+\log(O/H)$	$I(\lambda 4686)/I(H\beta)^b$	$I(\lambda 4686)/I_c(H\beta)^c$	$EW(\lambda 4686)^a$
0335-052	217.2	7.30	0.0262 \pm 0.0018	0.0105 \pm 0.0007	4.82 \pm 0.26
0553+033	272.2	8.09	0.0156 \pm 0.0026	0.0055 \pm 0.0009	3.61 \pm 0.45
0723+692	264.4	7.85	0.0093 \pm 0.0003	0.0018 \pm 0.0001	2.72 \pm 0.07
0749+568	117.1	7.85	0.0177 \pm 0.0084	0.0071 \pm 0.0034	2.20 \pm 1.00
0917+527	85.9	7.86	0.0229 \pm 0.0030	0.0092 \pm 0.0012	1.64 \pm 0.07
0926+606	108.6	7.91	0.0161 \pm 0.0024	0.0045 \pm 0.0007	1.64 \pm 0.05
0930+554	67.0	7.16	0.0340 \pm 0.0022	0.0156 \pm 0.0010	2.54 \pm 0.10
0947+008	124.3	8.07	0.0110 \pm 0.0047	0.0029 \pm 0.0012	1.17 \pm 0.23
0948+532	169.8	8.00	0.0150 \pm 0.0005	0.0060 \pm 0.0002	1.56 \pm 0.14
1030+583	84.1	7.79	0.0239 \pm 0.0021	0.0094 \pm 0.0008	1.91 \pm 0.07
1053+064	78.0	7.99	0.0055 \pm 0.0033	0.0021 \pm 0.0013	0.45 \pm 0.12
1102+450	56.0	8.12	0.0155 \pm 0.0052	0.0062 \pm 0.0021	0.78 \pm 0.13
1102+294	69.8	7.83	0.0249 \pm 0.0064	0.0100 \pm 0.0026	1.55 \pm 0.17
1116+583B	107.3	7.68	0.0245 \pm 0.0095	0.0098 \pm 0.0038	2.53 \pm 0.31
1139+006	48.9	7.99	0.0100 \pm 0.0034	0.0025 \pm 0.0008	0.48 \pm 0.09
1147+153	130.1	8.11	0.0089 \pm 0.0031	0.0041 \pm 0.0014	0.99 \pm 0.18
1150-021	87.8	7.95	0.0092 \pm 0.0024	0.0015 \pm 0.0004	0.83 \pm 0.10
1152+579	189.3	7.81	0.0129 \pm 0.0003	0.0052 \pm 0.0001	2.12 \pm 0.09
1159+545	249.3	7.49	0.0106 \pm 0.0006	0.0042 \pm 0.0002	2.29 \pm 0.20
1205+557	63.7	7.75	0.0181 \pm 0.0074	0.0072 \pm 0.0030	1.19 \pm 0.10
1222+614	85.2	7.95	0.0171 \pm 0.0017	0.0051 \pm 0.0005	1.30 \pm 0.05
1223+487	206.2	7.77	0.0117 \pm 0.0005	0.0038 \pm 0.0002	3.25 \pm 0.17
1249+493	124.1	7.72	0.0124 \pm 0.0010	0.0050 \pm 0.0004	1.32 \pm 0.22
1319+579A	173.0	8.11	0.0077 \pm 0.0014	0.0037 \pm 0.0007	1.60 \pm 0.05
1319+579B	64.6	8.09	0.0138 \pm 0.0044	0.0067 \pm 0.0021	1.21 \pm 0.07
1319+579C	16.6	7.92	0.0158 \pm 0.0135	0.0076 \pm 0.0065	0.30 \pm 0.25
1415+437	163.6	7.59	0.0251 \pm 0.0005	0.0100 \pm 0.0002	3.65 \pm 0.10
1420+544	217.3	7.75	0.0124 \pm 0.0005	0.0050 \pm 0.0002	2.42 \pm 0.17
1441+294	56.2	7.99	0.0189 \pm 0.0126	0.0076 \pm 0.0050	1.37 \pm 0.17
1851+693	368.4	7.79	0.0131 \pm 0.0012	0.0052 \pm 0.0005	4.90 \pm 0.14

^ain Å.

^bcorrected for interstellar extinction only.

^ccorrected for both interstellar extinction and aperture.

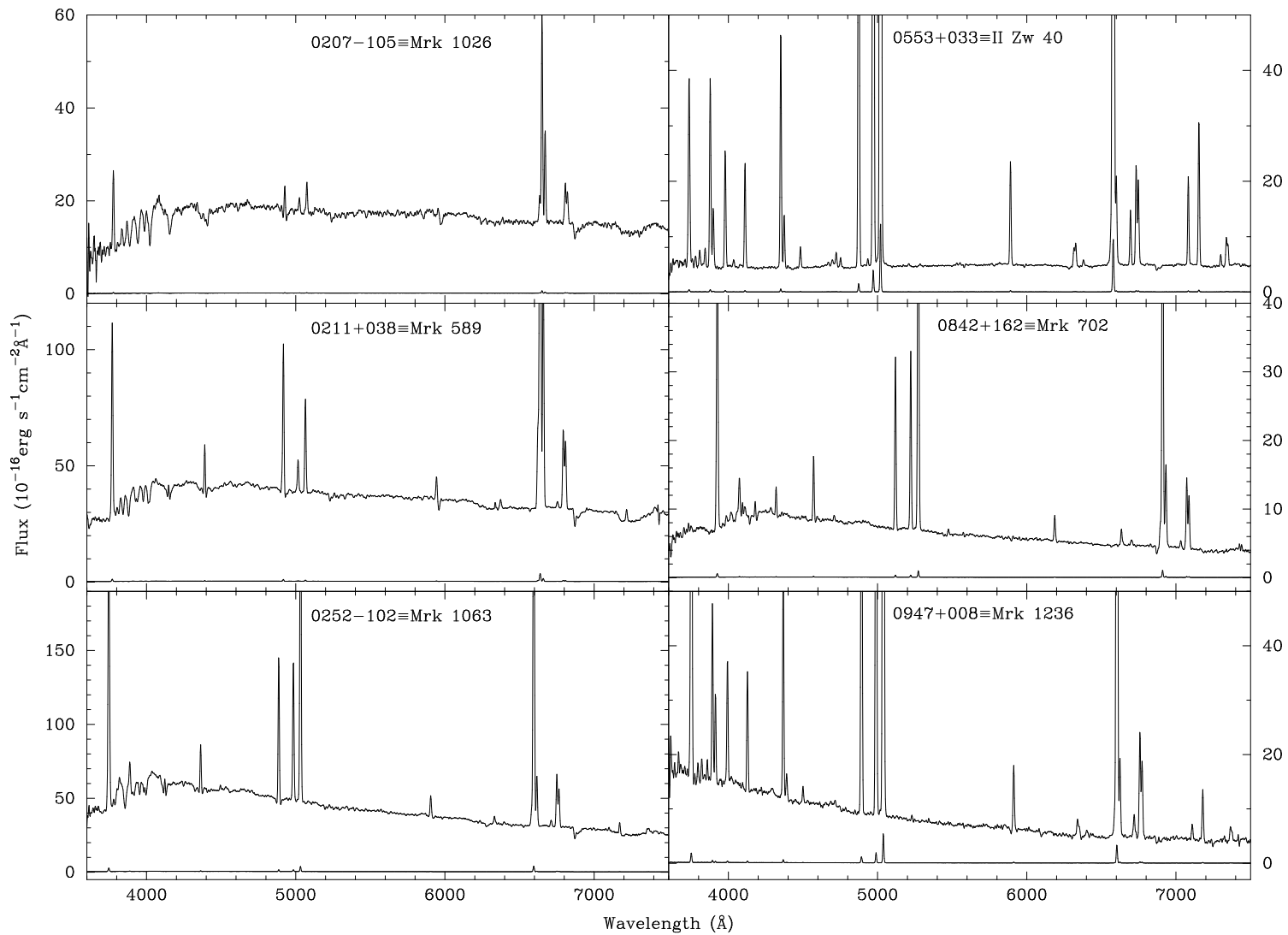


Fig. 1.— Spectra covering the whole optical spectral range of twelve galaxies in our WR sample. Spectra for the remaining WR galaxies can be found in previous publications (ITL94, ITL97, IT98, Thuan et al. 1995).

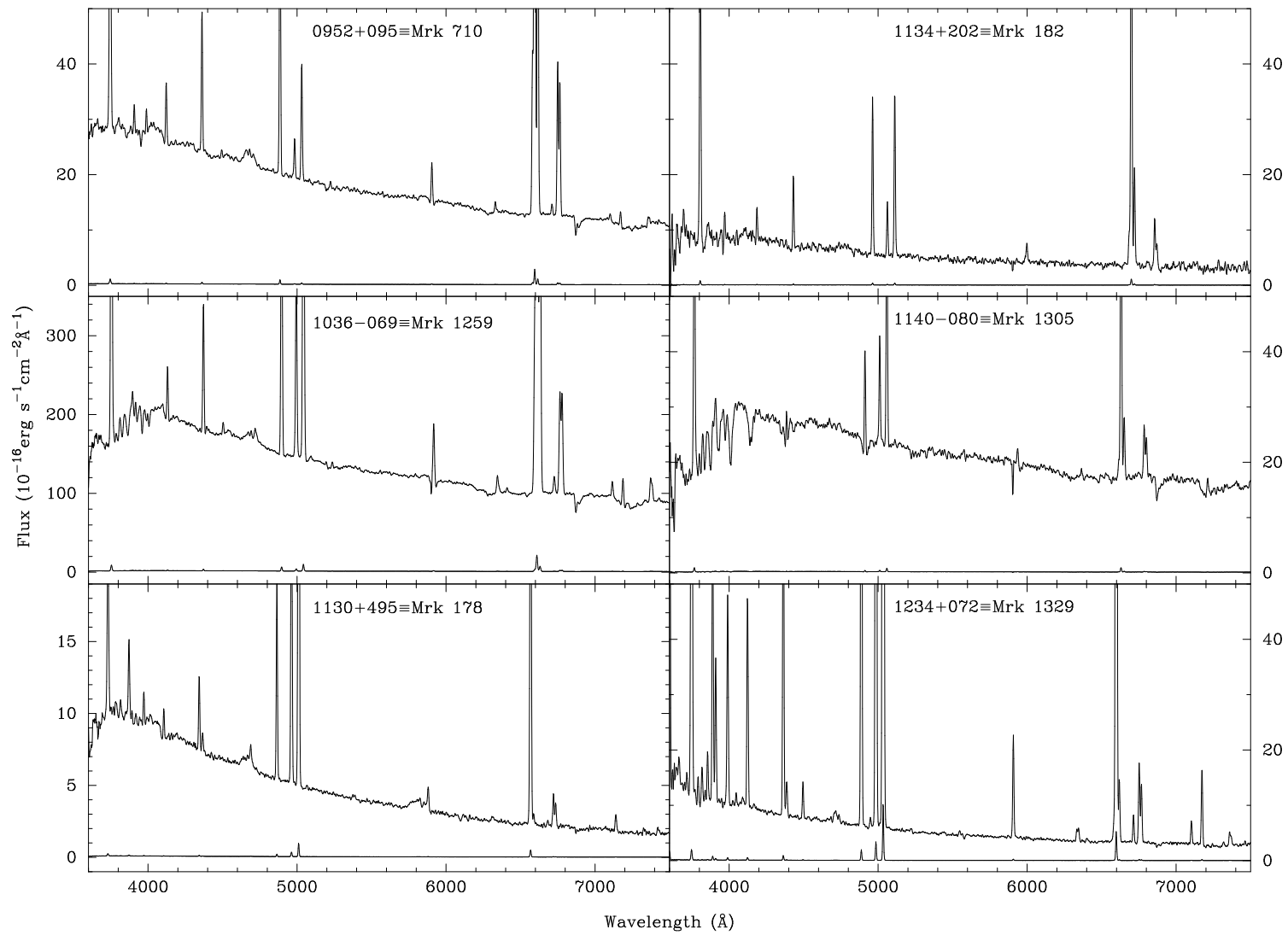


Fig. 1.— Continued.

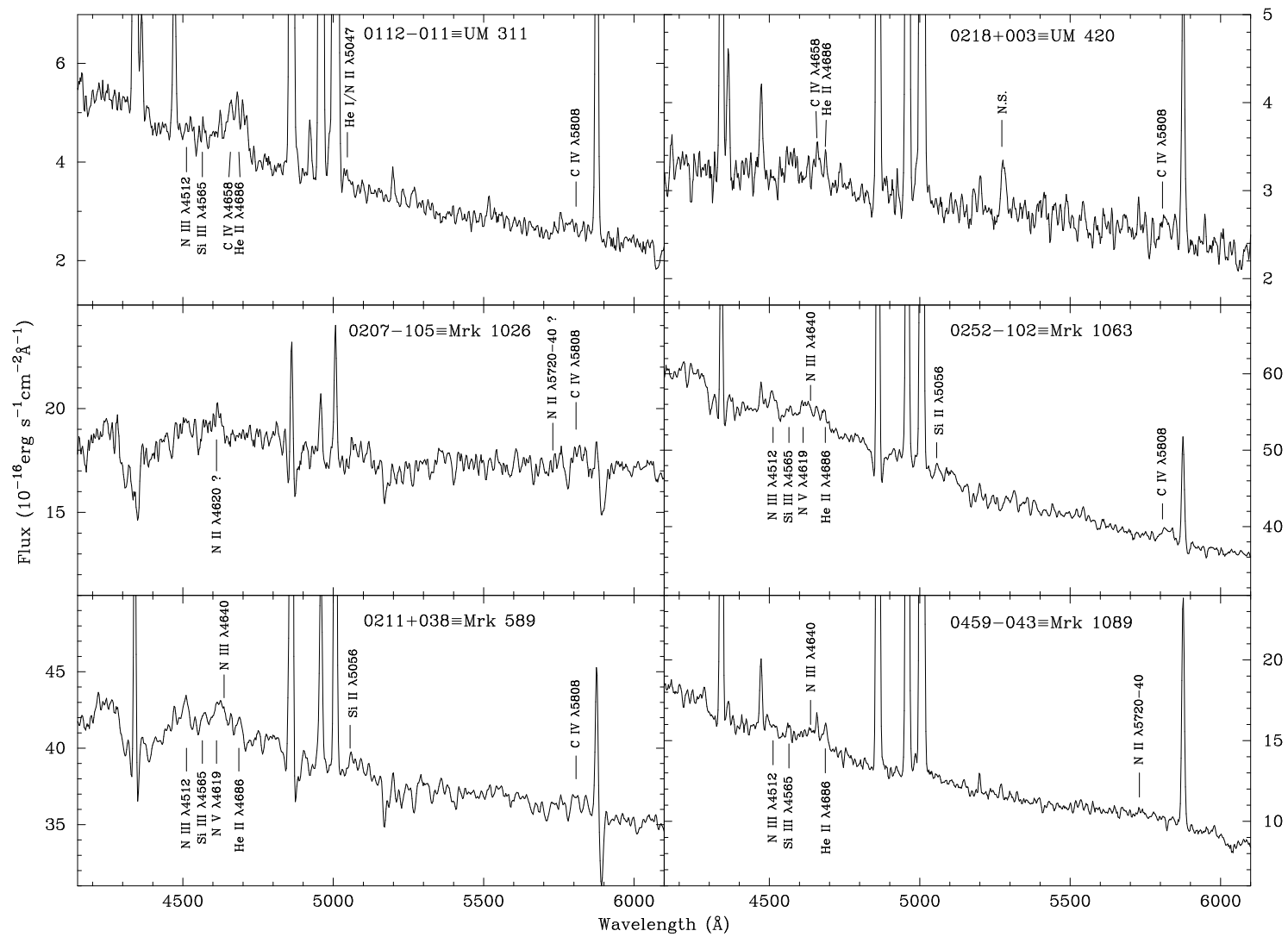


Fig. 2.— Spectra of all WR galaxies restricted to the wavelength range $\lambda\lambda$ 4150–6100 to emphasize the WR features. Definite and suspected WR lines are marked.

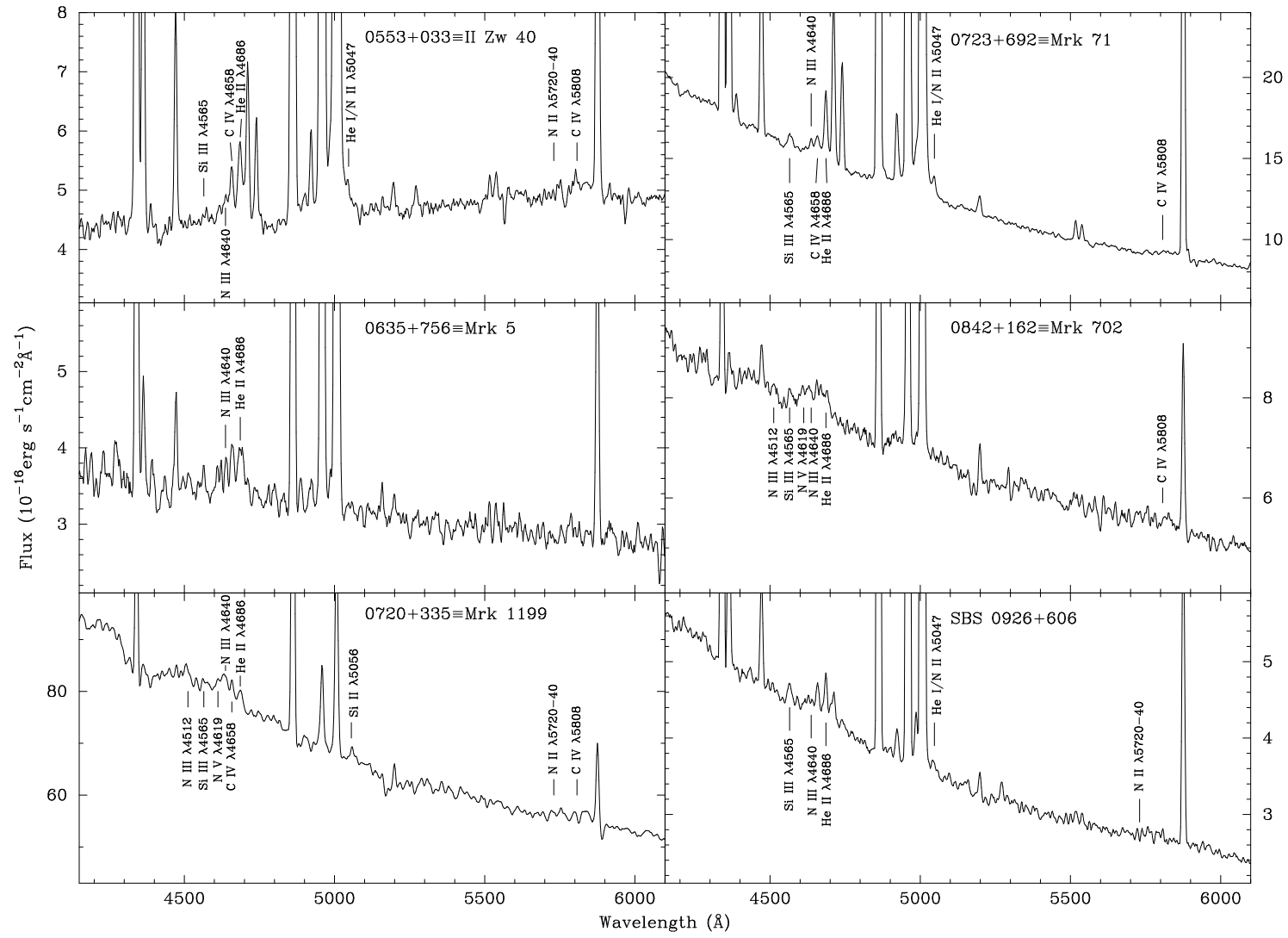


Fig. 2.— Continued.

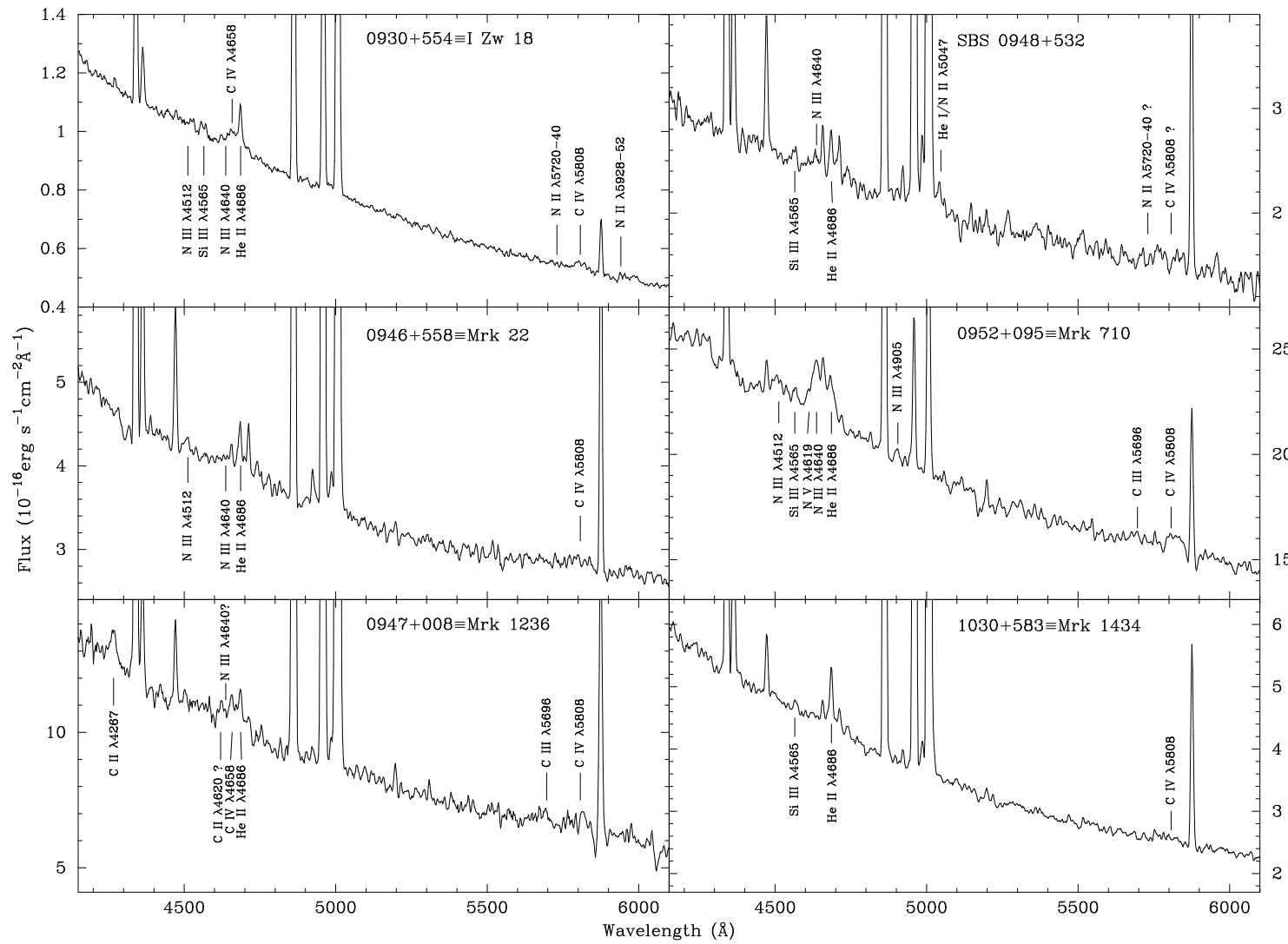


Fig. 2.— Continued.

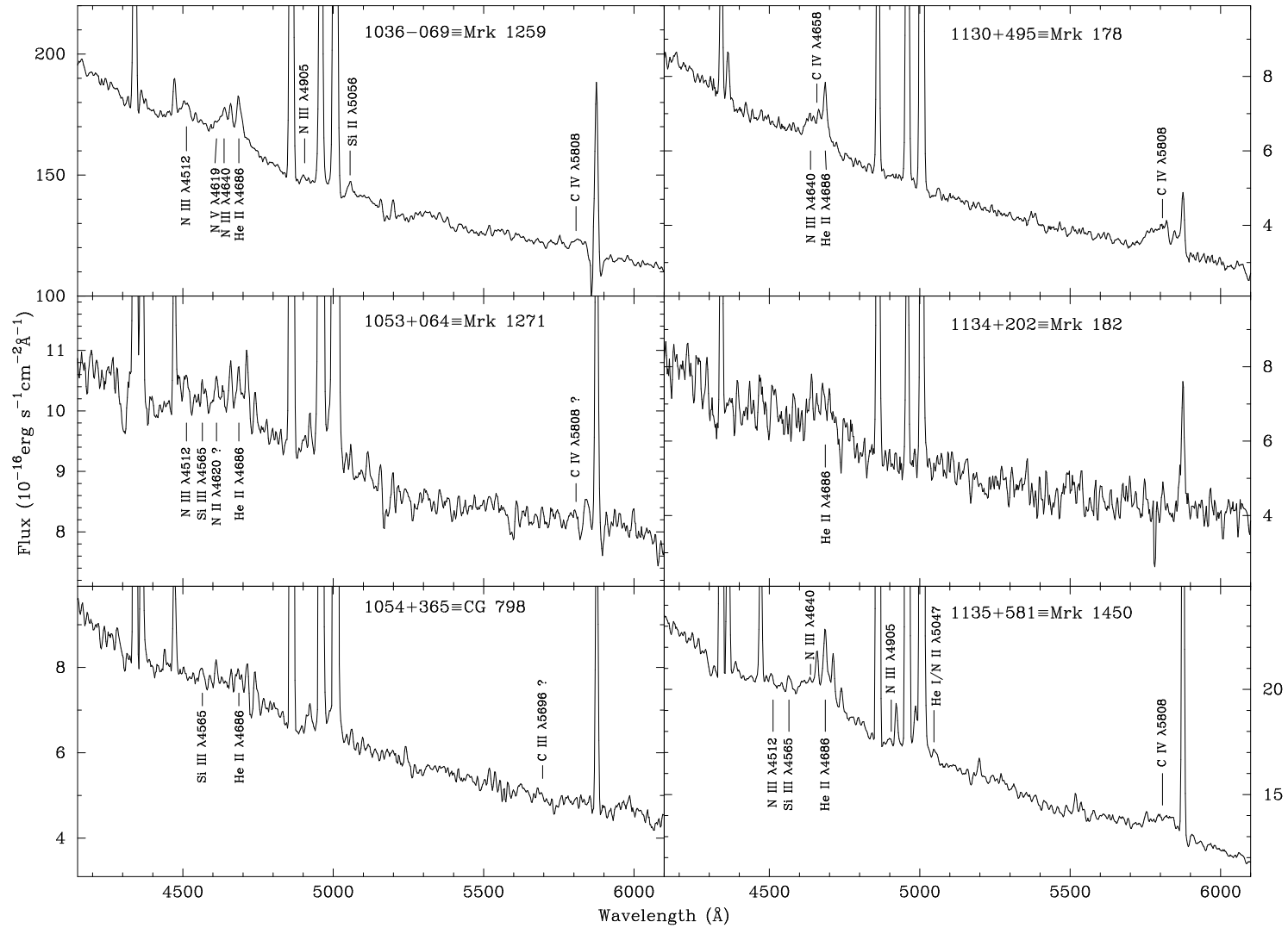


Fig. 2.— Continued.

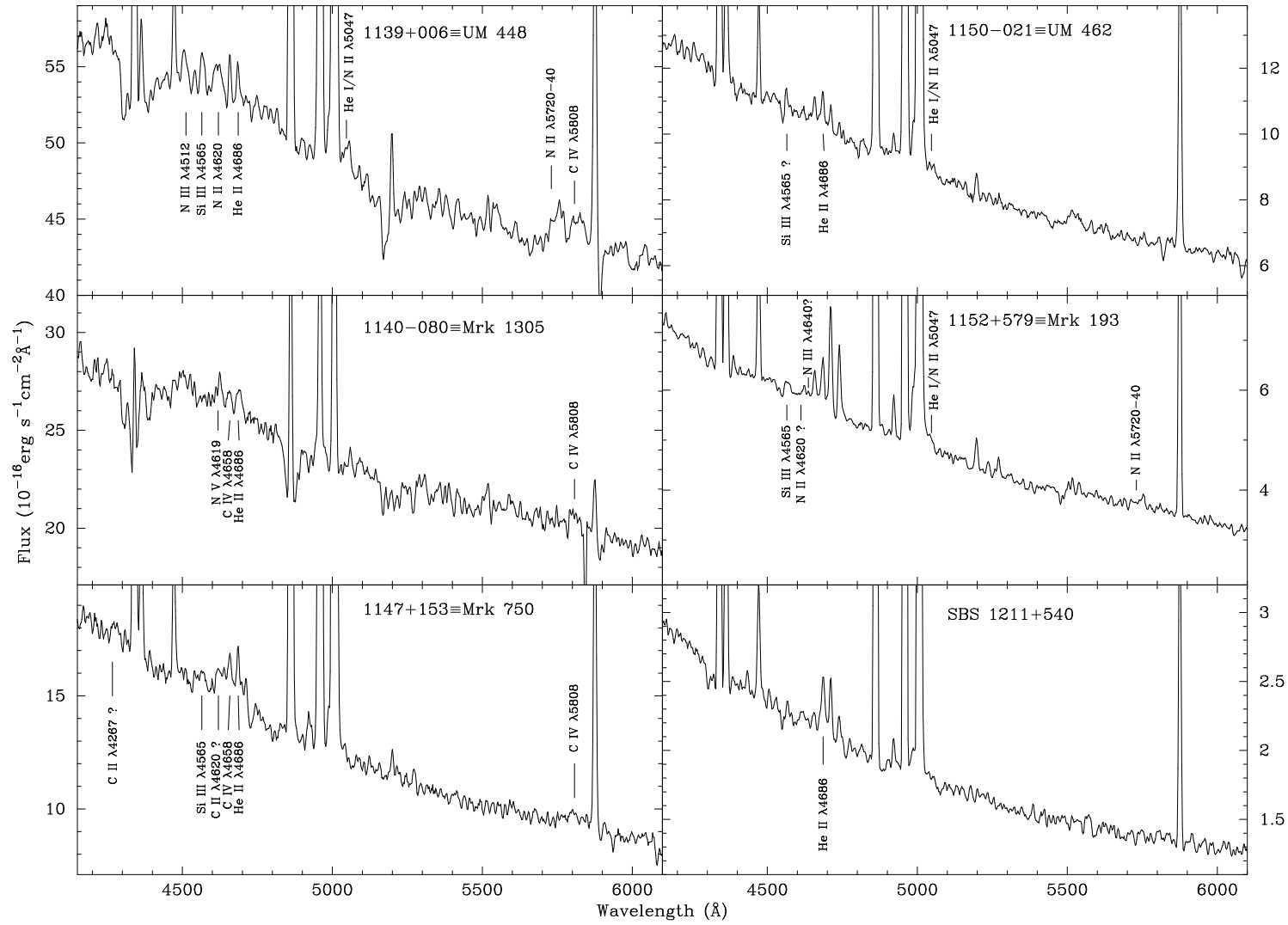


Fig. 2.— Continued.

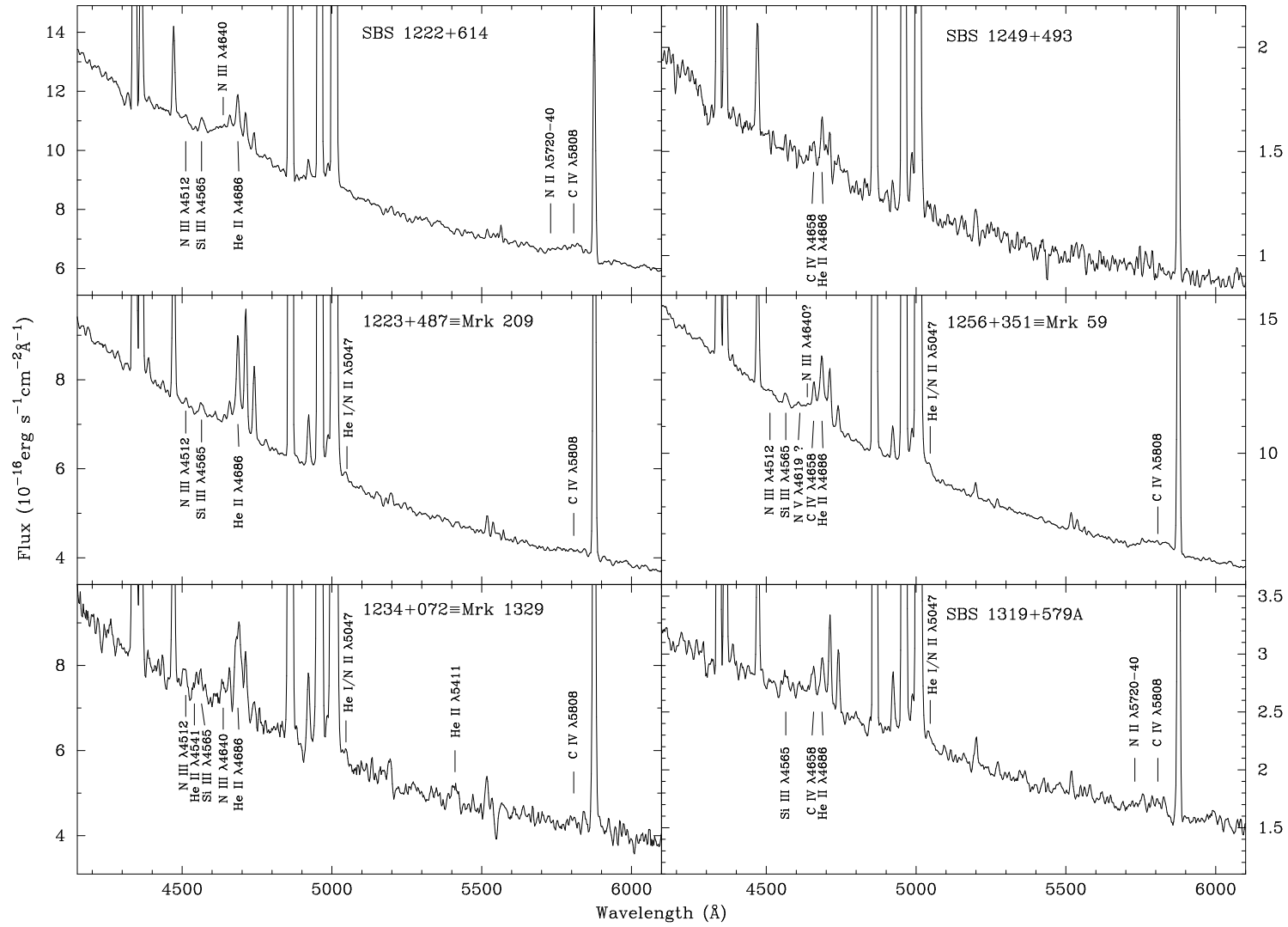


Fig. 2.— Continued.

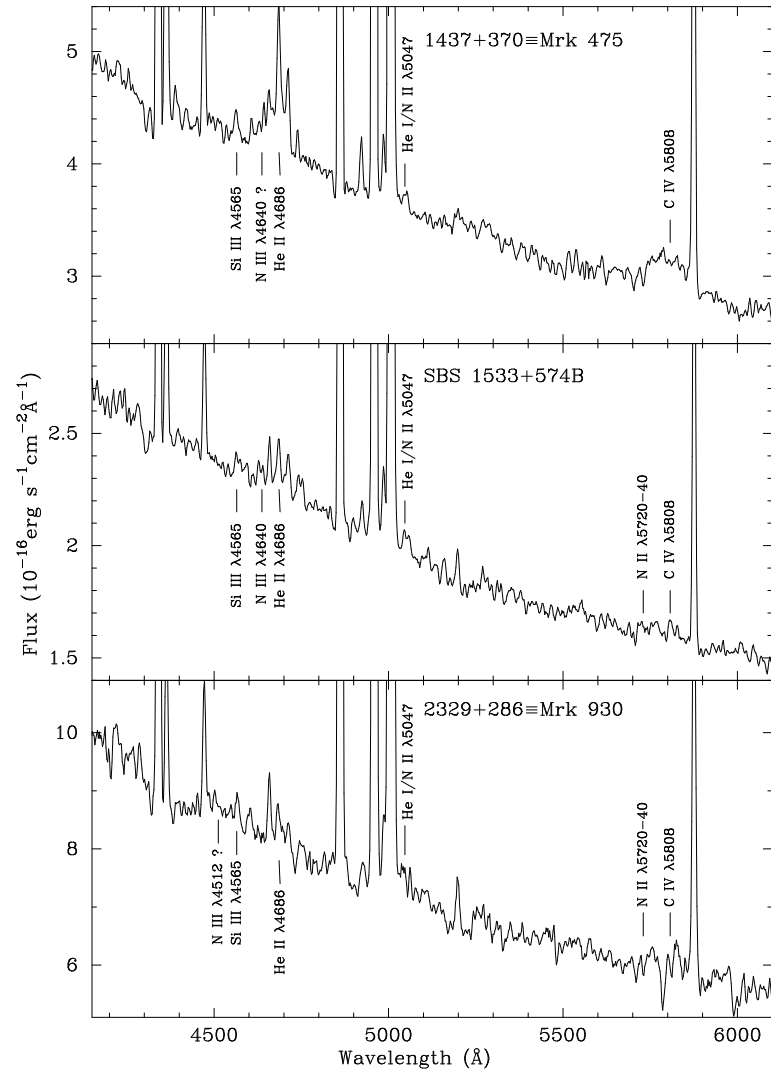


Fig. 2.— Continued.

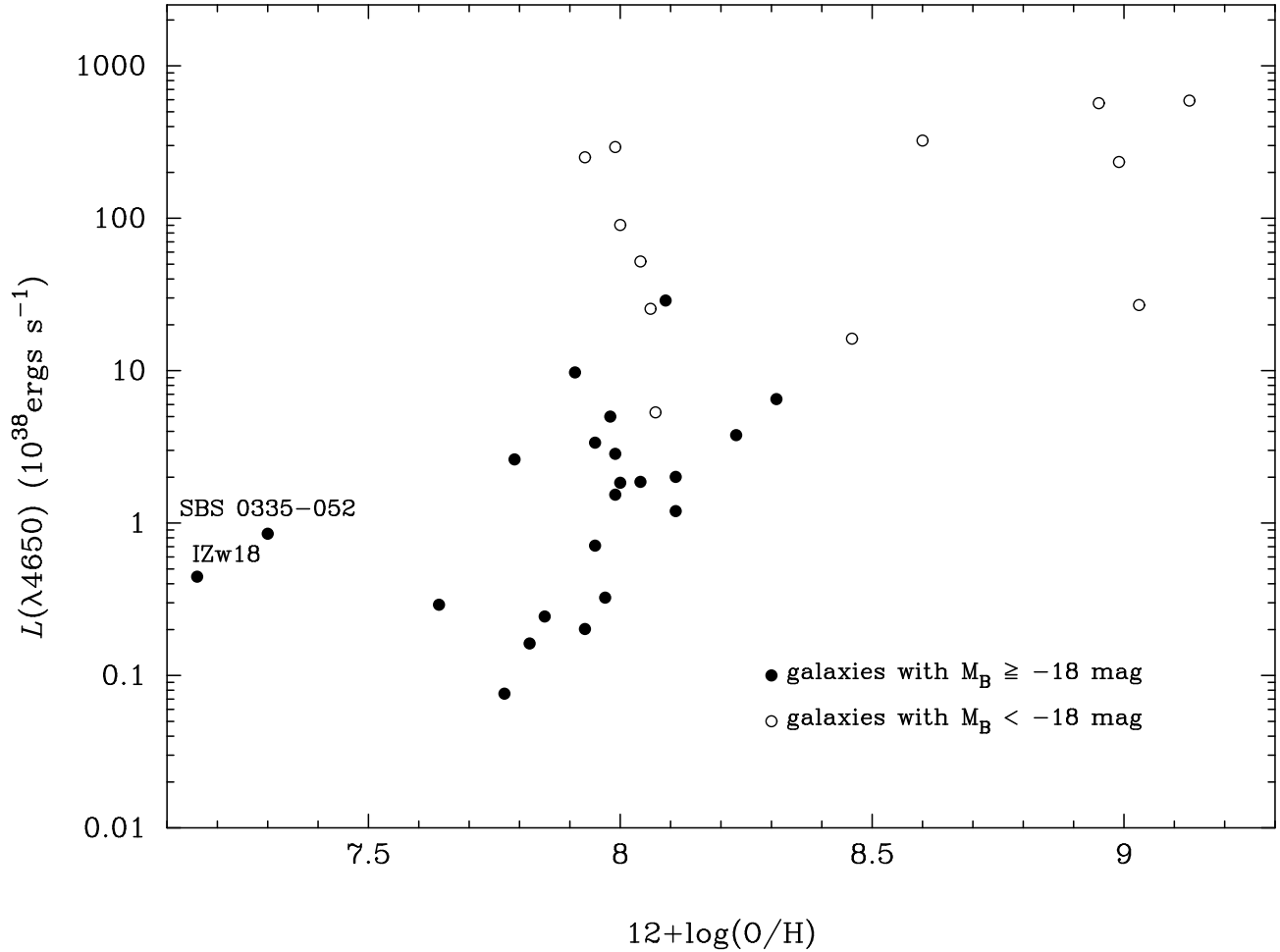


Fig. 3.— The luminosity of the blue bump $L(\lambda 4650)$ vs oxygen abundance $12 + \log(\text{O}/\text{H})$ for the WR galaxies. Filled circles denote galaxies with $M_B \geq -18$ and open circles those with $M_B < -18$. The data points belonging to the two most metal-deficient WR galaxies known, I Zw 18 (Izotov et al. 1997, this paper) and SBS 0335-052 (Izotov et al. 1999a), are marked.

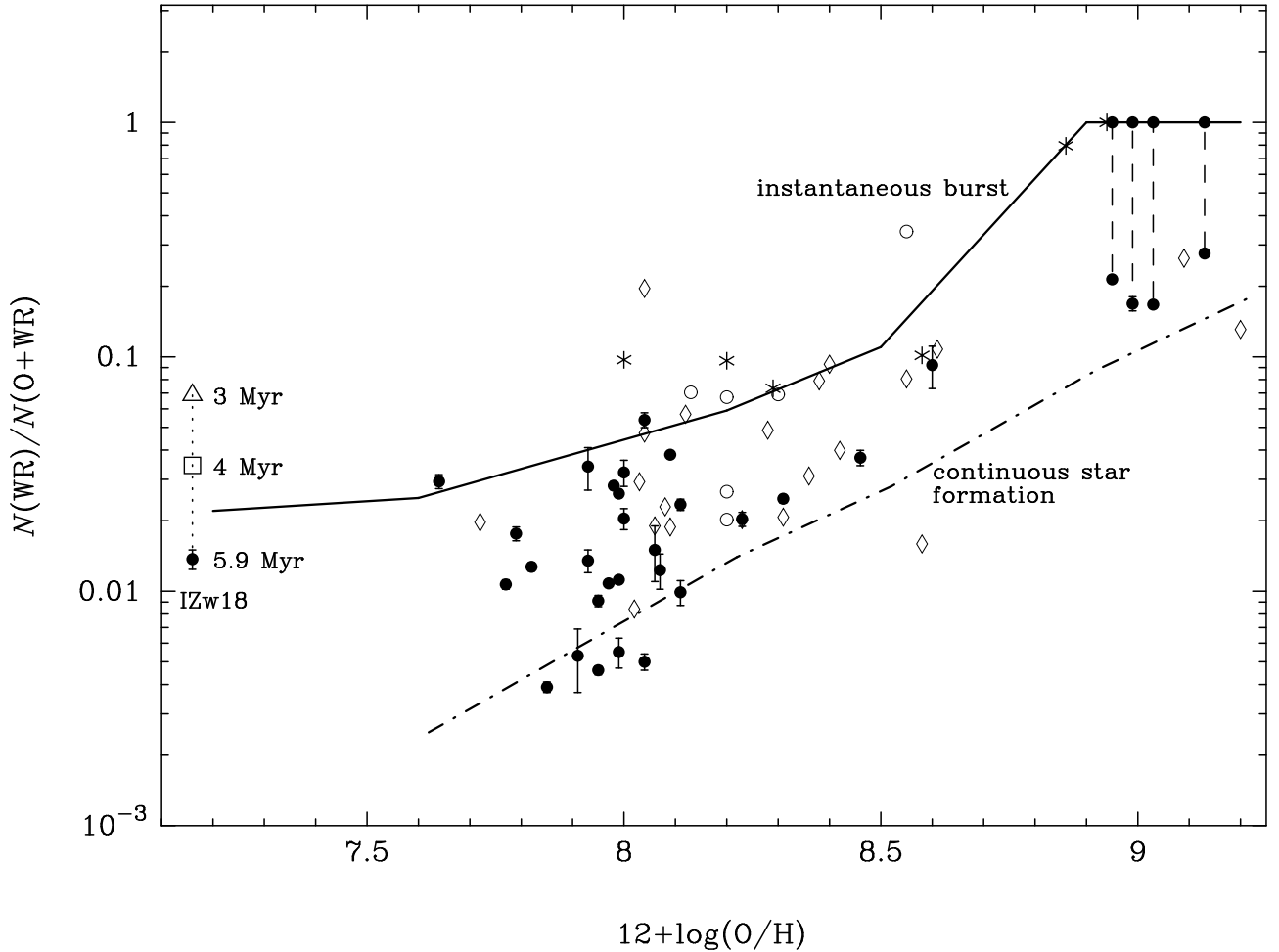


Fig. 4.— The relative number of WR stars $N(\text{WR}) / N(\text{O}+\text{WR})$ vs oxygen abundance $12+\log(\text{O}/\text{H})$ for the galaxies in our sample (filled circles), and from Vacca & Conti (1992) (diamonds), Kunth & Joubert (1985) (asterisks) and Schaerer et al. (1999a) (open circles). For I Zw 18, three $N(\text{WR})/N(\text{O}+\text{WR})$ values are shown for three choices of the parameter η_0 : 0.2 (filled circle), 0.5 (open rectangle) and 1 (open triangle) corresponding to burst ages of 5.9, 4 and 3 Myr respectively. At the high metallicity end, two values of $N(\text{WR})/N(\text{O}+\text{WR})$ are shown for each galaxy connected by a dashed line: 1 and the value corresponding to $\eta_0 = 1$. The solid and dot-dashed lines show the model predictions of maximum values of $N(\text{WR})/N(\text{O}+\text{WR})$ in the two limiting cases of an instantaneous burst and continuous star formation, respectively (SV98; Schaerer 1998, private communication).

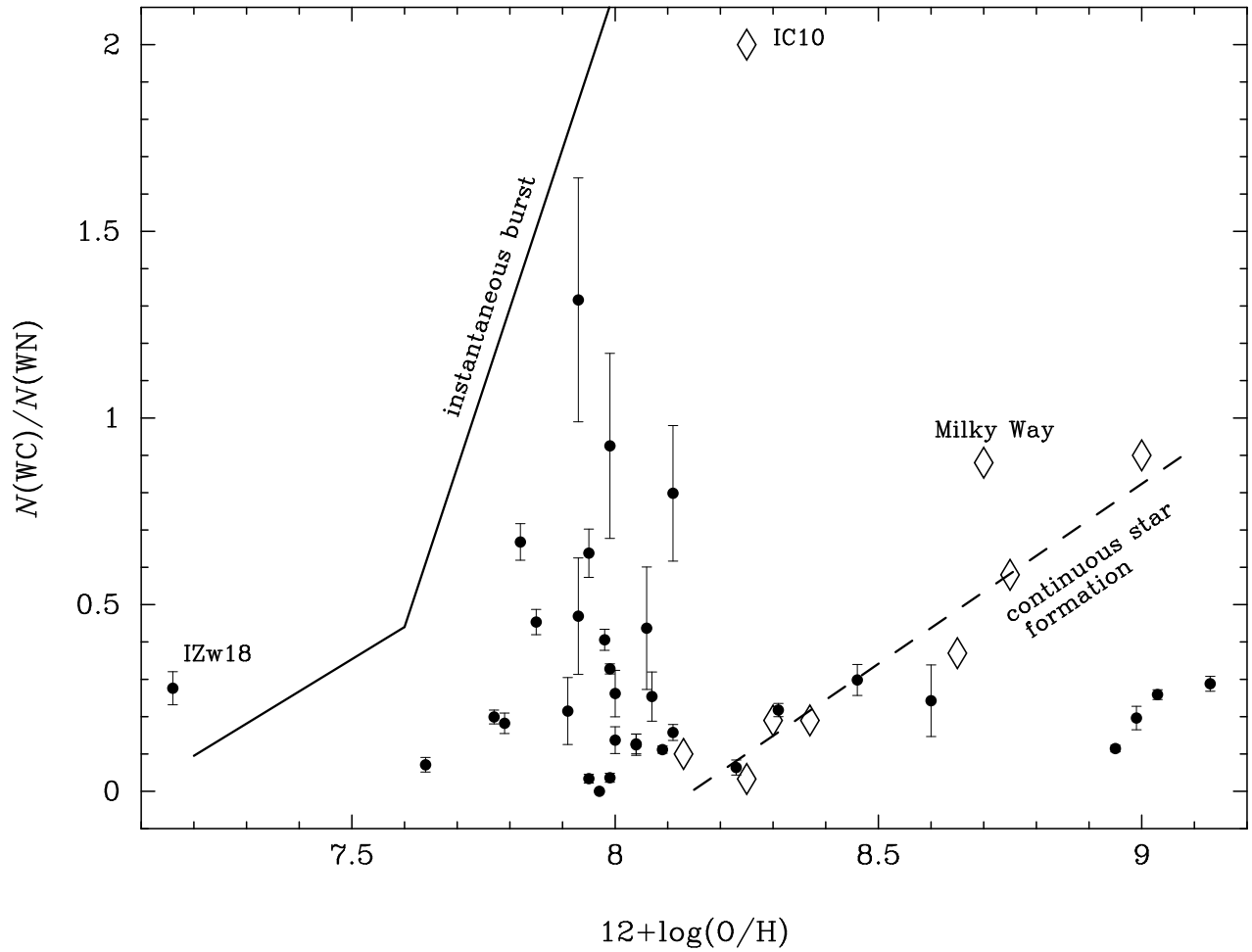


Fig. 5.— The ratio of the WC to WN star numbers vs oxygen abundance $12 + \log(\text{O}/\text{H})$ for the galaxies in our sample (filled circles). The solid line is the locus of maximum values predicted by evolutionary synthesis models for an instantaneous burst (SV98; Schaerer 1998, private communication). Diamonds are data from Massey & Johnson (1998) for Local Group galaxies. The dashed line is those authors' fit to their data and represents the case of continuous star formation.

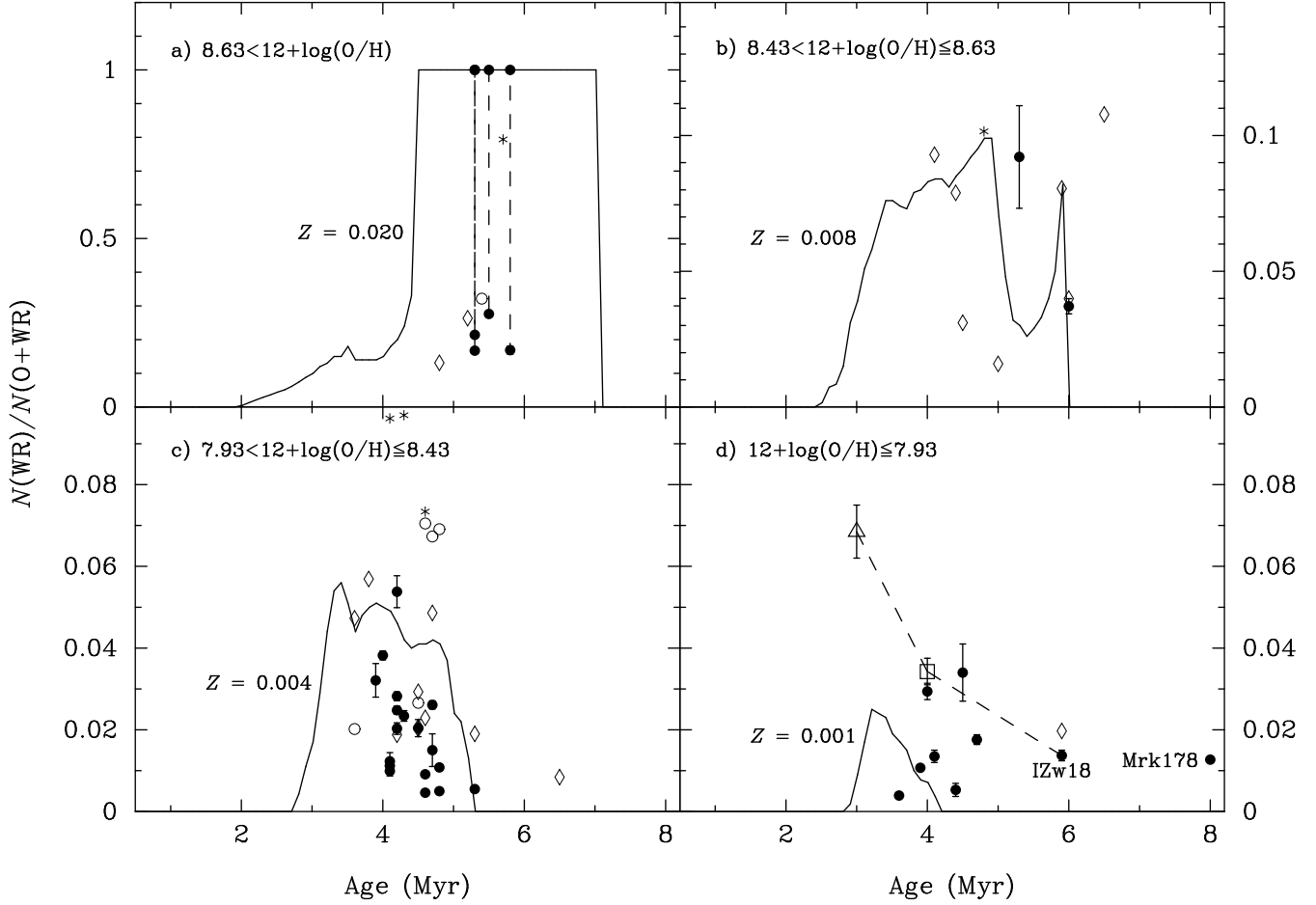


Fig. 6.— $N(\text{WR})/N(\text{O}+\text{WR})$ vs age of instantaneous burst diagrams for the galaxies from our sample (filled circles), Vacca & Conti (1992) (diamonds), Kunth & Joubert (1985) (asterisks) and Schaerer et al. (1999a) (open circles). The data are divided into four groups according to oxygen abundances: $12 + \log(\text{O}/\text{H}) > 8.63$ (Figure 6a), $8.43 < 12 + \log(\text{O}/\text{H}) \leq 8.63$ (Figure 6b), $7.93 < 12 + \log(\text{O}/\text{H}) \leq 8.43$ (Figure 6c) and $12 + \log(\text{O}/\text{H}) \leq 7.93$ (Figure 6d). In panel a) two values of $N(\text{WR})/N(\text{O}+\text{WR})$ are shown for each high-metallicity galaxy, connected by a dashed line (Figure 6a): 1 and the value corresponding to $\eta_0 = 1$. In panel d) three values of the $N(\text{WR})/N(\text{O}+\text{WR})$ ratio connected by a dashed line are shown for I Zw 18. They are derived for three values of the parameter η_0 : 0.2 (filled circle), 0.5 (open rectangle) and 1 (open triangle) corresponding to burst ages of 5.9, 4 and 3 Myr respectively. In all four panels solid lines represent model predictions by SV98. They are labeled by the heavy element mass fraction of the model.

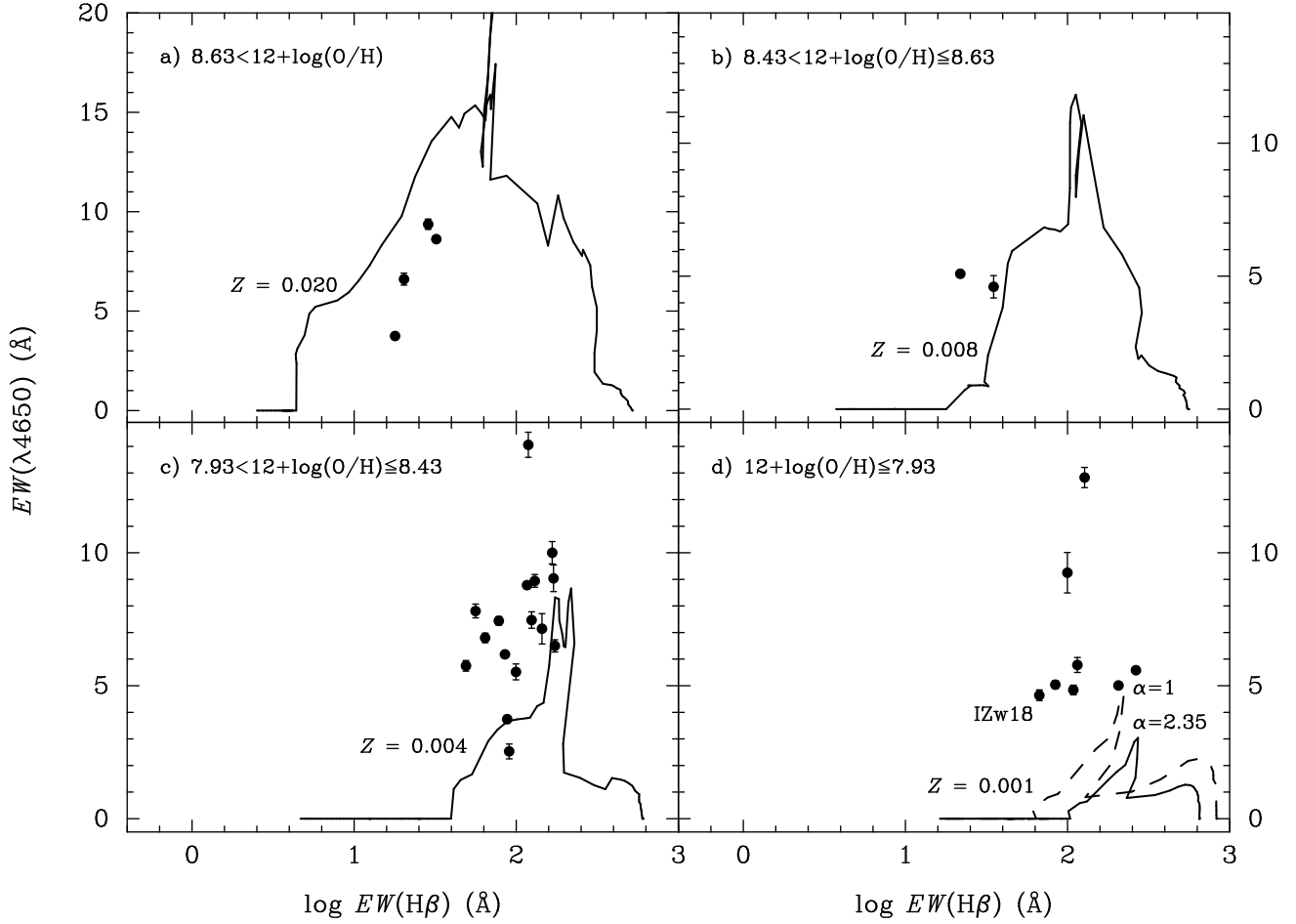


Fig. 7.— The equivalent width of the blue bump $EW(\lambda 4650)$ vs equivalent width $EW(H\beta)$ of the $H\beta$ emission line for our WR galaxy sample. The WR galaxies are divided into four groups with different ranges of oxygen abundance as in Figure 6. The solid curves in all 4 panels show theoretical predictions by SV98 for an instantaneous burst with an initial mass function slope $\alpha = 2.35$. In panel d), the predictions for an instantaneous burst with $\alpha = 1$ are shown in addition. Each model is labeled by its heavy element mass fraction.

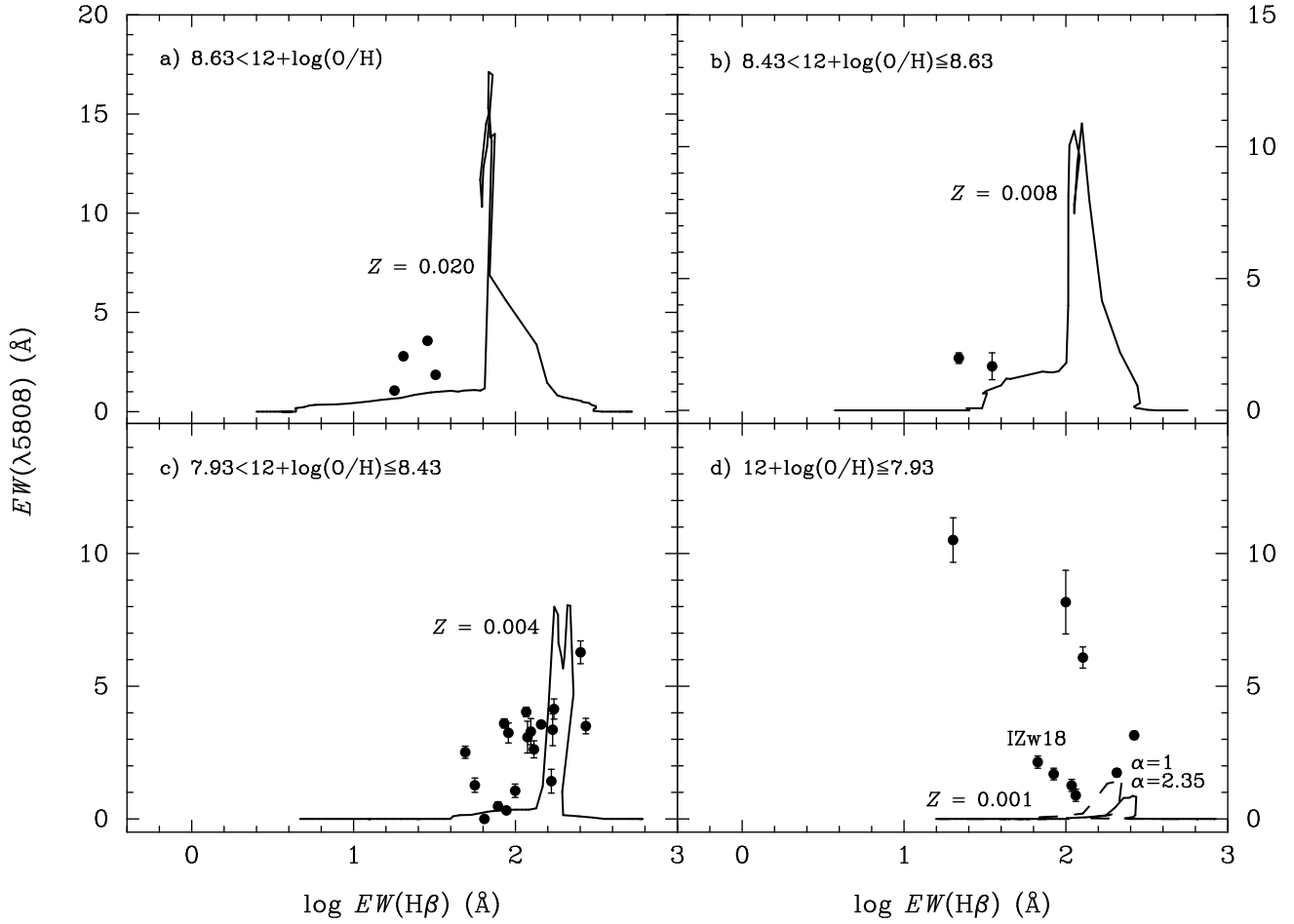


Fig. 8.— Equivalent width of the red bump $EW(\lambda 5808)$ vs equivalent width $EW(H\beta)$ of the $H\beta$ emission line for our WR galaxy sample. The WR galaxies are divided into four groups with different ranges of oxygen abundance as in Figure 6. The solid curves in all 4 panels show theoretical predictions by SV98 for an instantaneous burst with an initial mass function slope $\alpha = 2.35$. In panel d), the predictions for an instantaneous burst with $\alpha = 1$ are shown in addition. Each model is labeled by its heavy element mass fraction.

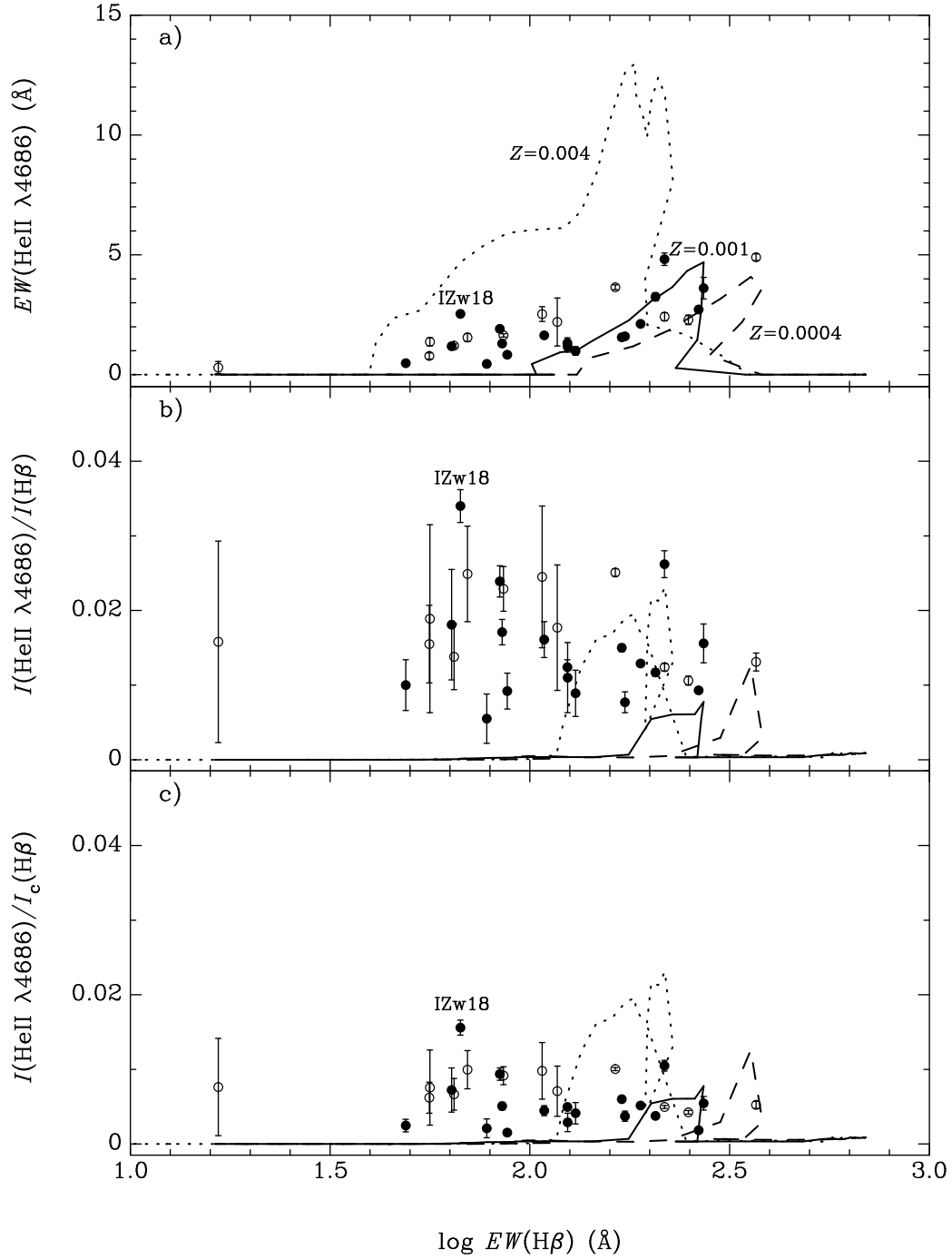


Fig. 9.— (a) Equivalent width of the He II $\lambda 4686$ nebular emission line vs equivalent width of the $H\beta$ emission line for a sample of 30 H II regions; (b) Intensity of the He II $\lambda 4686$ nebular emission line relative to $H\beta$, the latter not being corrected for aperture, vs equivalent width of the $H\beta$ emission line; (c) Intensity of the He II $\lambda 4686$ nebular emission line relative to aperture-corrected $H\beta$, vs equivalent width of the $H\beta$ emission line. In each panel, the lines show theoretical predictions for the heavy element mass fractions $Z = 0.004$ (dotted), 0.001 (solid) and 0.0004 (dashed) respectively (SV98; Schaerer 1998, private communication). H II regions with detected WR features are shown by filled circles while those with non-detected WR features are shown by open circles.